

Immune cell self-organization towards ongoing immune reactions on a tissue-mimicking microdevice

Giovanna Perinetti Casoni

June 2015

MASTER THESIS

Department of Molecular Medicine and Cancer Research, Faculty of Medicine
Norwegian University of Science and Technology

Supervisor 1: Professor Øyvind Halaas

Supervisor 2: Doctor Nimi Gopalakrishnan

Acknowledgment

This thesis was written at the Department of Molecular Medicine of the Norwegian University of Science and Technology (NTNU). I would like to thank the following persons for their great help during this project. To my supervisor, professor Øyvind Halaas, for being a vitally important reference and source of advices, guiding me during difficulties and bringing out the best of my capabilities: grazie mille (tusen takk).

To my co-supervisor Nimi Gopalakrishnan, for being helpful and resourceful in every situation, and for her great companion that I really missed during the last months of this work.

To all the students and the PhD candidates of our group that were always available for helping each other. It was a pleasure to be part of such a team. Thank you for the reciprocal help and for the knowledge we shared in every moment.

Special thanks go to Kjartan Wøllo Egeberg, Bjørnar Sporsheim, Gaute Brede, Markus Haug, Hany Ibrahim and Nisha Kannan, for suggestions and laboratory training. Particular thanks to Signe Åsberg for teaching me how to isolate and differentiate primary dendritic cells.

Thanks to my family that supported me and allowed me to do this experience abroad.

Thank you Aksel, for always being there when I needed it the most.

Thanks to my classmates for the great moments we shared together.

Finally, I would like to thank my italian friends, I miss you always and I am looking forward to seeing you again.

G.P.C.

Abstract

A tissue mimicking micro-device has been developed by our microfluidics group. The device has been designed in order to mimic complex *in vivo* scenarios of immune cell recruitment, where cells sense and are directed by soluble and structural signals in confined spaces. A maze-structured network of microchannels is connected to cell culture chambers where immune reactions can take part. Immune reactions represent a source of chemoattractants molecules for creating functional gradients across the network, possibly recruiting cells from other compartments. The device is composed of a patterned structure of polydimethylsiloxane (PDMS), an organosilane elastomeric polymer, bonded on a glass coverslid.

In this work, our newly designed fourth generation device has been tested under several experimental conditions studies in order to determine its critical points in the study of cell chemotaxis. First, some of the microfabrication operations necessary for the realization of the chip have been expanded and partly translated to the biology laboratory. Good microfabrication procedures have been proved to be fundamental for the functionality of the device, since a good bonding between the micropatterned PDMS and the glass is crucial to spatially control the flow of chemoattractant molecules. Second, a preliminary characterization of diffusion dynamics within the device was performed. The design fits the creation of gradients across the mazed-structured network, but gradients seem to require time to be established. Some suggestion are therefore proposed in order to accelerate this process, such as increased dimensions of the attractor culture chambers, that are likely to help in the accumulation of more chemokine-producing cells. In any case, some results suggest that established gradients may be maintained during prolonged time inside the network.

The device was then employed in biological experiments showing potential recruitment of bone marrow-derived dendritic (BMDC) cells. These cells invaded the network under certain experimental conditions and clearly localized towards the source of chemoattractant molecules. The long time needed for gradient formation and a degree of unpredictability of the dynamics in antigen-presentation reactions ongoing on-chip, did not demonstrated active recruitment of CD8⁺ and CD4⁺ T cell hybridomas. T cell hybridomas showed though a high motility inside the device and interactions between them and BMDC have been documented in real-time. Moreover, the design fits the employment of several microscopy techniques that can be used to address diverse questions regarding mechanisms regulating cells' routes and potentially (not present in this work) subcellular events during migration. The design was proven to organize the space surrounding migrating cells in a manner that is easily accessible to tracking and modeling techniques. Temporal components of migration still need to be fully elucidated and will require further work, also by coupling established biological assays, in order to fully benefit from device potentialities.

Contents

Acknowledgment	i
Abstract	ii
List of figures	vi
List of tables	vii
List of supplementary videos	viii
1 Introduction	1
2 Background theory	3
2.1 Leukocyte migration during homeostasis and inflammation	3
2.1.1 Chemotaxis and leukocyte migration:	3
2.1.2 Recruitment of dendritic cells and T-cells to lymph nodes and peripheral tissues during homeostasis and immune responses:	4
2.1.3 Leukocyte migration in different environments	6
2.2 Studying leukocyte migration	7
2.2.1 Classical biological macro-scale assays	7
2.2.2 Gel assays	9
2.2.3 Intravital microscopy	9
2.2.4 Studying cell chemotaxis with microfluidics and confined environments .	10
2.3 Device description and microfabrication techniques	11
2.3.1 Microfabrication and soft lithography	12
2.3.2 Third and fourth generation device designs	13
2.3.3 Objectives	15
3 Methods and solutions	16
3.1 Device Fabrication and Operation Procedures	16
3.1.1 Device features and fabrication steps	16
3.1.2 Device handling	18
3.2 Cell Cultures, Preparation and Loading	19
3.2.1 Base medium employed in cell cultures	19
3.2.2 Cell counting	19
3.2.3 Dendritic cells culture and preparation	19
3.2.4 MF2.D9 and RF33.70 staining and preparation	21
3.2.5 CD8 ⁺ and CD4 ⁺ T cells preparation and staining	21
3.2.6 Cell loading on fourth generation device	21

3.2.7	Administration of bioactive molecules and bacteria in-channel	22
3.2.8	Modeling diffusion and gradient establishment within the fourth generation device:	24
3.3	Analysis	24
3.3.1	Imaging	24
3.3.2	Flow cytometry	24
4	Results	26
4.1	Device fabrication and operation developments in fourth generation device . . .	26
4.1.1	Bonding and sterility	26
4.1.2	Device types and cell loading procedures	27
4.1.3	Administration of bioactive molecules/bacteria in channel	28
4.1.4	Modeling diffusion and gradient establishment within in fourth generation devices	30
4.2	Flowcytometry	32
4.2.1	BMDC staining and flow cytometry	32
4.2.2	MF2.2D9 and RF33.70 staining and flowcytometry	32
4.3	Cell recruitment and chemotaxis assays	35
4.3.1	Established method for chemotaxis analysis	35
4.3.2	Mouse CD4 ⁺ and CDS ⁺ T cells chemotaxis and recruitment	36
4.3.3	BMDC chemotaxis and recruitment	36
4.3.4	MF2.2D9 and RF33.70 recruitment towards antigen presentation reactions	44
4.4	Cell migration and interactions, in real-time observations in the Fourth Generation Device	50
4.4.1	BMDC behavior and migration in fourth generation device	50
4.4.2	MF2.2D9 and RF33.70 cells migration and behaviour	51
5	Discussion	54
5.1	Device fabrication and operations	54
5.2	Chemotaxis assays and antigen presentation reactions	57
5.3	Cell Recruitment and Migration in Real-Time	59
6	Future Developments	62
7	Conclusion	64
	Bibliography	65

List of Figures

1.1	Complex routes involved in dendritic and T cells homing and circulation within the human body:	2
2.1	Chemokines and leukocyte chemotaxis.	4
2.2	Localization of immune cells depend on their chemokine and migratory receptors.	5
2.3	Phenotypes of ameboid migration in immune cells:	7
2.4	Advantages and limitations of common assays for studying chemotaxis <i>in vitro</i>	8
2.5	Limits of intravital microscopy	10
2.6	Examples of microfluidics and microchannels applications for the study of leukocyte chemotaxis	11
2.7	Soft lithography technique for the fabrication of microfluidics devices in PDMS	13
2.8	Third generation device design	14
2.9	Fourth generation design.	15
3.1	Structural characteristics of Type 1 devices, fourth generation	17
3.2	Filling strategy for fourth generation device attractor/control chamber	22
3.3	In-channel administration strategy	23
4.1	How to evaluate device bonding efficiency in fourth generation devices	27
4.2	In-channel administration: diffusion dynamics in plugged devices	29
4.3	In-channel administration of CFP- <i>Micobacterium avium</i>	30
4.4	Modeling gradient diffusion inside the device	31
4.5	Flow cytometry analysis of <i>in vitro</i> differentiated bone marrow-derived dendritic cells	33
4.6	Flow cytometry analysis of MF2.2D9 cell line	34
4.7	Flow cytometry analysis of RF33.70 cell line	34
4.8	Identified subareas for chemotaxis analysis.	35
4.9	Chemotactic response of iBMDCs towards LPS stimulated BMDCs	37
4.10	BMDCs localization in different areas of the device 18 h after loading:	39
4.11	BMDCs localization in different areas of the device 24 h and 48 h after loading	40
4.12	Chemotactic response of iBMDCs towards LPS stimulated BMDCs	41
4.13	BMDCs localization in different areas of the device 16h and 48h after loading	41
4.14	Chemotactic response of BMDCs towards LPS stimulated BMDCs and distribution 24 h after loading	42
4.15	Chemotactic response of BMDCs at 15 h, 24 h and 48 hours towards <i>M. avium</i> infections and distribution of BMDC during chemotaxis	43
4.16	Chemotactic response of BMDCs at 20 h, 48 h and 72 hours towards <i>M. avium</i> infections	44

4.17	Localization of a mixture of RF33.70 and MF2.2D9 towards BMDCs or antigen presentation reactions	46
4.18	Chemotactic response of MF2.2D9 towards antigen presentation reactions: . . .	47
4.19	Localization of MF2.2D9 towards antigen presentation reactions:	48
4.20	Localization of MF2.2D9 and RF33.70 towards antigen presentation reactions .	49
4.21	Different Deep Red CellTracker dye intensities in cells within attractor and control compartments	50
4.22	Interaction from the uropod region between two RF33.70 cells	53

List of Tables

3.1	Types of silicon master utilized in this thesis	16
3.2	Antibodies used in flow cytometry analysis of bone marrow-derived dendritic cells	25
3.3	Antibodies used in flow cytometry analysis of T cells	25
4.1	Experimental setups CD8 ⁺ and CD4 ⁺ T cells fourth generation cell experiments	36
4.2	Experimental setups of chemotaxis experiments with BMDCs	37
4.3	Experimental setups of antigen presentation reactions and RF33.70 and MF2.2D9 chemotaxis experiments	45

List of supplementary videos

1. **Retention:** a large number of RF33.70 and MF2.2D9 seems to be retained in the compartment by probable interactions with BMDC cells 5 days after device loading. Due to the long time after cell labelling, dyes are no longer detected by the microscope. Time lapse of 15 min, pictures every 83 sec, EVOS FL Auto Cell Imaging System.
2. **Particular interaction:** Dendritic cell protrusions are sniking through the filters and interacting with RF33.70 and MF2.2D9 present in the loading channel. Due to the long time after cell labelling, dyes are no longer detected by the microscope. Time lapse of 15 min, pictures every 83 sec, EVOS FL Auto Cell Imaging System.
3. **Inside the attractor compartment:** Deep red labeled MF33.70 and maybe MF2.2D9 seem to have entered and proliferated inside the attractor compartment where an antigen presentation reaction between BMDC and MF2.2D9 was established. CMFDA labelling of MF2.2D9 is no longer visible, Deep Red dye (blue) of MF2.2D9 is slightly visible in cells inside the chamber and visible in some cells in the network. Time lapse of 2 h, pictures every 3 min, EVOS FL Auto Cell Imaging System.
4. **Inside the control compartment:** Deep red labeled MF33.70 and maybe MF2.2D9 seem to have entered the control compartment where unstimulated BMDC and MF2.2D9 were loaded. CMFDA labelling of MF2.2D9 no longer visible, Deep Red dye (blue) of MF2.2D9 is still visible. Time lapse of 2 h, pictures every 3 min, EVOS FL Auto Cell Imaging System.
5. **Pillar movement:** Movement of an unlabeled BMDC along the pillars of the control compartment. The cells exhibit a 2D migration and change shape while it translocate from a pillar to another. Pictures every 3 min, EVOS FL Auto Cell Imaging System.
6. **BMDC morphologies:** Multiple morphologies and migratory profiles of unlabeled BMDCs inside the network. Time lapse of 2h, pictures every 5 min. Zeiss LSM 510.
7. **Inside the lines:** Morphologies and migratory profiles of unlabeled BMDCs inside the lines towards attractor compartment. Time lapse of 2h, pictures every 5 min. Zeiss LSM 510.
8. **Entrance in the network:** Repolarization of BMDCs before entering the network from the migratory compartment. Time lapse of 2h, pictures every 5 min. Zeiss LSM 510.
9. **Adhesive rear:** The rear of some polarized BMDC seem to be uncoupled from leading edge protrusion and stick to the walls of the channel. Time lapse of 2h, pictures every 5 min. Zeiss LSM 510.
10. **BMDC under the filter:** unlabeled BMDC are observed protruding and moving under

the $2\mu\text{m}$ filter between control and arrival compartments. A Deep red labeled RF33.70 travels around. Time lapse of 4 h, pictures every 3 min, EVOS FL Auto Cell Imaging System.

11. **Manual tracking:** Overlay of dots and line obtained by manual tracking. MF2.2D9 and one BMDC moving inside the network 48 h after the starting of the experiment. Time lapse of 2 h, pictures every 3 min, EVOS FL Auto Cell Imaging System.
12. **Automated tracking:** Overlay of cells and lines obtained by automated tracking. Deep-red labeled RF33.70 moving inside the network 6-10 h after the starting of the experiment. Time lapse of 4 h, pictures every 3 min, EVOS FL Auto Cell Imaging System.
13. **Squeezing over:** a Deep Red labeled RF33.70 surpass a CMFDA-labeled MF2.2D9 by squeezing over. Pictures every 3 min, EVOS FL Auto Cell Imaging System.
14. **Encounters:** Deep Red labeled RF33.70 and CMFDA-labeled MF2.2D9 meet upon network bifurcations and interact for several min. Pictures every 3 min, EVOS FL Auto Cell Imaging System.
15. **Dragging from the rear:** Deep Red labeled RF33.70 and CMFDA-labeled MF2.2D9 interact and redirect each other from the rear of the cell. Pictures every 3 min, EVOS FL Auto Cell Imaging System.
16. **Full interactions:** Deep Red labeled RF33.70 and CMFDA-labeled interact with a BMDC, that can be recognized by the numerous elongated protrusions, in front of the entrance to the network. Time lapse of 2 h, pictures every 3 min, EVOS FL Auto Cell Imaging System.
17. **Link to Supplementary videos:** Supplementary videos can be downloaded from:
<https://www.dropbox.com/s/aqzrjq908gxi6dw/VIDEO%20THESIS.zip?dl=0>

Chapter 1

Introduction

It is not birth, marriage, or death, but gastrulation, which is truly the most important time in your life. *Lewis Wolpert (1986)*

Cell migration characterizes fundamental processes for living organisms such as ontogenesis, wound healing and immune responses against pathogens.

The function of the immune system is to eliminate the cause of primary inflammation within organs and tissues in order to preserve their physiological roles. Furthermore, it is also involved in tissue repair mechanisms and homeostasis^{1,2}. Immunity relies on both humoral and cellular components that discriminate between self and non-self/abnormal molecules, eliciting a proper response against potentially pathological situations, while maintaining tolerance towards self-antigens. Immunity is further divided into innate inflammatory responses and adaptive antigen-specific responses³.

Leukocytes are the major cells of the immune systems and are disseminated into many tissues and organs of mammals. Leukocytes either circulate in blood and lymphatics systems or travel across peripheral and lymphoid tissues during surveillance and effector responses⁴, as illustrated in Figure 1.1. The study of leukocyte migration is therefore complex and requires the development of platforms able to address specific questions regarding how different cells integrate external stimuli, such as chemokine gradients, spatial organization of surrounding and interactions with other cells, with the internal functional state of the cell. After a theoretical introduction to leukocyte migration, some of the tools currently employed in this field of study will be presented and compared to relatively new microtechnological developments. Finally, the microfabricated device designed and produce by our group will be presented. The device is major object of investigation during this work. The device is a new tool for studying cell migration during chemotaxis with the purpose to mirrow and resolve the complex *in vivo*.

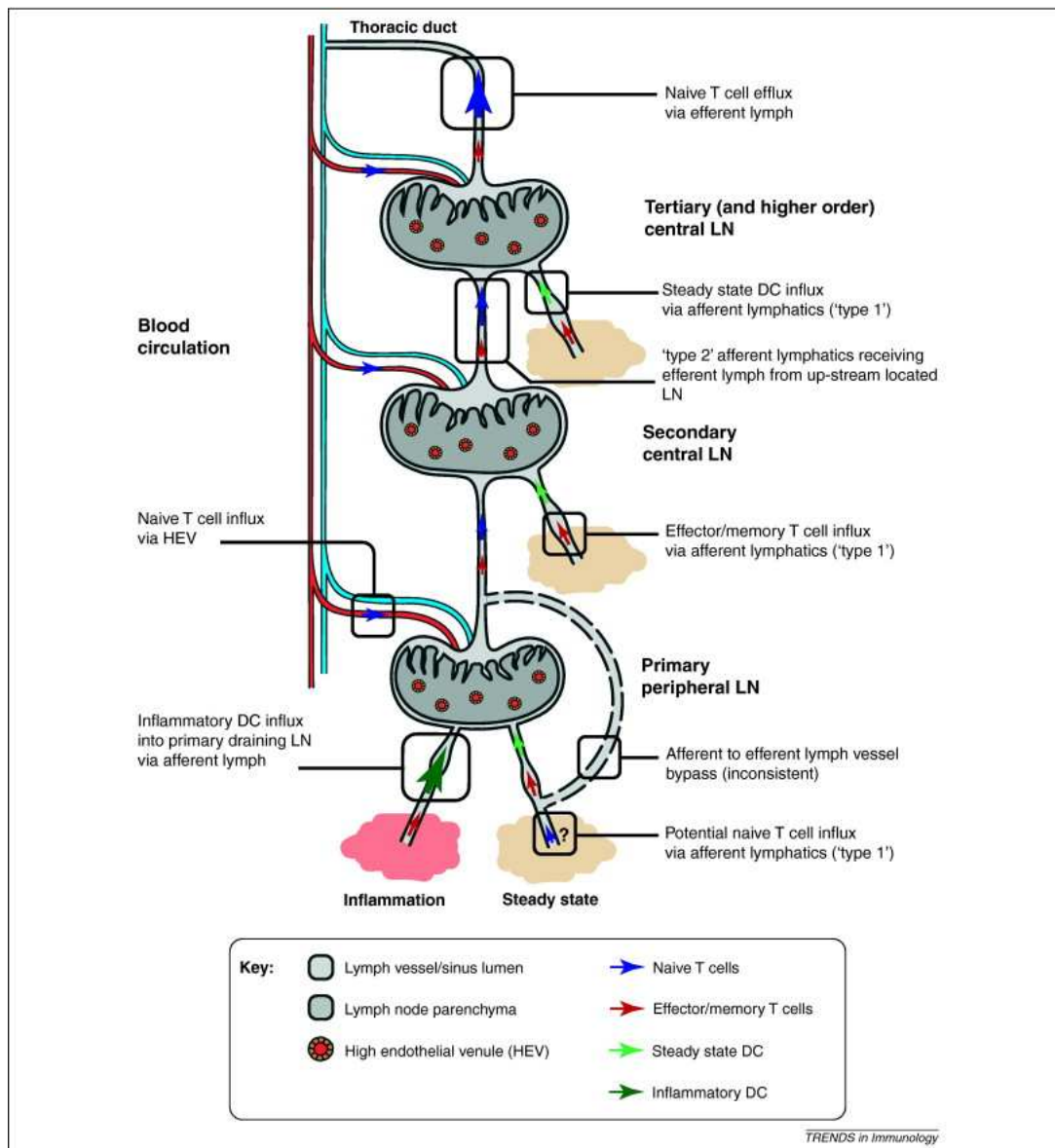


Figure 1.1:
Complex routes involved in dendritic and T cells homing and circulation within the human body: This figure summarizes the known migratory routes of T and dendritic cells in steady state and during inflammation. Immunity is a dynamic system and leukocytes circulate continuously along cell-specific routes during homeostatic and inflammatory migration. Adapted from⁵

Chapter 2

Background theory

2.1 Leukocyte migration during homeostasis and inflammation

Leukocyte localization is regulated in a spatio-temporal manner according to cell types and functions. Effector cells of the innate response are always available and are quickly recruited from interstitial tissues and blood circulation upon inflammation to relevant sites. On the other hand, T and B lymphocytes, the major cells eliciting acquired immune responses, become effective in an antigen-specific manner. The first antigen recognition happens in specialized secondary lymphoid tissues such as lymph nodes (LNs) and spleen⁶. Effector leukocytes can be found already inside tissues or being recruited through transmigration across venular walls in nearby blood vessels. Here, endothelial cells become activated through histamine and pro-inflammatory cytokines released by interstitial mast-cells and other sentinel cells. Endothelial cell activation leads to augmented adhesiveness of the venular walls and effector leukocytes start to crawl on it looking for exit signals such as chemokines that, together with endothelial cells and pericytes, guide leukocyte transmigration to the interstitium⁷. Leukocyte extravasation from blood and lymphatic vessels and migration within tissue interstitium are not only mere mechanical processes. They are instead regulated by environmental signals and interactions with other cell types, enabling leukocytes to acquire efficient migratory profiles necessary for quick localization to the inflammation sites and elicit the proper immune response⁸.

2.1.1 Chemotaxis and leukocyte migration:

Chemokines are chemotactic cytokines that, together with other bioactive molecules such as bioactive lipids and hormones, direct cell activation, migration and recruitment^{9,10}. Up to now more than 50 different chemokines have been discovered and they are divided into four families as illustrated in Figure 2.1a. Chemokines bind to seven transmembrane receptors (7TM) coupled to $(\alpha\beta\gamma)$ heterotrimeric G proteins called G protein coupled receptor (GPCR). Signaling through GPCRs cause morphological changes priming leukocytes to efficient migration. When a soluble gradient of external ligands is present, cells become polarized along ligand gradation and migration is directed towards higher concentration of attractant molecules in a process termed chemotaxis. Cells can also be guided by a surface-bound gradient of chemokines or extra cellular matrix (ECM) and cellular adhesion sites, this latter process is termed haptotaxis. Intracellular signaling pathways triggered by chemokine and adhesion receptors lead to morphological changes and different migratory modes are adapted by the migrating cells according to the surrounding and the nature of the stimulus, as depicted in Figure 2.1b.

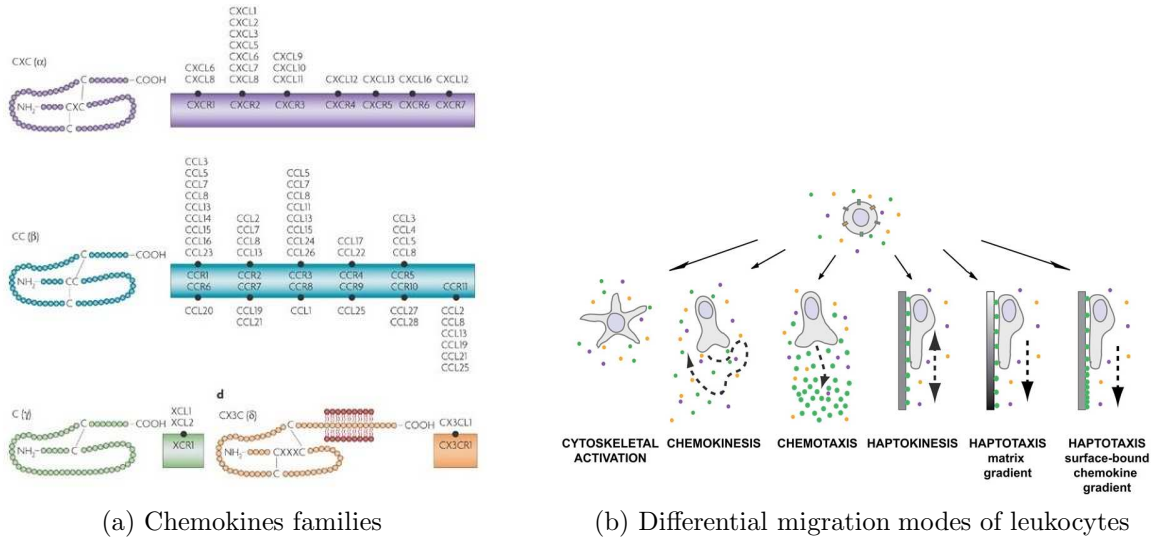


Figure 2.1:

Chemokines and leukocyte chemotaxis: a) Chemokine molecules and their receptor are divided into four families (CXC, CC, C, and CX3C) according to the position of cystein residues inside the ligands. Adapted from¹¹ b) Leukocytes sense a myriad of environmental cues, both soluble and surface-bound, determining (1) Morphological changes without cell movement, (2)(3) non-directed motility (chemokinesis) or directed motility along a gradient of soluble chemoattractant molecules (chemotaxis), (4)(5)(6) non-directed motility (haptokinesis) or directed motility along extracellular matrix gradient or along surface-bound ligands (haptotaxis). Adapted from¹²

2.1.2 Recruitment of dendritic cells and T-cells to lymph nodes and peripheral tissues during homeostasis and immune responses:

Signaling through G protein-coupled receptors (GPCRs) and other migratory receptors (MRs), such as selectins and integrins, determine immune cell localization in homeostatic migratory routes and cell recruitment during immune responses. Moreover, immune cells themselves express chemokines and other chemoattractant molecules in order to coordinate and interact with other cells. For example, in dendritic cells (DCs) chemokine receptors and secretion of chemotactic signals are rigorously time-regulated. Upon detection of pathogens and stress signals via Toll-like receptors (TLRs) and other pattern-recognition receptors (PRRs), they release and express inflammatory cytokines and chemotactic cytokines, such as $\text{TNF-}\alpha$, CCL3 and CCL5, activating endothelial cells and recruiting other effector leukocytes such as granulocytes and macrophages that will contribute to innate immune responses¹³. Immature DCs and their progenitors do also express receptors for inflammatory chemokines like CCR1, CCR2, CCR6 and CCR5. The expression of these receptors on cell surface is lost following maturation while expression of CCR7 and CXCR4 is upregulated^{14,15}. CCR7 binds to CCL21 expressed by endothelial cells of lymphatic vessels and guide maturing DCs through the gaps of the discontinuous basal membrane of the vessels. The contribution of other migration receptor (MRs) such as selectins and integrins is still unclear, also because DC cell migration into lymphatics has been found not to be dependent upon integrin-mediated adhesion¹⁶. It is thought that CCR7 independent signals rather contribute moderately to DCs entering in lymphatics⁵. In-

side the small lymphatics, DCs sense lymph flow and crawl along the endothelium until once they reach collecting lymphatics that through rythmical contractions pump the cells inside the subcapsular sinus⁵. During the travel DCs progressively downregulate the expression of most of the pro-inflammatory chemokines, but once arrived in secondary lymphoid organs the expression of chemokines attracting T lymphocytes (CCL17, CCL18, CCL19, CCL22) is upregulated and they can then present antigens to naïve T-cells in order to initiate adaptive immune responses^{14,17}. In secondary lymphoid organs DCs localized to T-cell zone haptotactically and chemotactically guided by CCR7 ligands (CCL21 and CCL19) that are produced by fibroblast reticular cells (FRCs), the stromal cells organizing T cell zones,⁵. Indeed the situation is much more complex *in vivo*, since DCs are a heterogeneous population in humans and mice, and are furthermore divided into multiple subsets according to their surface markers and functions¹⁸. Different subsets of DCs express distinct sets of chemokine receptors and travel across diverse anatomical sites¹⁵.

T cells migratory routes can be distinguished between naïve cells trafficking, and homing of effector cells to peripheral tissues after antigen recognition and differentiation. Naïve lymphocytes continuously recirculate between blood and lymph. Naïve T cells enter LNs from high endothelial venules (HEVs). The major MRs regulating naïve T lymphocytes extravasation are L-selectin(CD62L), CCR7 and LFA whose ligands(PNAd, CCL21 and ICAM-1) are all presented on HEV surface⁴. Once inside they are guided by CCR7 ligands produced by FRCs, localize in T-cell zones where they receive survival factors (IL-7) regulating their homeostasis, scan DCs and are eventually engaged in antigen-recognition reactions^{19,5}. After antigen recognition and priming in diverse, effector T cells express a variety of MRs that direct them to different locations of peripheral tissues, as depicted in Figure 2.2. Activated lymphocytes are first released into the circulation and then transmigrate to sites of inflammation by activated endothelium.

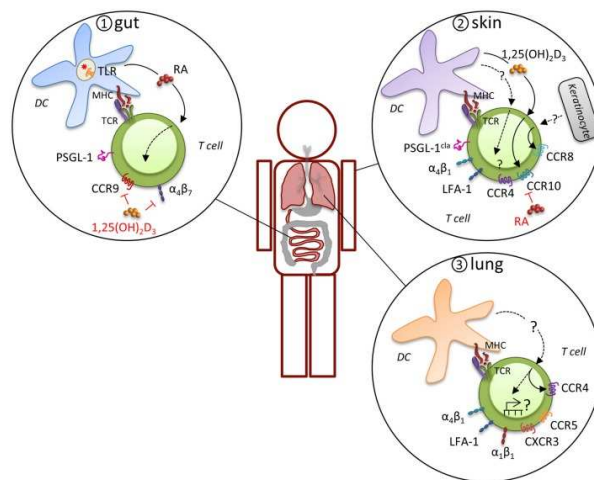


Figure 2.2:

Localization of immune cells depend on their chemokine and migratory receptors: Localization of immune cells is strictly dependent upon the combinatorial expression of receptors mediating their interactions with the environment. Diverse DCs subsets instruct T lymphocytes with tissue-specific migratory receptors that will guide effector cells to the correct region(for example: skin, gut or lung). Adapted from⁴

2.1.3 Leukocyte migration in different environments

Recruitment of circulating leukocytes through the inflamed venular walls is the most characterized process involving immune cell migration. It is divided into two steps: the leukocyte-adhesion cascade and the transendothelial migration (TEM) through the venular wall. First leukocytes adhere to the activated vascular surfaces, assume a flattened morphology and crawl (rolling) looking for chemotactic exit cues. Arrest occurs upon detection of a strong chemoattractant signal activating major lymphocyte integrins such as LFA-1 and Mac-1. Then leukocytes are able to transmigrate through the junctions of adjacent cells (paracellular TEM) or across endothelial cell membrane (transcellular TEM)⁷. Cytoskeletal rearrangement, chemokine-stimulated integrin-dependent adhesion and polarity induction are some of the chemokine-induced effects needed during directional motility on, and through, vascular walls^{8,7}. Once inside the tissue interstitium, leukocytes present a different morphology and are then able to migrate through a three dimensional (3D) spaces filled with extra cellular matrix (ECM), like in tissue interstitium, or cells, like in secondary lymphoid organs⁸. Establishment of front-back polarity occurs through cytoskeletal rearrangements and activation of polarity complexes. Generally speaking, the relocation of key regulators of cytoskeleton such as the members of the Rho family of small GTPases (Rac isoforms, Cdc42 and RhoA) organize a protrusive leading edge and a contracting rear, termed uropod²⁰. Rho GTPases were also found to interact with polarity complexes such as the partitioning defecting (Par) complex in T-cells²¹.

The morphology of migrating leukocytes in two-dimensional (2D) and three-dimensional (3D) environments is defined as ameboid, meaning that cells continuously change shape protruding and retracting extensions during translocation²². Ameboid migration relies on three major forces in order to generate movement: adhesion to the substrate, actomyosin contraction at cell rear and expansion of an actin network at cell front that creates diverse protrusive structures (lamellopodia, filipodia and pseudopodia)²². In order to promote motion, these forces need to be coupled and transmitted to the surrounding space. Also, regarding leukocyte, coupling mechanisms can be diverse and largely depend on environmental features. Dendritic cells are indeed able to migrate in a non-adhesive 3D substrate. When the integrin-mediated retrograde resistance for the actin flow at the leading edge is hindered, DCs change the actin polymerization rate at the leading edge until a new equilibrium with the constant membrane tension is reached²³. As depicted in Figure 2.3, leukocytes possess multiple migratory modalities, and are able to switch migration modes also according to attractant molecules distribution and/or genetic/pharmacological interferences with genes and proteins involved in cell migration in a cell-type-specific fashion¹². For each leukocyte, striking differences emerge when migration on 2D surfaces is compared to migration in 3D environments. Integrin-independent 3D migration has been demonstrated *in vivo* for activated interstitial DCs migrating towards lymphatic vessels¹⁶.

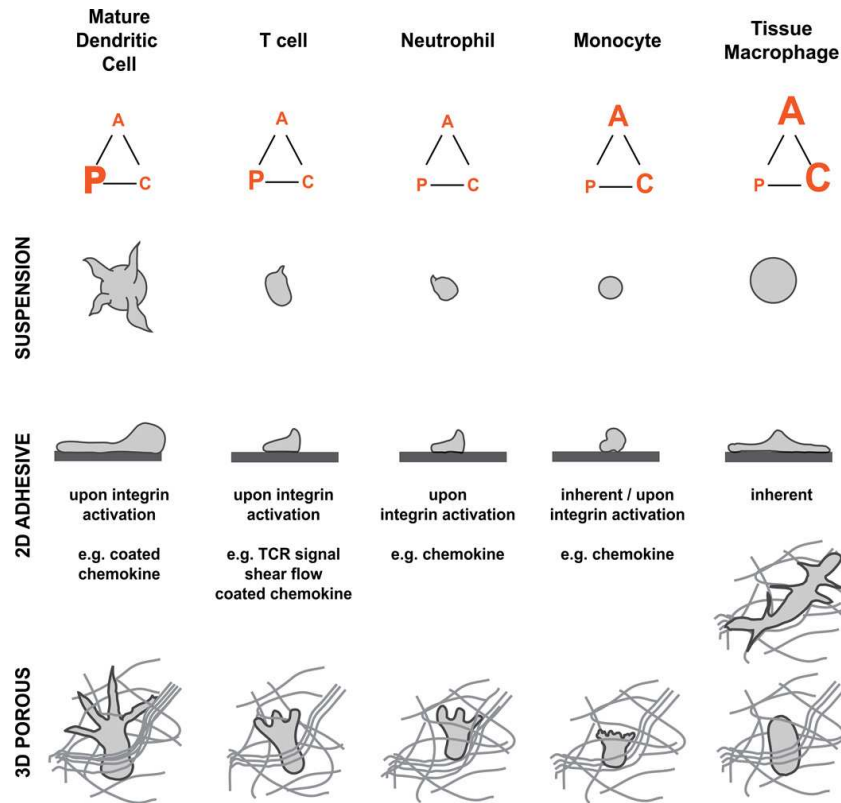


Figure 2.3:

Phenotypes of amoeboid migration in immune cells: The balance between different forces (A= adhesion, P= protrusion, C= contraction) plus environmental cues (e.g. substrate conformation) regulate leukocyte migration and morphology in a cell specific manner. Adapted from²²

2.2 Studying leukocyte migration

Leukocytes possess a big variety of migratory modes regulated by numerous mechanisms, both molecular and mechanical, as it was pointed out in section 2.1. The study of leukocyte migration is therefore complex and requires the development of platforms able to address specific questions regarding how different cells integrate external stimuli, such as chemokine gradients, spatial organization of surrounding and interactions with other cells, with the internal functional state of the cell. Many different assays have been developed during years and new approaches are continuously proposed. Studying cell migration can either aim to determine a general quantitative response to a chemotactic stimulus or to resolve quantitative and qualitative questions at single- and intra-cell level. Considering the huge variety of assays to choose from, specific questions need to be addressed with proper experimental tools taking into account the advantages and the disadvantages of each of them. In this section, some assays for studying cell migration during chemotaxis will be presented and compared.

2.2.1 Classical biological macro-scale assays

Since the 1960s, several *in vitro* chemotactic assays have been employed in the study of leukocyte migration. Among macro-scale assays, some of the most common are the Boyden cham-

ber, capillary chambers (Zigmond, Dunn and Insall), the under agarose gel assay and the micropipette assays²⁴. Some the advantages and withdrawals of these assays are recapitulated in Figure 2.4.

Boyden Chamber or Transwell assay²⁵ is one of the most established macro-assay for evaluating chemotaxis of leukocytes and other cell types. Two chambers filled of medium are separated by a porous membrane, where pore size is determined by the size of the analyzed cells. Cells are seeded on the upper chamber and can migrate through the porous membrane to the lower chamber where a chemotactic or repellent stimulus is present inside medium. Migrated cells on the lower part of the membrane are then fixed while cells in the upper part must be carefully removed. Quantification can then be done after staining transmigrated cells on the membrane, or by using a fluorescent reader after labeled cells use in the test are removed from the membrane²⁶. Among the advantages of the Transwell assay, there is its quick and non-demanding technology that can be easily employed in high throughout analyses. In any case, the test results often not reproducible, especially due to the step of manual cell removal and staining, that can compromise quantitative aspects of the assay²⁶. A common disadvantage for chemotaxis macro-assays is that migration is limited on a 2D space and these assays are cannot be used to evaluate migration in 3D environments. In a 2D ambient most cells migrate by using protrusive and unconstrained lamellopodia, they assume apical-basal polarity, since the adhesion with the substrate is restricted to an x-y plane, and can spread freely along the surface. Upon comparison with 3D environment strictly differences in migratory dynamics and emerge and highlight why the study of cell migration is moving towards three-dimensional environments²⁷.

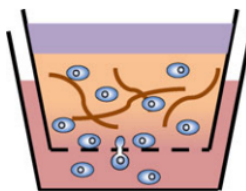
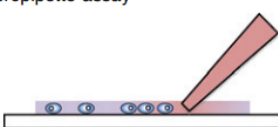
	Advantages	Limitations
<p>Boyden chamber</p> 	<ul style="list-style-type: none"> • Multiwell plate format that allows for a large number of screenings • Convenient and easy to use • System can be modified to introduce fluid flows • Cells can be embedded in a 3D matrix, which is a better mimic of <i>in vivo</i> microenvironments 	<ul style="list-style-type: none"> • Population-based • Gradients are not well defined • Does not distinguish chemotaxis from chemokinesis • Not compatible with live cell imaging • Unknown membrane pore effect
<p>Zigmond or Dunn chamber</p> 	<ul style="list-style-type: none"> • Allows for video imaging • A nearly linear steady state gradient 	<ul style="list-style-type: none"> • Poor reproducibility • 2D studies only • Short term experiments only • Low throughput
<p>Under agarose gel assay</p> 	<ul style="list-style-type: none"> • Allows for video imaging • Easy to use 	<ul style="list-style-type: none"> • Poor reproducibility • 2D studies only • Low throughput
<p>Micropipette assay</p> 	<ul style="list-style-type: none"> • Compatible with optical microscope for the case of 2D studies • 3D studies possible 	<ul style="list-style-type: none"> • Not a steady state gradient • Short-term experiments

Figure 2.4: Advantages and limitations of common assays for studying chemotaxis *in vitro*: Adapted from²⁴

2.2.2 Gel assays

In many of the biological processes explained in the previous section, cell migration occurs either within the organized and molecularly complex extra-cellular matrix (ECM) or in cell-filled environments such as lymph node cortex, where migratory cues guide migratory cells by 3D interactions with their transmembrane adhesion proteins and receptors. In order to confine migrating cells in such a 3D environment biomaterial such as cell-derived matrices (Matrigel) and fibrillar collagen gels. Even though cell-derived matrices highly resemble *in vivo* microenvironment, providing growth factors and physiological linear elasticity of fibers²⁸, its molecular complexity is a disadvantage for the standardization of migrational assays. Collagen gels have a more defined composition and allow squeezing and nonproteolytic migration of leukocytes²⁹, some parameters such as pore sizes and physical properties of the polymer remain uncertain¹². Moreover their 3D features hinder the access to common microscopic techniques in the event that migration of cells want to be directly visualized and require the use of sophisticated tools to image inside the gel.

2.2.3 Intravital microscopy

In order to observe leukocyte dynamics *in situ* one of the first techniques utilized was organ explant systems, where collected secondary lymphoid organs are placed and heated with oxygenated media. Excised organs anyway lack perfusion thorough vascularization of blood and lymphatics and therefore important dynamics regulated by biomechanical fluid flows cannot be studied in such a preparation³⁰. Therefore modern approaches for *in situ* visualization of immune responses involve the use of single-photon(1P-IVM) or two-photon (2P-IVM) microscope for intravital microscopy. Those approaches are extremely advance and permit to observe cellular dynamics on organs still linked to the animals, preserving most of the physiological parameters of the tissues^{31,30}.

In 2P-IVM studies the non-optical effect of the second harmonic generation(SHG) can resolve structural components of the matrix, such as collagen fibers³¹. Structural characteristics or the surrounding can therefore be coupled to migratory behaviours of cells in order to investigate reciprocal interactions and influences. However the structure visualized is complex and resolving migratory routes according to the structural architecture of the surrounding require considerable technical efforts, and results are often non-univocal, as shown in Figure 2.5. Still distance tissue imaging and visualization of regions may be disturbed by involontarian movements like respiration. Plus there is poor control over the oxygen levels and administrated substances in a particular areas¹². All those fact may affect the reproducibility of observations and therefore a considerable number of animals may be required, increasing the costs and the time of experiments. Access and manipulation of specific cell population such as specific subsets of dendritic cells, most employing *in vitro* generated dendritic cells injected administrated to the animals, or technical demanding techniques to identify subpopulations inside tissues³².

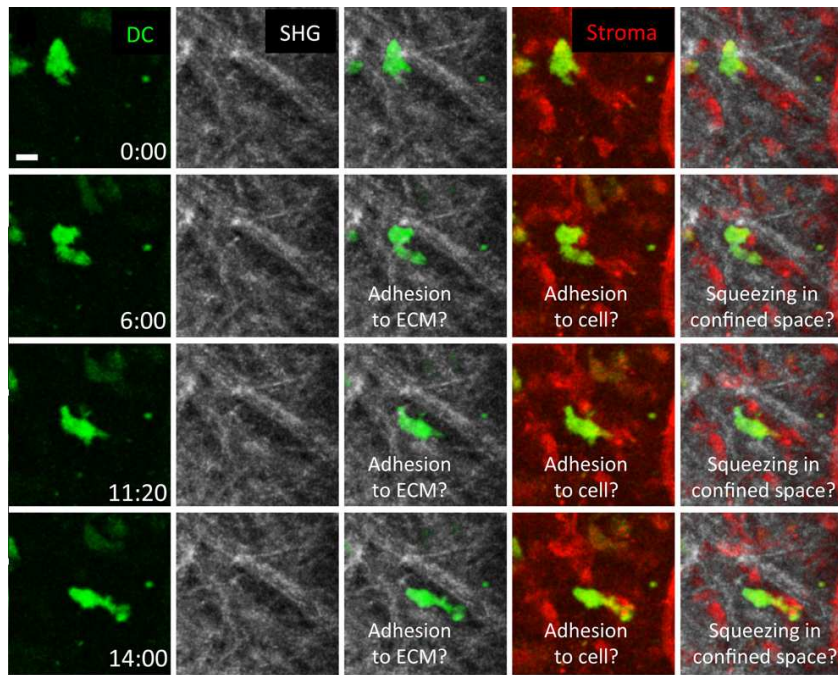


Figure 2.5:

Structural Limits of intravital microscopy: Migration of a yellow fluorescent protein (YFP)-expressing DC (green) on the ear skin of a transgenic $DsRed^{+/+}$ $CD11c-YFP^{+/-}$ B6.Albino. 2P-IVM is able to resolve collagen fibers inside the tissues (SHG) and also DsRed expressing stromal cells (red) can be visualized. It is difficult though to resolve all the interactions between moving cells and the environment. Adapted from¹²

2.2.4 Studying cell chemotaxis with microfluidics and confined environments

One of the newest advancements for the field of leukocyte chemotaxis is the employment of microfabrication technology for the realization of biocompatible microfluidic devices. Recent advancements in microfabrication techniques using biocompatible materials have let researchers and engineers to collaborate for the realization of custom-made devices. Microtechnological chemotaxis assays rely on two diverse features that can either be exploited alone or combined in chemotaxis studies. First fluid microdynamics can be exploited inside channels in order to generate controlled chemotactic gradients across different compartments, and directed cell migration by soluble ligands distribution. Gradients can be generated by pump-driven convective flows or passive molecular diffusion²⁴. Second cells can be forced to stay and migrate in the geometrically constrained space of microchannel systems. Migration inside a channel is 1D directed, but if the channel has a diameter comparable with cell dimensions, migration acquires a 3D component due to the contact between cells and channel walls³³. Microchannels can therefore be used to mimic *in vivo* architectures and environments encountered by cells and study migration in geometrical defined spaces.

A common advantage for microfluidics and microchannels assay is that, being micro-assays, less cells are required for analysis, and they could therefore fit the investigation of rare cell populations that are difficult to isolate for macro-assays and to visualize *in vivo*. Moreover since it is a semi-3D space they can be adapted to any type of microscopy are easy to utilize in life-imaging and cell-tracking techniques^{33,34}. Anyway the technical efforts required in order

to establish those system are variable, depending on the complexity of the system (a pump-coupled system is more demanding than a diffusion-based design) and demand ample technical efforts and collaboration from many scientific fields. Some examples of microfluidic applications are depicted in Figure 2.6.

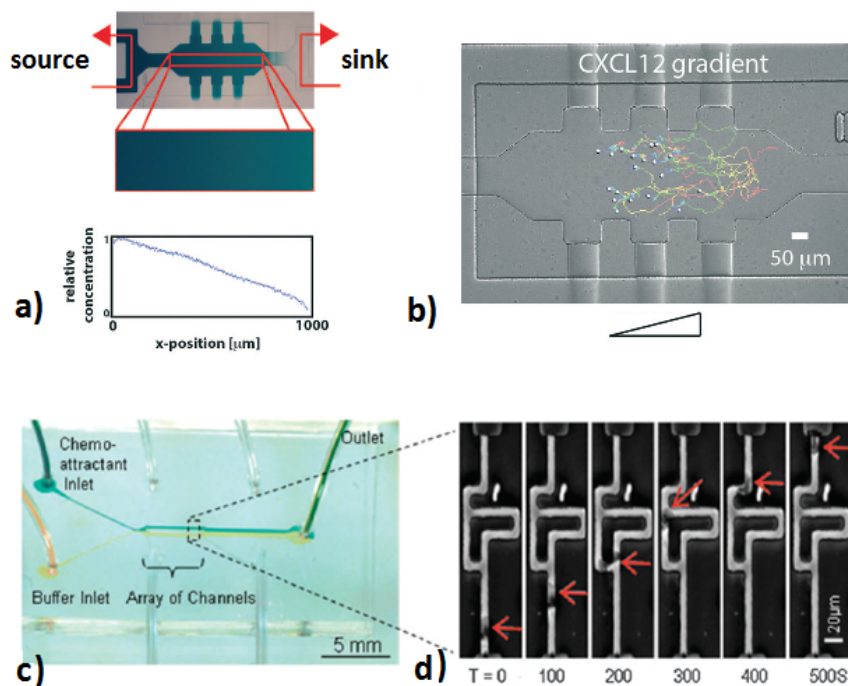


Figure 2.6:

Examples of microfluidics and microchannels application for the study of leukocyte chemotaxis:

a)b) A microfluidic device for studying cell migration in a chemotactically controlled chamber. A diffusion-based chemotactic gradient is created inside the chamber by flushing different chemokines in the source and the sink channels (a); Cells are seeded from the parallel and migration can be visualized and tracked in real-time(b). Migrated cells can be recollect at different positions and be further be analyzed.

Adapted from³⁴. c)d) A microfluidic device designed for the evaluation of cell decision-making during migration. The microfluidic device creates a stable chemoattractant gradient across the microchannels between the green and the yellow line(c); fluorescein, green, is used to check the stability of the system. Figure freely adapted from¹³ d) A neutrophil cell, indicated by the red arrows, is moving through the asymmetrical maze towards the greater concentration of the chemoattractant, the cell chooses the shortest path in the

microchannels. Adapted from³⁵

2.3 Device description and microfabrication techniques

In our group we aim to build functional tissue units to understand the complexity of cellular self organization in the immune system through soluble, surface-bound and cell-associated molecular cues. Among our projects, there is the design of a practical chip device in order to study in real-time cell migration in confined space and at a single-cell level towards immune reactions. The device could potentially be used to study chemotactic cell recruitment to relevant immunological sites such as infections in tissue interstitium and lymph node zones. We

therefore chose to investigate how such a device can be employed in the study migration towards infection-like reactions and lymph node areas. Our approach would rather be systemic using cell reactions, instead of single chemoattractant molecules, in order to generate chemoattractant gradients. We are attempting in this way to mirror the physiology of migration within living organisms as described in the previous section, 2.1.

Generally speaking attractor cells and bacterial mixtures are isolated in a compartment of the device, while migrating cells are loaded in a different compartment. The two compartments are linked by a network-like structure of microchannels that allows attractive and activating molecules, i.e. chemokines and cytokines, to freely flow from the attractor compartment, possibly creating a increasing gradient towards it. Attractor cells and eventually bacteria are isolated in attractor side by a narrow filter-like microchannel structure placed before the network, while migrating cells are the only ones able to enter the network. In the device it is always present a internal control compartment designed as the attractor compartment. In this work of thesis a fourth generation design of the device has been employed in the experiments. The fourth generation architecture was designed based on the results obtained from a previous model, the third generation, that was used for testing chemotaxis and migration in the Master thesis of Ryan Hannam, spring 2014, "*Monitoring Chemotaxis Towards Immune Reactions in a Microcompartmentalised Device: Real-time is King*". The results obtained with the third generation design will be summarized in section 2.3.2, and then the design of the fourth generation will be illustrated.

2.3.1 Microfabrication and soft lithography

The micro-scaled features of the device are obtained using a technique called soft lithography. A mixture of an elastomer, polydimethylsiloxane or PDMS, and a curing agent is poured on on a reusable patterned silicon wafer referred as master or mould. The photomask employed in this work was designed by by doctor Nimi Gopalakrishnan. The silicon master mould employed in this work was created by optical lithography and physical and chemical etching by doct. Jonas M. Ribe, see Figure2.7a,b. The casted polymer is cured into a solid gel by heating. The micropatterned PDMS can be bound by physical activation, such as oxygen plasma and corona bonding, on a glass coverslip, see Figure2.7c. The device obtained in this manner is transparent and modern microscope techniques can be employed in order to monitor the cells within it.

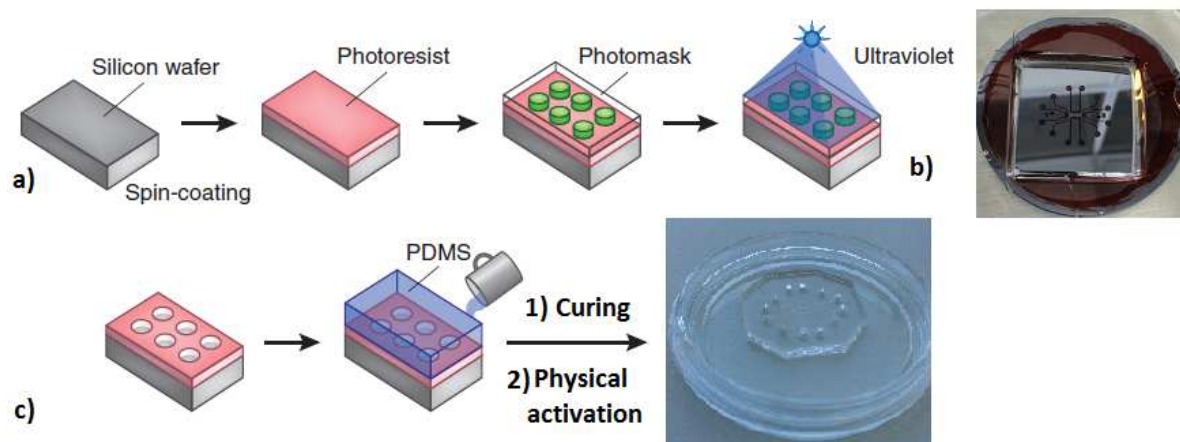


Figure 2.7:

Soft lithography technique for the fabrication of microfluidics devices in PDMS: a)

Photolithography: a photomask is first designed with the features of the chip such as channels, network and cell compartments. A silicon wafer is spin coated with a SU-8 photoresist. When UV light is sent through the mask, the light crosslinks the resist according to the patterned design. The uncrosslinked resist can then be removed and the silicon wafer is further patterned by chemical and physical etching in order to obtain the desired feature profile (b). Then PDMS elastomer can be casted and cured in order to obtain a patterned device that is bonded onto glass by physical methods. Adapted from³⁶

PDMS is composed by repeated units of $-O - Si(CH_3)_2-$, surface application of oxygen plasma and corona discharges introduce hydrophilic silanol ($-OH$) groups taking the place of hydrophobic methyl groups ($-CH_3$)^{37,38}. The surface can then be bonded to other activated surfaces such as plastic, glass and PDMS^{39,38}. The acquired hydrophilicity is beneficial for biological application, but PDMS is likely to recover hydrophobicity in a second time^{39,40}. Hydrophilicity can be preserve by exposing PDMS to water and organic solvents, but PDMS is still likely to regain hydrophobic properties later³⁹. A possible cause for the regain of hydrophobicity after oxygen plasma treatment is due to the trafficking of low molecular weight PDMS oligomers that remain uncrosslinked during the curing process, and/or the replacement of the surface polar hydrophilic groups by unpolar methyl groups from the bulk material⁴⁰. A possible solution in order to hinder hydrophobic recovery in oxygen plasma activated surfaces could be thermal aging achieved with an extended curing time that should therefore significantly reduce the number of low molecular weight PDMS chains within the bulk material⁴¹. Alternatively, activated PDMS surface can be functionalized and coated with protein such as collagen and fibronectin that increase the biocompatibility of the environment for cell cultures⁴².

2.3.2 Third and fourth generation device designs

Four generations of the device have been designed by the group. The third generation have been described in details in the Master thesis of Ryan Hannam, spring 2014, "*Monitoring Chemotaxis Towards Immune Reactions in a Microcompartmentalised Device: Real-time is King*" and in the article of Gopalakrishnan et al.⁴³. The microfluidic device is in both case constituted by flow-free co-culture compartments linked by mazed-structured networks of microchannels where confined cell migration can take part.

Third generation device The third generation design is illustrated in Figure 2.8.

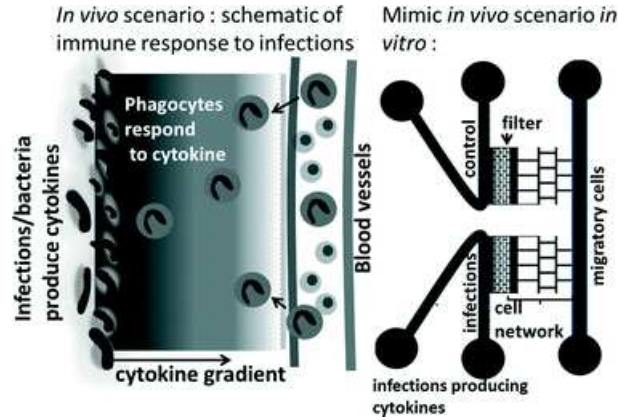


Figure 2.8: **Third generation device design:** A channel loaded with migratory cells face two $500\ \mu\text{M}$ long network structures of $6\ \mu\text{M} \times 6\ \mu\text{M}$ channels. One network is connected to an attractor compartment where infections and chemoattractant reactions reaction can be established, while the other network can be used as intern control. A filter $2\ \mu\text{M}$ high allows for bacterial compartmentalization in the attractor compartment. Adapted from⁴³

Rapidly moving cells as MF2.2D9 cells, an I-A^b-peptide restricted T-cell hybridoma cell line, seemed not to clearly migrate preferentially towards the attractor compartment, where different immune reactions, such as antigen-presentation reaction by immunogenic peptide loaded macrophages, were tested. Sometimes MF2.2D9 seemed instead to preferentially migrate towards the control side. This event was hypothetically addressed to the facts that gradients due to the attracting reactions were not generating as it was thought, and also to the eventual pre-activation of migrating cells during cell preparation procedure that would therefore hint the respond to an activating gradient of chemokines produced by immunological reactions. Another cause to be mentioned is the difficulty of loading the attractor compartment with a consistent amount of attracting cells in such a design. It was therefore suggested to increase the dimensions of the attractor compartment and to adopt a design that facilitates such a loading. Due to the high motility of MF2.D9 it was also suggested that cells may enter the device before being stimulated by gradients that, according to the obtained results, seemed to require more hours to be established. The design resulted to be well suited for in real-time observation and the investigation of migratory behavior at a single-cell level. Decision making, speed and memory of migrating cells could be evaluated in such a maze-structured network. A chemotactic response was observed in later experiments, when bone marrow-derived dendritic cells were used in a series of chemotaxis experiments towards antigen-presentation reactions, CCL19 and *Mycobacterium avium* infections. In all experiments a significant migration in the network facing the attractor compartment was observed respect to the control network,⁴³. Another withdrawal of third generation devices that needed to be solved was the uneven partition of cells in the migratory compartment, that can potentially influence chemotaxis results, especially if highly motile cells are used in the device. All those considerations were taken into account during the design of the fourth generation, that aimed to correct the lacks of the third one.

Fourth generation design The fourth generation mask design was elaborated by Nimi Gopalakrishnan with the collaboration of the whole group and two different types of silicon masters were produced from the design, the properties of the two masters are described in chapter 3, section 3.1.1. The general common features of the fourth generation design are depicted in Figure 2.9. Compared to third generation devices the fourth generation design is characterized by a single mazed-structured network surrounded by cell chamber compartments. A sink compartment is introduced in the design opposite to the entrance from the migratory cell compartment in the network, while equally attractor/control compartments are at the side of the network connected by linear channels. Attractor/control compartments are served by lateral channels designed to administrate in-channel bioactive molecules and bacteria.

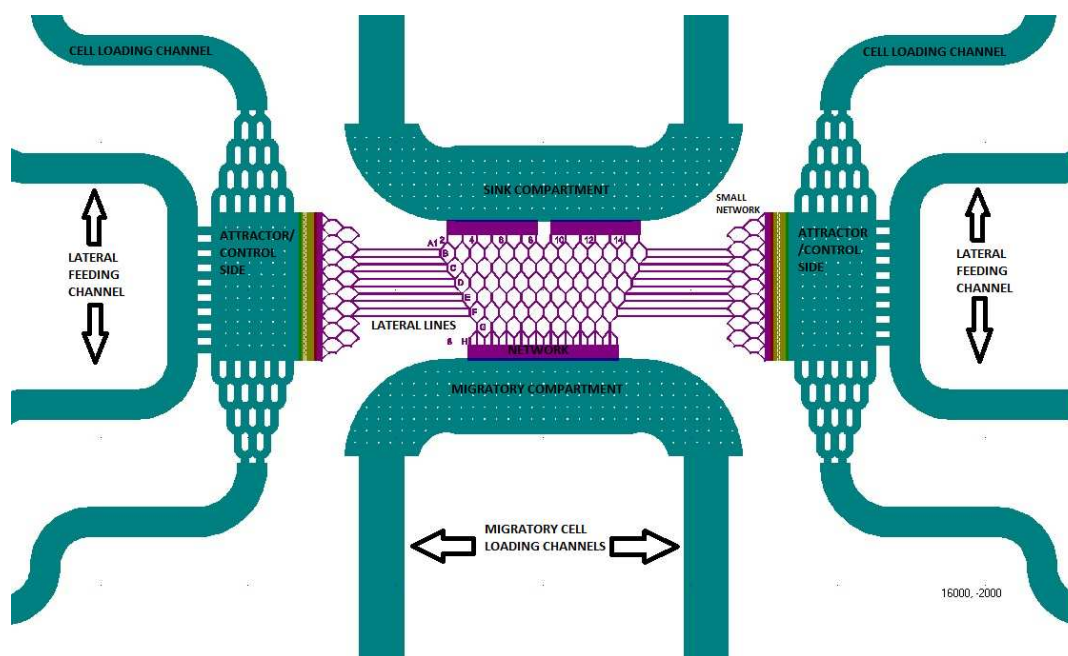


Figure 2.9: **Fourth generation design:** The fourth generation design is characterized by a sole network in front of a migratory compartment. On the other side of the network there is a sink compartment specular to the migratory compartment. From the major network lateral straight lines end to a smaller network in front of attractor/control compartments. The attractor/control compartment are connected with cell loading channels through a branched structure and with a lateral feeding channel

2.3.3 Objectives

The aim of this thesis was to assess the structural progresses of our newly designed fourth generation device. Specifically, I have explored new potential applications, such as in-channel administration of bioactive molecules and bacteria. In addition to this, I have evaluated the potentials of such devices in the study of immune cell chemotaxis towards relevant immunological reactions. In order to achieve these objectives, it has been necessary to perform some microfabrication steps, i.e. the bonding of PDMS onto glass, in the biology laboratory, for not to be strictly dependent on the Nanolab during the microfabrication operations of the device. The steps necessary to be done have also been illustrate in this thesis.

Chapter 3

Methods and solutions

3.1 Device Fabrication and Operation Procedures

Our group aims to create an end-user device that can be assembled and used in a simple and inexpensive manner in biology laboratories. Therefore we attempted to transfer the microfabrication steps following PDMS curing down to the biology laboratory. The new procedures tested during this work will be described in this section after elucidating some technical features of the fourth generation device.

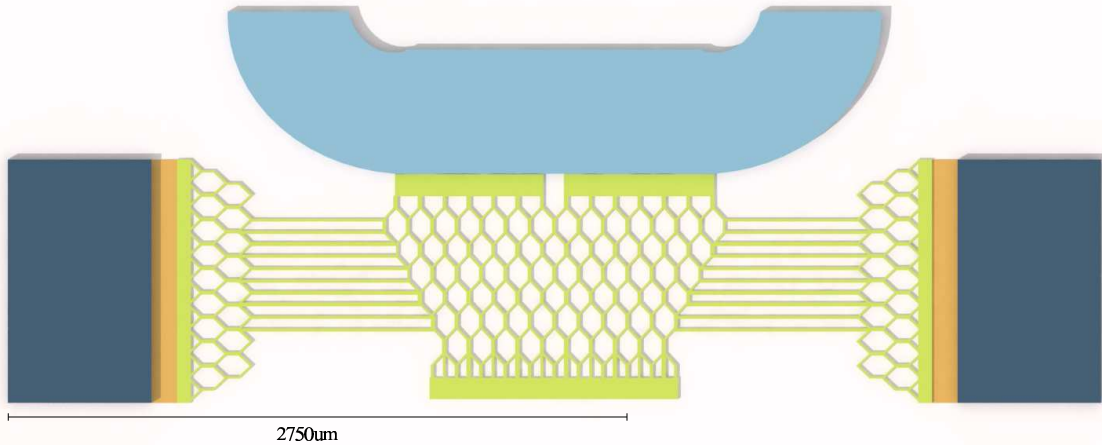
3.1.1 Device features and fabrication steps

Fourth generation master types: Two silicon masters differing in the height of the loading channels and in the width of the network channel were prepared using the fourth generation mask.

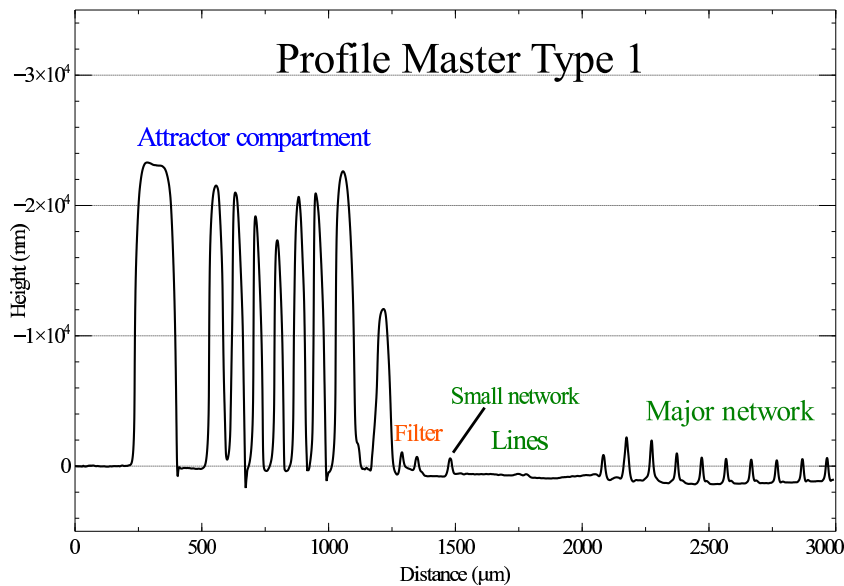
Master type	Loading channels (height)	Network channels (width)
Type 1	28 μm	8 μm
Type 2	9 μm	6 μm

Table 3.1:
Types of silicon master utilized in this thesis

Type 1 devices the most used during this work and a profile was taken at Nanolab with a contact stylus profilometer (*Dektak 150*), as depicted in Figure 3.1



(a) Profile



(b) Profile of Type 1 master

Figure 3.1:

Structural characteristics of Type 1 devices, fourth generation: (a) The highlighted line was profiled at Nanolab. (b) Profile of fourth generation device: Attractor compartment with pillars, filter and small network, mines (the machine hit the space between the lines), major network

PDMS casting, curing and washing steps: In order to produce PDMS devices the elastomer (*Sylgard 184 silicone elastomer, Dow Corning*) is first mixed with a cross-linking agent (*Sylgard 184 curing agent, Dow Corning*) at a ratio of 10:1. The mix is then distributed on the silicon mould and degassed in a vacuum chamber in order to eliminate air bubbles that would disturb the pattern formation within PDMS. Then the polymer is cured into a solid gel for 1h at 70° degrees Celsius or 40 min at 80° C.

After PDMS curing, the device is peeled from the master, cut and all the inlets and outlets are punched as illustrated in figure. These steps and oxygen plasma bonding were performed in the clean room of Nanolab at NTNU.

In order to eliminate organic residues the polymer is washed with acetone, ethanol and isopropanol. The PDMS is now ready to be bond to a cover glass (Menzel, Gläser, Ø 50/47 mm x 150 μm (No1.5), *Thermo Scientific*) previously washed with acetone, ethanol and isopropanol. Bonding is achieved by oxygen Plasma in Nanolab: the device is place in the oven (80deg) 5 min before plasma bonding, then the glass and PDMS are inserted in Plasma Cleaner Femto (*Diener Electronics*) and after vacuum creation inside the machine, oxygen plasma is applied with 50% O₂-gas and 50 W power for 12 sec, the PDMS is immediately placed on the glass, and gently pressed down. Then the device is place again in the oven for 5-10 min. Then the device can be filled with sterile water, maintaining in this way sterilization obtain through oxygen plasma application.

Alternatively, in order to move microfabrication steps down to the biology laboratory, Corona (BD-20AC, *Electro-Technic Products*) bonding was performed outside the clean room of Nanolab, on a unsterile bench in the biology laboratorium and also this process needed to be optimized during this work.

Corona bonding: The initial procedure of Corona bonding (apply Corona to a clean glass and to the washed PDMS for 1 minute each, press gently together and add water after 30 min) provided inefficient bonding of the fourth generation devices, even though the same procedure had granted satisfactory results with the third generation. For this reason a new procedure was developed in order to achieve a successful bonding:

1. The washing steps of devices and of cover glasses are performed at least one day prior bonding;
2. The clean glass and the PDMS are placed on a semi-conductive surface (Silicon plate). Corona plasma is then applied using the one inch disc electrode for 2 min on the cover glass and for 1 min of both PDMS and cover glass, with a maximum of ca 30 s application on the PDMS.
3. The activated surfaces are then gently and evenly pressed together, and the device is placed for 10 min at 70°.
4. The device is then left undisturbed for at least 2h. In the meantime it can be mounted to a plastic surround (MAT-B-5040, *Willco Wells*);
5. A rapid reactivation of channels hydrophilicity is achieved by max 30 s application of Corona treater and the device is rapidly filled with sterile water for storage.

3.1.2 Device handling

Device storage and sterility: Devices prepared as described in section 3.1.1 are filled and submerged with sterile water, close with a transparent plastic lid (MAT-B-5040, *Willco Wells*) and stored in the fridge. Corona bonding is performed on an unsterile bench. When a mounted and submerged device is covered with the lid, flow leakage is usually generated creating another access point for bacterial contaminations. Several procedures are taken into account in order to increase the sterility within the system:

- Devices are exposed to 320 nm UV light on a UV Table(*UVP*) for 7minutes/2h before being employed in biological experiments.
- Devices are washed with ethanol 70% and the device is then placed at 80° in order to let the solvent evaporate.
- Antibiotic Ciprofloxacin (*Cellgro*) is always added to media employed in cell experiments.

Media exchange operations: PDMS needs to be primed in order to become, as much as possible, a cell-friendly environment. Uncrosslinked PDMS oligomers could be toxic for cells and PDMS is likely to adsorb hydrophobic components of cell medium, see section 2.3.1. As established in the Master Thesis of Ryan Hannam, stored device are refilled with serum-free base medium RPMI-1640(*Sigma-Aldrich*), see section 3.2.1, at least one day before cell experiments and kept inside a petri dish in the cell incubator. This is likely to allow saturation of PDMS surface with hydrophobic components. The medium is then exchanged with 2% Fetal Calv Serum (FCS, *Invitrogen*) and 50 μ M 2-Mercaptoethanol (ME) additioned base RPMI at least 30 min prior cell loading in order to partly remove PDMS oligomers leaching into solution. Channels can also be rinsed from eventual fibers or PDMS fragments identified at the light microscope.

3.2 Cell Cultures, Preparation and Loading

3.2.1 Base medium employed in cell cultures

For base medium we intend RPMI-1640 addictionated with 10 μ M Ciprofloxacin, 25 mM HEPES (*Gibco, Life Technologies*) and 2 mM L-glutamine(*Sigma-Aldrich*). Base medium was employed in most of the cell cultures and further reagents added to it are specified for every cell culture/experiment. The cell lines and of the primary cells employed in this work were maintained in RPMI base medium addictionated with cell specific reagents.

3.2.2 Cell counting

According to necessity (culture passages, staining and loading on the device) cells were counted with a Countess Automated Cell Counter (*Invitrogen*) by mixing them at 1:1 ratio with Trypan Blue (*Life Technologies*, according to manufacturers protocol). The dye is excluded from live cells and a rough viability count is obtained. Further calculations were based upon live cell concentration.

3.2.3 Dendritic cells culture and preparation

Bone marrow-derived dendritic cells isolation, differentiation and culture: Bone marrow-derived dendritic cells, BMDC, were differentiated *in vitro* from bone marrow cells using the following protocol:

Differentiating medium: RPMI-1640 + 10 μ M Ciprofloxacin + 25 mM HEPES + 2 mM L-glutamine + 10% FCS + 50 μ M 2-ME + 20 ng/mL GM-CSF (*Biolegend*).

1. Femur bones and tibiae are removed from an euthanized C57BL/6 wild type mouse and collected in 25 mL Hanks solution in ice.

2. The bones are then placed in a dish with 96% EtOH for few min and the bones were cleaned from remaining meat.
3. The clean bones are rapidly washed from etOH in RPMI with antibiotics(Ciprofloxacin), cutted at both ends and flushed down in a 50 mL Falcon tube with ca 10 mL RPMI (+ Ciprofloxacin) each until they turn white.
4. If necessary the tube it filled up to 20 mL, cells are then spin for 6 min at 460xg and resuspended in 2-3 mL Red Blood Cell lysis buffer (*eBio*) for 3 min. The tube is again filled up to 20 mL with RPMI (+ Ciprofloxacin + 10% FCS) and cells are spin down again.
5. Bone marrow cells are resuspended in 10 mL of differentiated medium containing GM-CSF and counted at the Countess system.
6. 1 million of cells are then plated in petri dishes containing 10 mL of differentiating medium and incubated at 37° with 5% of CO
7. After 3 days 10 mL of GM-CSF containing medium are added to the petri dishes and after 3 more days 10 mL of medium are removed and 10 mL of fresh differentiating medium are added.

BMDC following this protocol can be matured by 24 hours stimulation with 100 ng/mL of LPS(*E. coli* O111:B4, *InvivoGen*). BMDC were used in migratory experiments and flow cytometry analyses between eight and fourteenth days after preparation.

BMDC used during experiments BMDC are very delicate and sensible to manipulation and activation is likely to happen during common cell routines such as centrifugation and concentration. Staining of BMDC followed by 3 washing steps with serum-free RPMI-1640 before and with 10% FCS RPMI after staining procedure was abandoned since it lead overly to cell death. A mild staining procedure was tested using 1 wash before and after staining with 0.8 μ M of CMFDA for 20 min in warm bath. Reaction was quenched with with 50% FCS. Cells were afterward tested for LPS-induced activation, as explained in section 3.3.2.

Non adherent cells were carefully collected from culture dishes and used as unstimulated dendritic cells, adherent cells were usually collected after stimulation with LPS. It was found that scraping those cells on ice, reduced cell death and it was chosen to always observe this procedure. Still cell death was consistent, as a lot of debris were eventually load on the device. In a final experiment it was chosen to use EDTA 0,02% in PBS to loose stimulated adherent cells. Stimulated cells were washed once or twice from LPS with cold RPMI serum-free. In order to avoid unwanted maturation of immature BMDC they were always kept and manipulated at 4 deg and spin down at 200g for 10 min. Cells were concentrated to 2x10⁷ mL⁻¹ in medium supplied with 2% FCS and 50 μ M 2-ME before loading. In antigen presentation experiments cells were pulsed with 10 μ M of Ovalbumin 323-339 peptide (ISAVHAAHAEINEAGR-*AnaSpec*) on ice for 1h and resuspended in 2% FCS RPMI (+ Ciprofloxacin, + L-1) medium containing 10 μ g/mL of the peptide and 20 ng/mL GM-CSF, since it has been reported that dendritic cells cytokine and chemokine production is enhanced by constituents of the DC growth/differentiation medium and other T-cell derived cytokines such as IL-4 and GM-CSF,⁴⁴.

3.2.4 MF2.D9 and RF33.70 staining and preparation

MF2.D9 and RF33.70 culture Non-adherent MF2.D9 and RF33.70 (Respectively a MHC class II-restricted Ova(323-339)-specific CD4⁺ T cell hybridoma and a MHC class I-restricted SIINFEL OVa(257-264)) a gift from Dr Kenneth Rock, *University of Massachusetts, Worcester*) were maintained in 75 cm² flasks. Upon thawing cell growth was more contained and require 1:60 dilution and passage every 3 days and a 1:80 dilution and passage every 4 days. Cells growth usually augmented after 5 to 10 passages and needed to be increased up to 1:80 dilution every 3 days. Cell culture medium consisted of base RPMI-1640 medium, with addition of 10 μ M of Ciprofloxacin, 25 mM HEPES, 2mM L-Q, 10% FCS and 50 μ M 2-ME. According to experimental needs between 2 and 10 million cells were stained using either CellTracker Green CMFDA(5-Chloromethylfluorescein Diacetate), CellTracker Deep Red Dye or CellTracker Violet BMQC (*Molecular Probes, Life Technologies*). Celltrackers are cytoplasmic fluorescent probes that freely pass cell membrane and react either with thiol groups (CMFDA and Violet BMQC) or amine groups (Deep Red) inside cells and cannot exit the membrane anymore, they are transferred to progeny but cannot be passed to adjacent cells, so they can be employed in multiplexing imaging. CellTrackers were diluted from stock solutions (respectively 10mM, 1mM and 10 mM in DMSO) to a 2x concentration of 2 μ M in serum-free RPMI-1640. Cells in suspension were collected from flask cultures and counted at the Countess system. Cells were centrifuged 460xg for 6 min and washed in warm serum-free medium three times before being resuspended in serum-free RPMI. The staining volume depended on the initial number of cells: each million of cells was stained in 1 mL of 1 μ M of CellTracker, i.e. 2 millions cells were stained in 2 mL, 5 millions in 5 mL. Cells were kept in water bath at 37C during staining for 30 min and the reaction was then quenched with 50% FCS for 3 min. Cell were then centrifuged and washed 3 times in complete base medium and rested overnight in 75cm² flasks, eventually splitting them according to their rapid growing nature. Before loading on the device cells were counted and concentrated at 2x10⁷ mL⁻¹ in experimental medium: RPMI base medium supplied with 2% Fetal Calv Serum (FCS, Invitrogen) and 50 μ M 2-ME. Cells were kept on ice before loading.

3.2.5 CD8⁺ and CD4⁺ T cells preparation and staining

Mouse spleens from euthanized C57BL/6 wild type were collected in Hanks solution on ice at the animal facility. Spleen were then opened with a scalpel over a 40 μ m cell strainer and cells were squeezed through it by using a syringe plunger. Prior erithrocytes lysis the rough number of cells isolated from one spleen was 210x10⁶ cells, after erithrocytes with RBC lysis buffer one spleen yielded circa 90x10⁶ cells. Dynabeads Untouched Mouse CD8 (*Invitrogen*) and Dynal Mouse CD4 Negative Isolation Kit(*Invitrogen*) were used to isolate CD4⁺ and CD8⁺ T lymphocytes. Cells were usually coloured using CellTracker dye at concentration of 1 μ M and a mild procedure was chosen for cells employed in chemotaxis experiments with just one wash before and after staining. Before loading cells were counted and concentrated to 2x10⁷ mL⁻¹ in 2% FCS and 50 μ M 2-ME. Cells were kept on ice before loading.

3.2.6 Cell loading on fourth generation device

A good cell loading strategy in the different compartments of the fourth generation was established during initial tests of type 1 and type 2 devices. Before loading cells device dish are

emptied from medium and let dry superficially, eventually using some sterile paper without fibers. A good flow is usually achieved by letting cells flow from a pipette tip with $5\mu\text{m}$ of concentrated cells and placed on the correct inlet of the feeding channel filled with a drop of cold medium while the other wells of the compartments are left empty, as depicted in Figure 3.2. The tip needs to be lift up and put back again some times in order to let pressure and capillary forces draw cells inside the network, upon arrival in front of the attractor chamber cells are sucked up from the lateral small channels connecting the feeding channel to the cell chamber, where a lower pressure was probably created by emptying the other wells. Tips should be changed when cells get warm and start to stick to each other. In order to see when tips need to be lift and changed a light microscope is cleaned with ethanol 70% and placed under the sterile bench. With this strategy all compartments can be loaded at the same time. The well developed attractor and migratory compartments are usually filled in 10-15 min, while filling the overdeveloped control compartment increase the loading time up to 30-40 min. The device is then submerged with warm experimental medium and the time is taken as starting point for experiments. The results of this loading strategy are further illustrated in section 4.1.2 of chapter 4 and in section 5.1 of chapter 5.

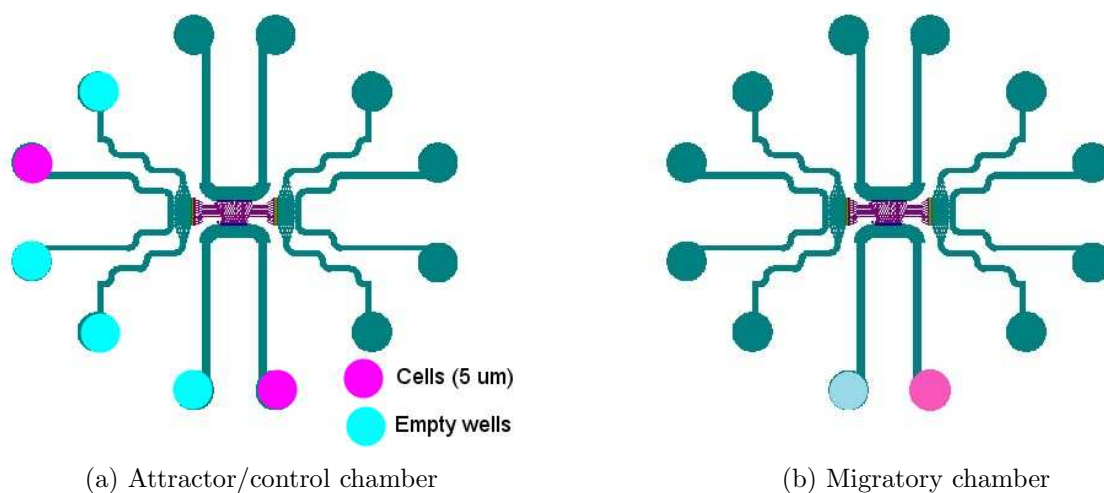


Figure 3.2:

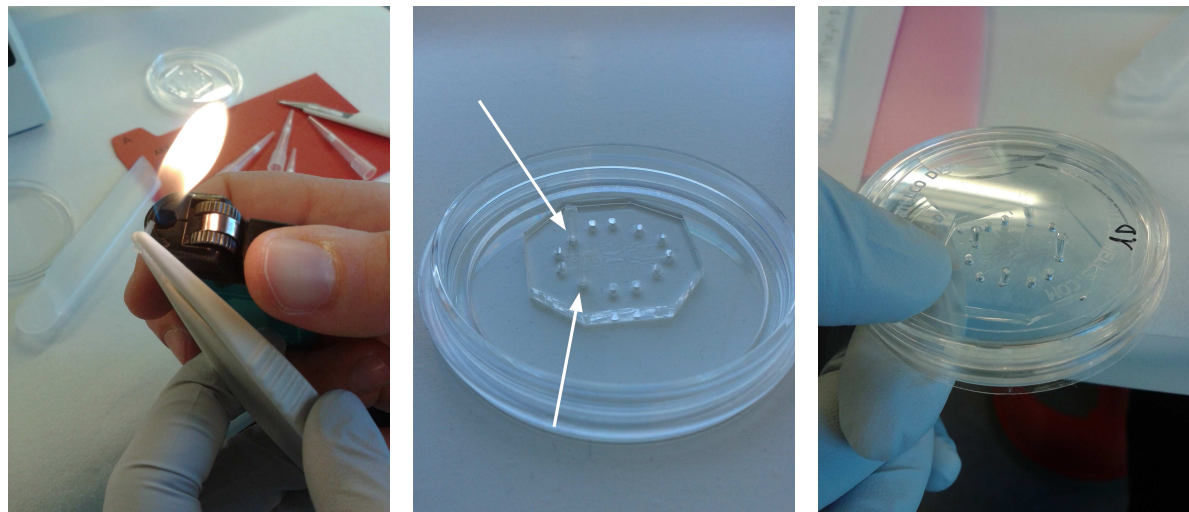
Filling strategy for fourth generation device attractor/control chamber: A tip with $5\mu\text{L}$ of concentrated cells is placed on the correct inlet well while the other wells of the compartment are emptied.

3.2.7 Administration of bioactive molecules and bacteria in-channel

Fourth generation devices offer the chance to administer bioactive molecules and/or bacteria to cells already loaded in attractor/control compartments. The device is designed with a lateral channel that feeds the attractor and the control sides and will be therefore referred to as the feeding channel, see Figure 2.9. Some experiments were performed with food dyes in order to test the potentialities of in-channel administration, results are reported in section 4.1.3.

The strategy depicted in Figure 3.3 was used to administer CCL19 (*R&D systems*) and TNF (*R&D systems*) chemokines in experiments using CD4^+ and CD8^+ T cells, see Table 4.1. Chemokines were administered to empty attractor channels for 10 min in every experiment by creating a

lateral flow in the lateral feeding channels, while the wells of the attractor and control compartment were plugged with burned pipette tips. Then the device was closed and plugs were kept inside it.



(a) Pipette tips are cut and burned
 (b) Pipette tips are placed on the attractor/control compartment wells
 (c) After in-channel administration, the device can be filled up and closed

Figure 3.3: In-channel administration strategy: a) Creation of pipette plugs, plugs were then sterilized with EtOH 70%. b) Pipette plugs are placed in the correct wells c) The device can be filled up with medium (water is used in this example) and closed with the plugs still inside

CFP-*Mycobacterium avium* (Prepared at this lab, obtained from⁴⁵) was administered to iDC loaded 3-4 h before on the left attractor channels. Administration strategy was similar to the one explained above, but plugs were not used in this case, a flow was in the feeding channel was established by emptying the chosen outlet well and by placing a tip with bacteria on one inlet well, the other wells were kept filled with a drop of medium. Since cells are already loaded in the channel it was difficult to define the MOI, and different administration amounts were tested. During the first experience bacteria were diluted first to the concentration of 1.5×10^5 cfu/ μL in experimental medium and administered ($1\mu\text{L}$) for 4 min through the flow generated in the feeding channel. Since no response was noticed, they were administered again during the second day at a concentration of 3×10^5 cfu/ μL ($2\mu\text{L}$) for 2 min. In another experiment bacteria were administered at a concentration of 3×10^5 cfu/ μL ($2\mu\text{L}$) and the established flow was allowed for 10 min. After every administration the wells of the attractor side were emptied from remaining bacteria and the device was covered with medium.

For in-channel activation of dendritic cells, cells were loaded on a device Type one, all the wells, except for the feeding channel wells, were plugged with burned pipette tips and a lateral flow was created in the feeding channel by placing a tip with $4\mu\text{L}$ of 200 ng mL^{-1} of LPS and $10\mu\text{g/mL}$ on the inlet, while the outlet was left open. After four hours in the incubator the LPS tip was removed and the device was washed with medium, before carefully removing the plugs and loading the other cells on the device.

3.2.8 Modeling diffusion and gradient establishment within the fourth generation device:

In order to visualize and try to model chemokine diffusion and gradient establishment within the device in different conditions, we performed some experiments using a 3kDa large fluorescent dye Dextran TRIC Biotin (DTB) (*InvitroGen*) loaded in the left attractor compartment from the feeding channel. Sometimes plugs were employed in order to verify their utility and some other times the dye was left diffuse without plugs. Device were either submerged with PBS or left uncovered. Image were taken at the confocal microscope (Zeiss LSM 510) using 11 air unit in order to measure the mean fluorescence of a thick slice.

3.3 Analysis

3.3.1 Imaging

Microscopy : Three diverse microscope were employed during this work of thesis. During cell culture routine and passages an Olympus CKX41 inverted light microscope was used. The microscope was also used to monitor devices and count cells that were not stained in chemotaxis experiments. EVOS FL Auto Cell Imaging System, an automated fluorescent microscope, was used in order to monitor Celltracker labeled cells in chemotaxis experiments and to take tapse-lapse of the devices. The system utilizes LED light cubes combining excitation and emission filters for determined light intervals. It is coupled to an Onstage Incubator used to maintain cell viable conditions in long time imaging. A Zeiss LSM 510 inverted confocal microscope was utilized visualize CFP-*M.avium* localization during in-channel administration procedures and to analyzed diffusion of the fluorescent dye DTB inside the device.

Image processing : Images were processed in Fiji is just image J(v. continuous release) in order to augment the contrast between background and signal, generate LUT, make stack montages, track cells and optimize time-lapse quality.

Cell counting from pictures: Fourth generation devices allow many cells to enter the network and manual counting at the bright microscope was not actual. Pictures of devices where taken either at the Olympus camera or at the EVOS microscope with 10 or 20x objectives and processed in order to augment the contrast between cells and background. Cells were then counted using the Cell Counter plug-in of Fiji and subdivided in different areas as reported in section 4.3.1.

3.3.2 Flow cytometry

Flow cytometry was used to test whether cell activation was enhanced or hindered after cell staining with CellTracker dyes. Dendritic cells were analyzed with BD FACS Canto II flow-cytometer and BD LSR II flowcytometer was used for T-cell hybridomas analysis using FACS Diva(6.1, *BD Biosciences*). Autofluorescent control sample is gated for high forward scatter (large particles), the alive cell population, and all events are registered until 10,000 events were reached within the gated population. Data analysis was performed in FlowJo(V.10).

Sample preparation

Primary dendritic cells: Bone marrow-derived dendritic cells (BMDC) were tested for CD86 expression following 5 hours administration of LPS 100ng/mL. BMDC from different batches were routinely tested for CD11c expression. BMDC either stained, as described in section 3.2.3, or not BMDC were stimulated for 5 hours with 100 ng/mL in 6-well petri dish. Cells were scraped on ice, collected and divided into different flow tubes always kept on ice. Samples were centrifuged at 4deg, 200xg for 10 min and supernatant was poured. Before antibody (Ab) staining, 0.5 μ L Fc block were administered to each tube. Staining with 0.5 μ L of each Ab, see Table 3.2, was performed on ice, in dark for 30 min. Cells were then washed 1x with 1-2 mL of cold washing buffer(PBS, 2% BSA) and resuspended in 500 μ L of cold washing buffer. Flow tubes were kept in dark and ice and were briefly vortexed before analysis.

T-cells RF33.70 and MF2.2D9 cell lines were stained from culture flasks. Cells were stained with CellTracker CMFDA according to protocol described in section 3.2.4 with 1 μ M of CMFDA staining solution. After staining, control cells and stained cells were divided in 6-well petri dish plates and some of them were stimulated with Cell Stimulation Cocktail(Phorbol 12-Myristate 13-Acetate 40.5 μ M), Ionomycin(670 μ M), *eBioscience*) (4 μ M in 2 mL cell medium). Stimulation lasted 18 hours. Cells were collected and divided into different flow tubes and kept on ice. Samples were centrifuged at 4deg, 460xg for 10 min and supernatant was discarded. Staining was performed on ice, in dark for 30 min using Ab (0.5 μ L) reported in table. Cells were then washed 1x with 1-2 mL of cold washing buffer(PBS, 2% BSA) and resuspended in 500 μ L of cold washing buffer. Flow tubes were kept in dark and ice and were briefly vortexed before analysis. Cell viability was tested with 1 μ L of Propidium iodide added shortly before measurements (Channel Used PE-A).

Antigen (target)	Fluorochrome	Ab clone	Laser Line	Emission Filters	Source company	Cat. No.	Isotype	Channel used
CD11c	FITC	HL3	488 nm	525/50	BD	553801	Armenian Hamster IgG	FITC
CD86	PE	GL1	561 nm	585/20	BD	553692	rat IgG2a, K	PEA

Table 3.2: Antibodies used in flow cytometry analysis of bone marrow-derived dendritic cells

Antigen (target)	Fluorochrome	Ab clone	Laser Line	Emission Filters	Source company	Cat. No.	Isotype	Channel used
CD4	eFluor450	GK1.5	405 nm	450/51	eBioscience	48-0041-02	rat IgG2b, K	eFluor 450
CD8a	eFluor450	53-6.7	405 nm	450/50	eBioscience	48-0081-82	rat IgG2a, K	eFluor450
CD44	PE/Cy9	IM7	561 nm	780/60	BioLegend	103030	rat IgG2b, K	PE/Cy9
CD86	PE	GL1	561 nm	585/20	BD	553692	rat IgG2a, K	PEA

Table 3.3: Antibodies used in flow cytometry analysis of bone marrow-derived dendritic cells

Chapter 4

Results

4.1 Device fabrication and operation developments in fourth generation device

Several procedures were tested in order to explore and take advantages of the fourth generation design features. In-channel administration of bioactive molecules and bacteria by the lateral feeding channel is a new exciting possibility, but it needed to be optimized in order to obtain efficient results. Device microfabrication and handling was sometimes troublesome, especially when the bonding step was moved from Nanolab to the biology laboratory. Bonding resulted to be a fundamental step in order to fully employ the device in chemotactic experiments and it was therefore important to find the correct procedure in order to obtain reproducible results. Good cell preparation and loading procedures within the fourth generation device needed to be established.

4.1.1 Bonding and sterility

During experiments it was found how bonding efficiency can be evaluated in fourth generation devices. In well-bonded devices letters and symbols close to the network grid remain empty upon device filling with water and medium. When the bonding is inefficient, liquids leak under PDMS and there is no color distinction between channels and symbols close to the network. This phenomenon is illustrated in Figure 4.1. Both oxygen plasma bonding and Oxygen plasma bonding procedure needed to be optimized since poor bonding was observed quite often, and it can actually be considered a probable cause for inconclusive results in cell experiments. Oxygen plasma bonding procedure was optimized with the collaboration of Lisa and Nimi as explained in section 3.1.1. The amended procedure for Corona bonding of PDMS on the cover glass partly solved the problem of inefficient bonding: upon filling with sterile water bonding seemed to be efficient. Nevertheless after some days, in some devices used in cell experiments, it seemed that PDMS and glass lost their bonding strength, as the letters and symbols were progressively filled with medium. Moreover the reactivation step, when Corona was applied for 30 s in order to let PDMS to regain hydrophilicity, was found to be troublesome. Sometimes there were created holes inside the filter of the attractor and control sides. When filter damages occurred, cells were able to squeeze through them during experiments.

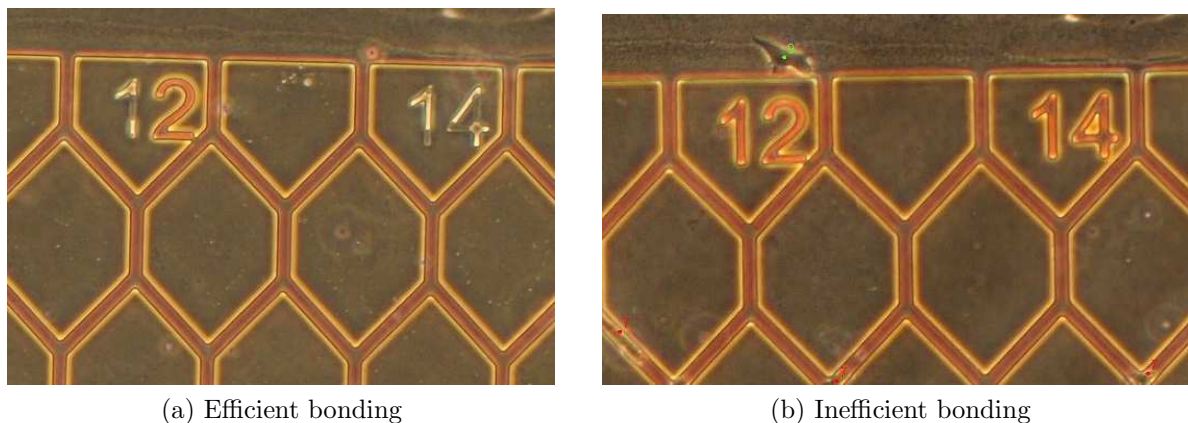


Figure 4.1:

How to evaluate device bonding efficiency in fourth generation devices:a) The different colours of numbers 1 and 2 characterized a well-bonded device. b) Bad bonded device do not have colour differences, meaning that liquid leaks under the PDMS.

Corona bonding was usually performed outside the clean room of Nanolab on a unsterile bench leading to more infections inside the device, even though devices were handled carefully and antibiotics were always added to cell medium. Infections were tried to reduce either by EtOH washing followed by solvent evaporation at 80deg or by using a UV light table(details) high. Indeed ethanol washing managed to reduce infections, but there were some concerns about ethanol retention within the pores of PDMS. Devices were then exposed to UV light at high intensity (302 nm) for 7 minutes. The exposure time was probably too short, since infections in UV exposed devices were still present. So far EtOH washing remained the most efficient sterilization method, but increase surface hydrophobicity was notice after ethanol washing of both corona and plasma bonded devices.

4.1.2 Device types and cell loading procedures

Type 1 and 2 masters of fourth generation device were profiled at Nanolab as shown in section 3.1.1. A block partially occluding the migration channel was found in Type 2 master. The initial channel designed for cell loading resulted to be unsuitable because cells tended to stick on the ramifications and cell loading required too many and long manipulations. For this reason an efficient strategy for cell loading was established by exploiting the lateral feeding channel, as described in 3.2.6.

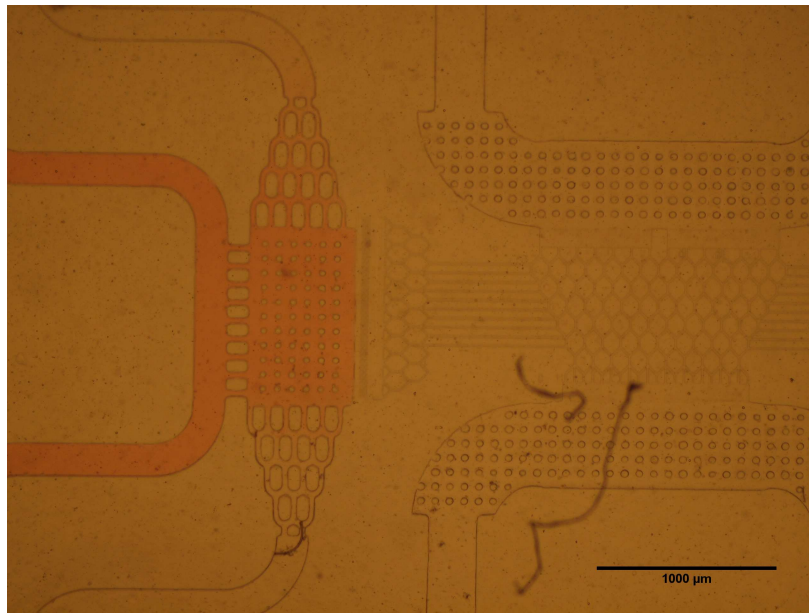
With the help of a clean light microscope under bench, it was possible to correctly determine when pipette tips needed to be adjusted or changed. Overall loading time was reduced to 30-40 min when all the compartments (migratory, attractor and control) were filled at the same time. A problem encountered in Type 1 master is that the features within the control side that connect the feeding channel and the attractor compartment were overdeveloped. Since the strategy described in section 3.2.6 depends on the access to the attractor side from the feeding channel, often a low amount of cells was loaded on the control, especially when bone marrow-derived dendritic cells were used. Therefore it is sometimes difficult to evaluate the control side role in some cell recruitment experiments. In some occasions the control side was left

empty while in some experiments a good loading was achieved. Well-developed compartments (migratory and attractor) could actually be filled in 10-15 min.

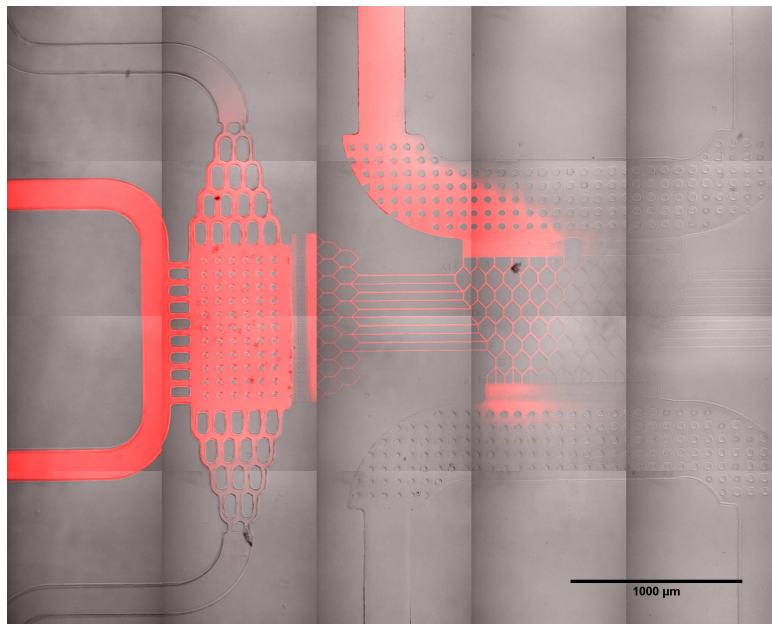
Cell dimensions also played an important role in loading procedures, since dendritic cells are broader and are prone to stick on the walls of loading channels. It was therefore more challenging to obtain equal filling in all compartments with this cell type, compared to MF2.2D9. Type 2 devices, with $9\mu\text{m}$ high loading channels, were inappropriate for both MF2.2D9 and BMDC cells, since most of the cells stuck on the channels before reaching cell compartments. For these reasons it was decided to use type 2 devices in experiments with spleen CD4^+ and CD8^+ T lymphocytes, see section, 4.3.2, which have a diameter of ca $6.5\mu\text{m}$ (according to Countess system).

4.1.3 Administration of bioactive molecules/bacteria in channel

The feeding lateral feeding channel was designed in order to administer bioactive molecules and bacteria to cells already loaded in the attractor/control compartments. First it was studied how to generate, in the simplest manner as possible, a flow only inside the the feeding channel with the aid of food dyes and plugs, see Figure 4.2a. In order to generate a flow only in the feeding channel, it seemed necessary to plug the other wells of the attractor compartment, while keeping the outlet of the feeding channel open, as described in section 3.2.7. The flow reached the side of the attractor compartment within few minutes and passively diffuse to the loaded cells. The plugs created a positive pressure that concentrated the dye in the cell compartment, hindered dye dilution from other wells of the compartment and and let molecules passively diffuse from the attractor compartment to the network. This hypothesis was later confirmed with Confocal microscopy where the diffusion of Dextran TRICT Biotin (DTB) in plugged device confirmed this diffusion dynamic, see Figure 4.2b.



(a) Food dye diffusion

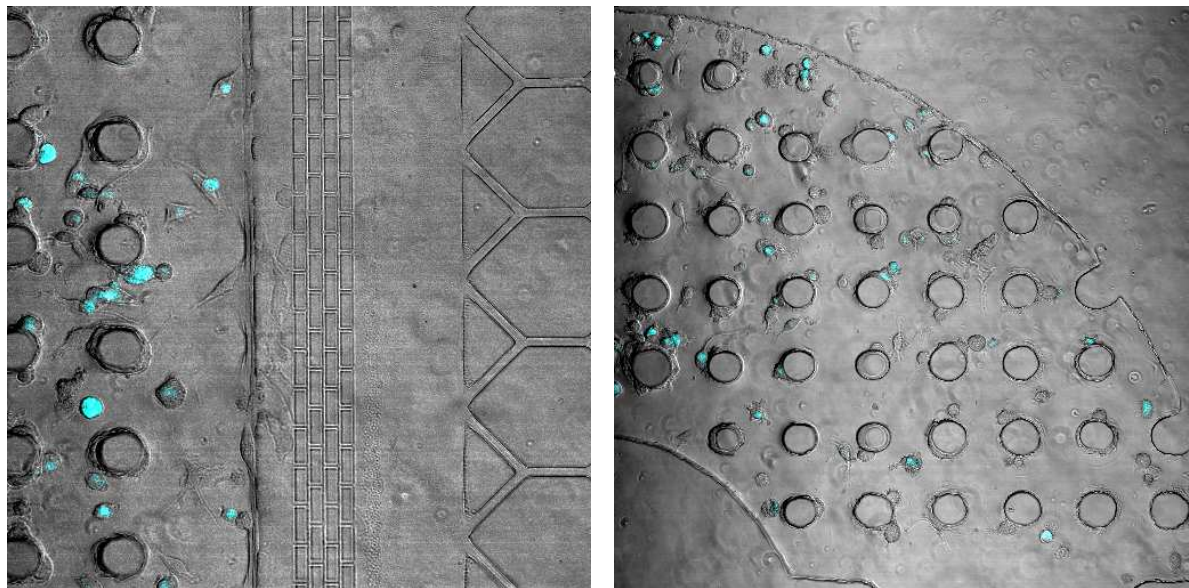


(b) DTB diffusion

Figure 4.2: **In-channel administration: diffusion dynamics in plugged devices:**a) Passive diffusion of $2 \mu\text{L}$ of food dye in a device where the wells of the attractor/control sides are plugged. The image was taken at light microscope. b) Passive diffusion of $2 \mu\text{L}$ of DTB in a device where the wells of the attractor/control sides are plugged. The image was taken at LSM 510 Confocal microscope.

This strategy was first applied to experiments with CD8^+ and CD4^+ T cells explained in Table 4.1. Nevertheless experiment results and, in a second time, confocal microscopy showed that plugging in this manner is not optimal, because tips are not fixed and they move upon device submerging, currents are created inside the channels, as reported in section 4.3.2.

Bacteria were therefore administrated in-channel to bone marrow-derived dendritic cells (BMDC) without the use of plugs, by creating a later flow in the left feeding channel as described in section 3.2.7. During a second experiment the flow was maintained for a longer time in order to seed more bacteria. At confocal microscopy, 20 h after bacterial administration, it was clearly observed that cells already in the channel were able to take up bacteria administrated from the lateral feeding channel, as shown in Figure 4.3a. Nevertheless bacteria were found also in cells of other compartments such as migratory and control sides. Cells that were found inside the network, and that had entered 1 h after bacteria administration, had no or few bacteria and some cells in front of the arrival compartment have not taken up bacteria at all. This indicate that bacteria passed from the other openings of the device and not through the 2 nm filter.



(a) Bacterial uptake in the attractor compartment (b) Bacterial uptake in the migratory compartment

Figure 4.3: Bacteria administration in channel: CFP-*M. avium* were administered by the lateral feeding channel to cells already loaded in the attractor compartment. Images of diverse cell chambers and network were taken 20 h after bacterial administration using the Zeiss LSM 510 confocal microscope. a) The attractor compartment, where CFP-*M. avium*(cyan) have taken up by previously loaded BMDCs. b) BMDC in the migratory compartment where contamination from CFP-*M. avium*(cyan) have happened

4.1.4 Modeling diffusion and gradient establishment within in fourth generation devices

Diffusion of DTB dye loaded from the left upper feeding was imaged at the confocal microscope. In this way it was attempted to have a general idea regarding diffusion dynamics inside fourth generation device. When the device was left uncovered with plugged wells, 2 μ M of DTB were inserted by creating a lateral current in the feeding channel, as described in sec sssec:adm. The dye diffused rapidly (within 1 min) from the left attractor compartment to the left part of the network and was mostly drained by the left sink compartment, as depicted in Figure ???. This partly confirmed the function of the sink compartment in maintaining a differential gradient between the left and the right side.

When the device was covered with medium and no plugs were used, dye diffusion was slower and it was difficult to image the diffusion inside the network. In one experiment a series of 6 pictures were taken across a period of 25 minutes using the same settings at confocal microscopy. The images were further analyzed and fluorescence intensities of different points (the arrival in front of the attractor compartment, the beginning and the end of the lines) were plotted against time. This revealed a linear increase of the gradient during time in every point. The analyzed points are also depicted in Figure 4.4. According to the trend lines obtained, a general doubling time of 20 min for of dye intensity (i.e. concentration of the dye) at the end of each line was calculated. Moreover, the doubling time was different for the three points analyzed and the lines seemed to be the slowest place for dye diffusion. This analysis was just a general representation for diffusion dynamics inside the network, but it may imply that gradients needs some hours to be established and that they can be maintained for long times inside the device.

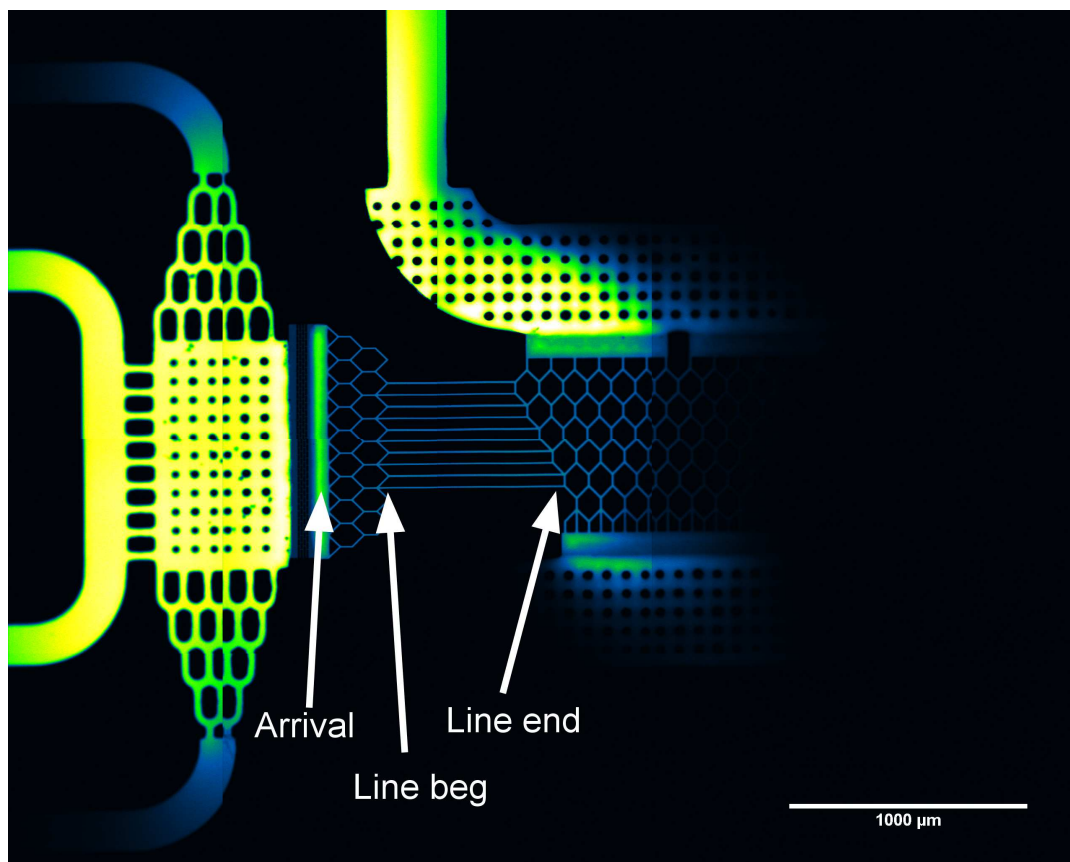


Figure 4.4:

Modeling gradient diffusion inside the device: Diffusion of DTB dye 10 min after loading in the upper well of the lateral feeding channel of a plugged and uncovered type 1 device. A Green-Blue fire LUT was generated in Fiji, highlighting high intensity areas in yellow/green, while low intensities area are blue. The dye is drained by the left sink compartment and does not consistently diffuse in the right network. In the figure the points analysed in further calculation of gradient diffusion are depicted. The Image was taken with Zeiss LSM 510 Confocal microscope.

4.2 Flowcytometry

4.2.1 BMDC staining and flow cytometry

Bone marrow-derived dendritic cells (BMDCs) were differentiated following the protocol described in section 3.2.3. They were analyzed with flow cytometry for CD11c expression at 6 days (in-between the differentiation protocol) and after 11 days (completed protocol) of *in vitro* differentiation. When the protocol is completed, cells are positive for CD11c expression with a Mean Fluorescence Intensity (MFI) of 570, compared to the isotype control (MFI:120), see Figure 4.5a).

BMDCs stained with 0.8 μ M of CMFDA were tested for activation following administration of 100 ng/mL of LPS for 5 hours in terms of CD86 expression. CMFDA Labelled BMDC could be activated by LPS as a shift was observed in CD86 expression, as depicted in Figure 4.5d) and and e). Anyway severe cell death was observed(data not shown) and it was decided not to dye this cell type. A consistent part of unstimulated BMDC were already expressing CD86, depicting how much these cells are prone to activation during handling procedures, as can be observed in Figure 4.5c). Therefore, in order to reduce handling as much as possible, it was decided to utilize non adherent BMDC as immature dendritic cells in further experiments. CD86 expression increase during the next 24 and 48 h following activations stimulus, as it was observed in other flow cytometry analyses (data not shown).

4.2.2 MF2.2D9 and RF33.70 staining and flowcytometry

MF2.2D9 and RF33.70 were tested in order to see whether activation was hindered or induced by staining procedures. Labeled cells and control were activated with Cell Stimulation Cocktail, according to sectionssec:flow. CD44 expression, a marker for T cell activation, was analyzed with flow cytometry and also expression of CD4 and CD8 were checked for MF2.2D9 and RF33.70 respectively. From flow cytometry results it is possible to observe that CMFDA staining does not alter MF2.2D9 activation since the expression of CD44 increased at comparable rates in both control and labeled MF2.2D9 cells, as depicted in Figure 4.6. Most of MF2.2D9 expressed CD4, as can be observed in Figure 4.6b), c), e) and f). Also RF33.70 expression of CD44 increased at similar rates in control and CMFDA labeled cells, but the complexive expression was much lower than MF2.2D9 cells, as can be observed in Figure4.7b), c), e) and f). Moreover RF33.70 do not express much CD8 and the expression was checked in another flow cytometry analysis revealing that the isotype control had a higher MFI than CD8 sample: 105 vs 72 checking(data not shown).

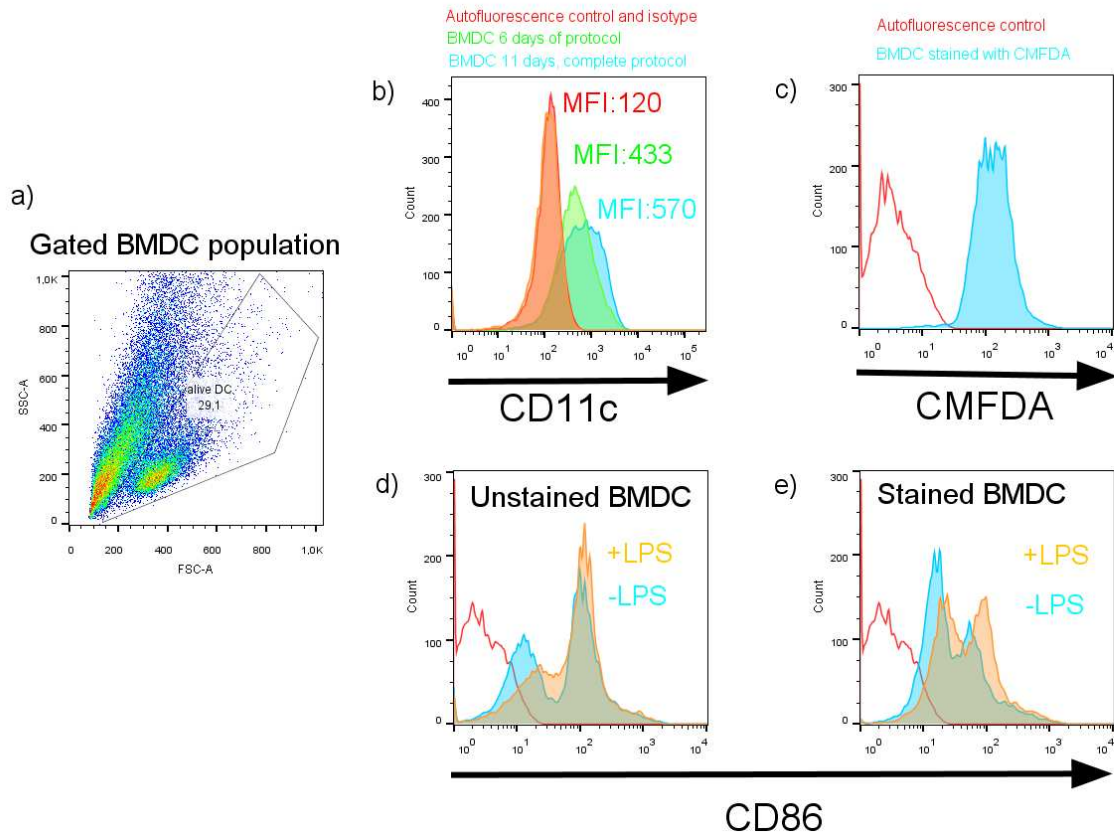


Figure 4.5:

Flow cytometry analysis of *in vitro* differentiated BMDCs a) Gated population of BMDC in the autofluorescence control sample b) CD11c expression of BMDCs at 6 and 11 days after isolation and starting of differentiation c) BMDC stained with CMFDA (cyan) compared to autofluorescence control (red line) d) CD86 expression of unlabeled BMDC with control medium (cyan), with 100 ng/mL LPS for 5 h (orange), autofluorescence control (red line) e) CD86 expression of CMFDA labeled BMDC with control medium (cyan), with 100 ng/mL LPS for 5 h (orange), autofluorescence control (red line).

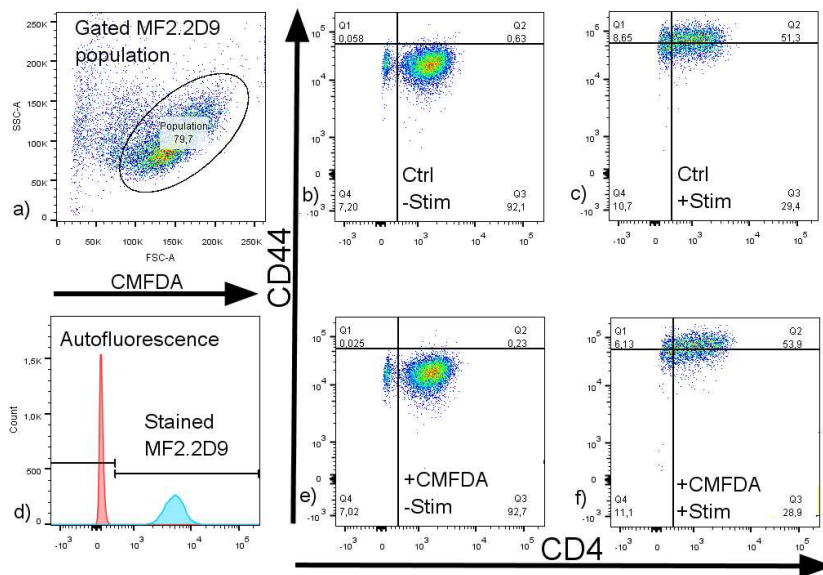


Figure 4.6: **Flow cytometry analysis of MF2.2D9 cell line:** a) Gated population of MF2.2D9 in the autofluorescence control sample b) CD44 and CD4 expressions of unlabeled MF2.2D9 cells without stimulation c) CD44 and CD4 expressions of unlabeled MF2.2D9 cells with Cell Stimulation Cocktail 18 h d) MF2.2D9 stained with CMFDA (cyan) compared to autofluorescence control e) CD44 and CD4 expressions of CMFDA labeled MF2.2D9 cells without stimulation f) CD44 and CD4 expressions of unlabeled MF2.2D9 cells with Cell Stimulation Cocktail 18 h

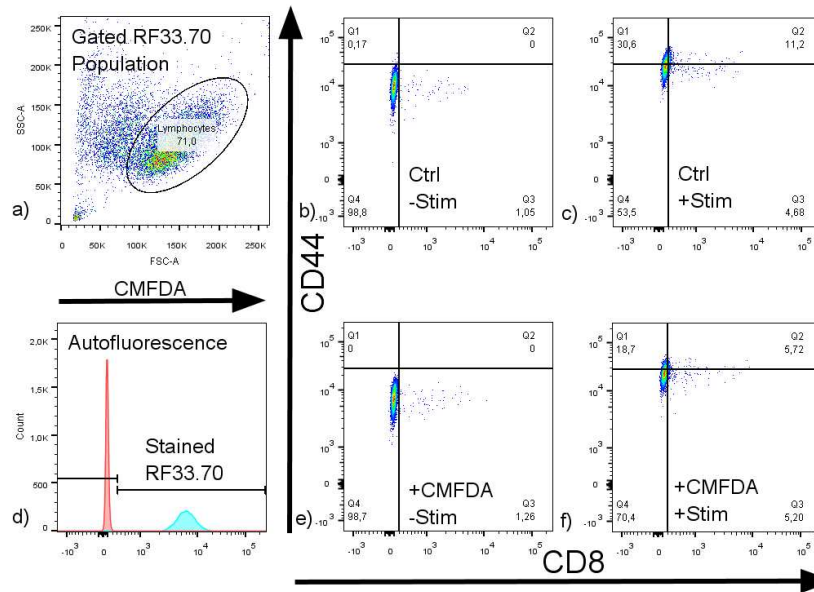


Figure 4.7: **Flow cytometry analysis of RF33.70 cell line:** a) Gated population of RF33.70 in the autofluorescence control sample b) CD44 and CD8 expressions of unlabeled RF33.70 cells without stimulation c) CD44 and CD8 expressions of unlabeled RF33.70 cells with Cell Stimulation Cocktail 18 h d) RF33.70 stained with CMFDA (cyan) compared to autofluorescence control e) CD44 and CD8 expressions of CMFDA labeled RF33.70 cells without stimulation f) CD44 and CD8 expressions of unlabeled RF33.70 cells with Cell Stimulation Cocktail 18 h

4.3 Cell recruitment and chemotaxis assays

Once loading and in-channel administration techniques were established for different cell types, fourth generation devices were employed in chemoattractant experiments, where the number of migrated cells towards either a chemoattractant reaction or a control was evaluated. Many different potentially chemoattractant immune reactions were tested on the new fourth generation device. Some of them were able to produce a significant chemoattractant gradient inside the device resulting in cell migration pointing towards the attractor compartment. A special effort was put in trying to understand when migration due to chemotaxis was happening and how the phenomenon could be observed inside the device. Therefore, a strategy, explained below was established in order to analyze cell recruitment and localization in different subareas of the device. Possible causes for inconclusive results were also highlighted in order to improve the use of the device in the future.

4.3.1 Established method for chemotaxis analysis

As illustrated in Figure 4.8, the device was divided into subareas in order to identify regions of interest for studying cell localization and migration inside the device. Due to master fabrication, the right cell compartment of devices type 1 was always more difficult to fill with cells and was utilized as a control side, often filled with a lower amount of cells. The left cell compartment was used as the attractor side where attractor cells and reactions were loaded during experiments. Cell distribution in the different subareas was analyzed at different time points attempting to understand whether and when a chemotactic gradient was present inside the device.

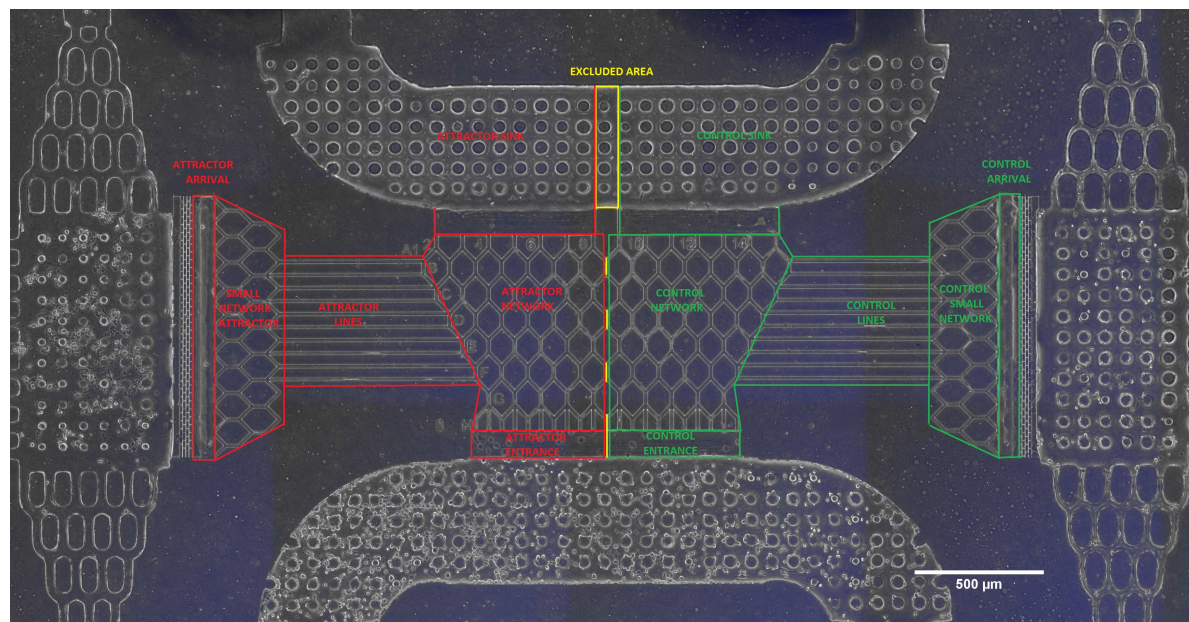


Figure 4.8:

Identified subareas for chemotaxis analysis: The device was divided into six areas: entrance, network, lines, small networks, arrivals and sinks. Shared areas like the entrance, the major network, and the sink sink were divided into left and right subareas, and central parts, highlighted in yellow, were excluded from the count. Red= attractor, green= control

4.3.2 Mouse CD4⁺ and CD8⁺ T cells chemotaxis and recruitment

In two occasions mouse CD4⁺ and CD8⁺ T cells were isolated from mouse spleen and labeled, as described in section 3.2.5. Cells were employed in two series of experiments, as illustrated in table 4.1. In the first experiments we aimed to test whether a gradient of chemoattractant molecules (CCL19 and TNF) created inside the device was able to recruit primary naïve T lymphocytes. CD4⁺ and CD8⁺ T cells were labeled respectively with CMFDA and Deep Red CellTracker and loaded on devices obtained from master Type 2 and attractant biomolecules were administered for 10 minutes by a flow created in the lateral feeding channel of the attractor side. The wells of the attractor compartment had been previously plugged with burned pipette tips that were kept inside the device. In this experiment it was found that the use of movable plugs in order to avoid chemokine dispersion from attractor compartment wells is not optimal. One pipette plug created a sucking pressure towards the lower well of the attractor compartment and compromised the result in CCL19 experiment. Cells loaded on the device containing TNF did not move during the next days.

Migratory side	Attractor side	Stimulation of attractor side	Control side	Medium
CD8+ and CD4+ T cells 1:1	CCL19	none	medium	2% FCS
CD8+ and CD4+ T cells 1:1	TNF alpha	none	medium	2% FCS
CD4+ T cells	BMDC	100 ng/mL LPS overnight	unstimulated BMDC	2% FCS
CD8+ T cells	BMDC	100 ng/mL LPS overnight	unstimulated BMDC	2% FCS

Table 4.1: **Experimental setups CD8⁺ and CD4⁺ T cells fourth generation cell experiments:** Labeled CD8⁺ and CD4⁺ T cells were loaded in devices of type 1 and 2 in order to test their response towards attractant biomolecules or mature dendritic cells. Chemokine experiments were performed in type 2 devices and experiments with BMDC were performed in type 1 devices.

The second time that mouse CD4⁺ and CD8⁺ T cells were employed, experiments aimed to investigate T cell recruitment from matured BMDC. Devices type 1 were chosen, since it is difficult to load a good quantity of BMDC cells in the Type 2 devices, as explained in section 4.1.2. Deep Red labeled CD4⁺ and CD8⁺ T cells (loaded in two different devices) didn't move from the place they were seeded. Moreover it was observed that a concentration of 2×10^7 cells mL⁻¹ is not optimal for loading this cell type on the device, cells are very small (6.5 μ m of diameter at Countess system) and should therefore be concentrated more.

4.3.3 BMDC chemotaxis and recruitment

Since bone marrow derived dendritic cells (BMDCs) had shown promising and directed migration inside PDMS channels of third generation devices⁴³, it was decided to use this cell type in order to investigate chemotactic recruitment of immature BMDCs by stimulated BMDCs within the fourth generation device. Cells were first used alone in a series of experiments where attractant cells were either stimulated with LPS before loading, and then it was attempted to mimic recruitment upon bacterial infection using CFP-Micobacterium avium administrated in-channel, as reported in Table 4.2. BMDCs were treated and loaded on devices type 1 following diverse procedures in order to optimize these steps when using these delicate cells.

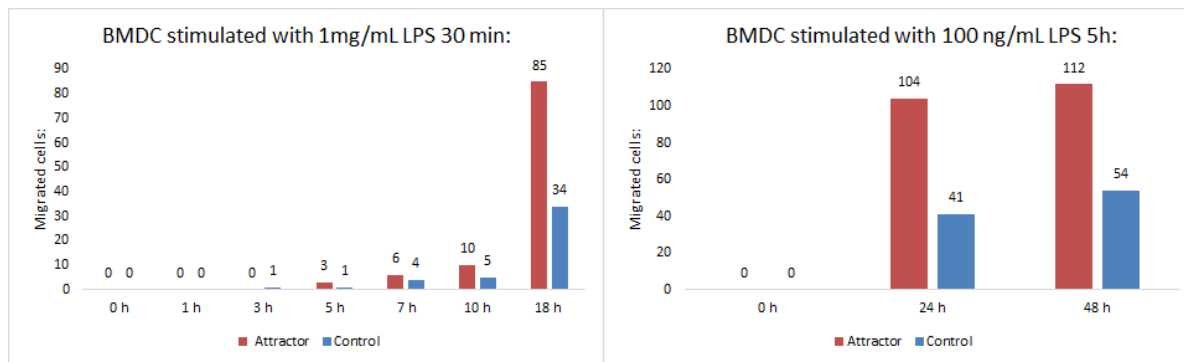
Migratory side	Attractor side	Stimulation of attractor side	Control side	Medium
Unstimulated BMDC	Stimulated BMDC	LPS in petri dish	Unstimulated BMDC	2% FCS
Unstimulated BMDC	BMDC infected with <i>M. avium</i>	<i>M. avium</i> administration in-channel	Medium/unstimulated BMDC	2% FCS

Table 4.2: **Experimental setups of chemotaxis experiments with BMDCs:** Recruitment of immature BMDC was evaluated towards two different attractor reactions. LPS was used for stimulating BMDC cells at either 100 or 200 ng/mL for 5/7h or at 1 mg/mL for 30 minutes. CFP-*Mycobacterium avium* was administered in-channel, as explained in section 3.2.7

BMDC stimulation with lipopolysaccharide:

During experiments involving BMDC as migrating and attractor cells, immature non-adherent dendritic cells were carefully collected and kept on ice while the rest of BMDCs were stimulated with LPS.

BMDCs were first stimulated for 30 min with a high dose of LPS (1 mg/mL), loaded on the attractor chamber, while the control was filled with few iBMDC, and recruitment of iBMC from the migratory chamber was observed during the first 18 hours. Cells started to move towards the network after 3 h and the first cells entered during the fifth hour following loading. Not so many cells entered between the first and the tenth hour, but a consistent migration towards left attractor area was noticed at the 18th hour, as reported in Figure 4.9a. A time-lapse of the left network was taken between the 20th and the 22nd hour, but just few cells were seen advancing toward the attractor compartment. At 24 h the situation was not considerably changed and cells were not counted.



(a) BMDC migrated during the first hours

(b) BMDC migrated at 24 and 48 hours

Figure 4.9:

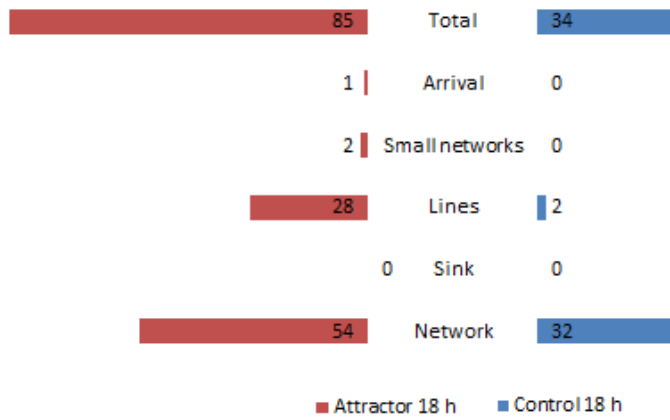
Chemotactic response of iBMDCs towards LPS stimulated BMDCs: (a) BMDC migrated towards attractor (red) vs. control (blue) compartment. (b) BMDC migrated towards attractor (red) vs. control (blue) compartment.

Cell distribution was analyzed in different subareas, identified by the method explained in section 4.3.1. Figure 4.10a is a butterfly graph depicting differences in cell distribution between the left and the right part of each subarea (respectively the attractor and the control sides of each subarea), cells were counted from Figure 4.10b. As can be observed in Figure 4.10a, most of the cells localized in the network, and most importantly, in every subarea there was a clear trend toward the left side. Many cells were found in the lower lines, maybe depicting

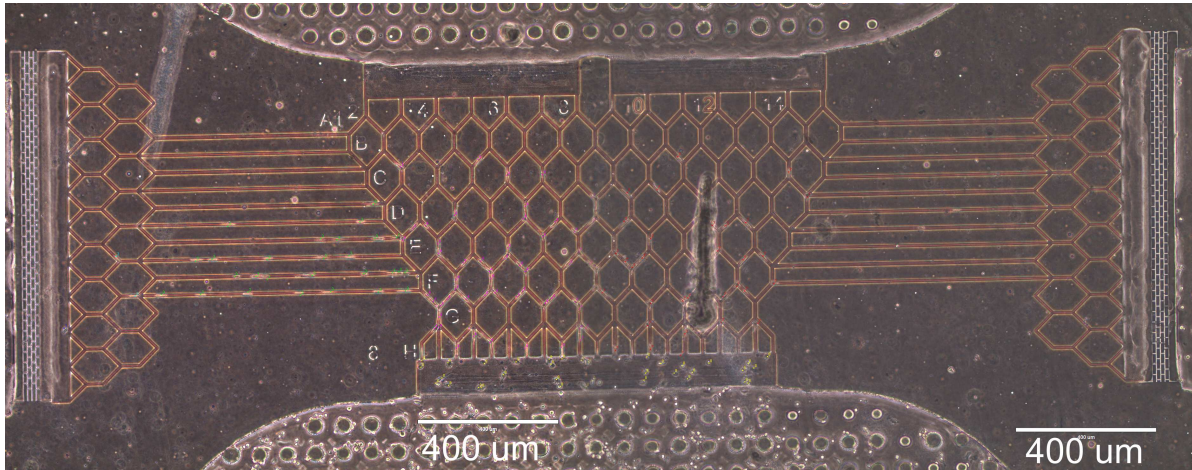
how a chemoattractant stimulus was sensed before advancing towards the higher parts of the network.

In another experiment, BMDCs were stimulated for a longer period with less LPS (5 hours with 100 ng mL^{-1} LPS in the petri dish). Stimulated cells were then loaded on the attractor side and migration of unstimulated BMDCs was evaluated after 24 and 48 hours. Also in this case, the control was filled with few iBMDC. A more consistent migration was noticed inside the device at 24 h towards the attractor compartment. As shown in Figure 4.9b, LPS seemed to trigger the production of chemotactic molecules actively recruiting cells towards the attractor compartment mostly during the first 24 hours. Indeed the number of migrated cells did not significantly increase in the following 24 hours. When cell distribution was analyzed in the second experiment, it was possible to see that after 24 hours more cells were found in every left/attractor subarea compared to the right/control, see Figure 4.10. Moreover most of the cells were located either in the network, of both sides, or in the lines especially towards the attractor compartment and in the arrival in front of the attractor compartment. Also in this case, in line subareas most cells were present in the lower line, but more cells compared to experiment of Figurefig:butterfly5feb had reached the arrival compartment. In the following 48 hours, cells inside the device continued to move and partly relocated to other subareas, with a more homogeneous distribution in the left attractor subareas. Since more cells reached the arrival compartment in front of the attractor side when attractor cells were stimulated for 5 h with LPS, it was decided to use longer stimulation times in further experiments. The control side of these first experiments had few unstimulated BMDC.

BMDC localization at 18 h:



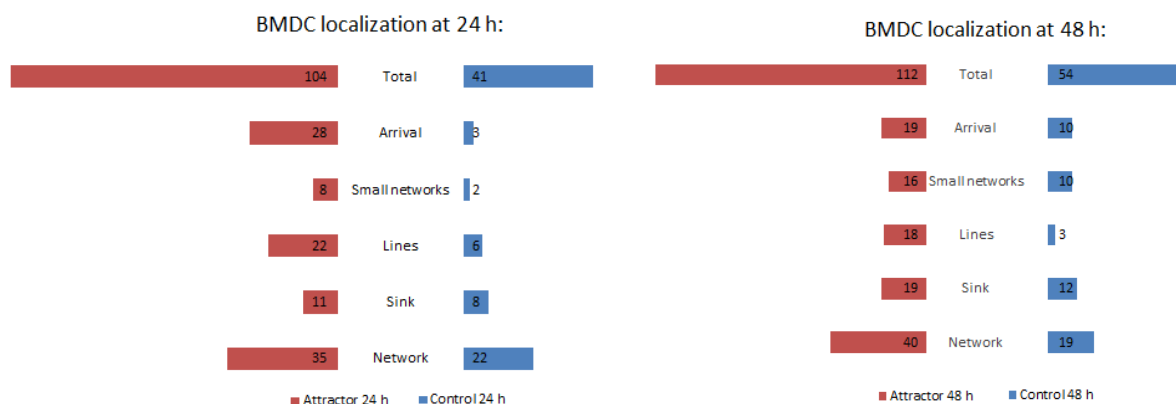
(a) Stimulation attractor: 1 mg/mL LPS 30 min



(b) BMDCs localization inside the device

Figure 4.10:

BMDCs localization in different areas of the device 18 h after loading: a) BMDCs distribution was analyzed in different subareas of the network, according to strategy explained in 4.3.1 b) Contrast phase image of BMDCs inside the network, from which BMDCs were counted using Cell Counter plug-in in Fiji.



(a) Stimulation attractor: 100 ng/mL LPS 5h

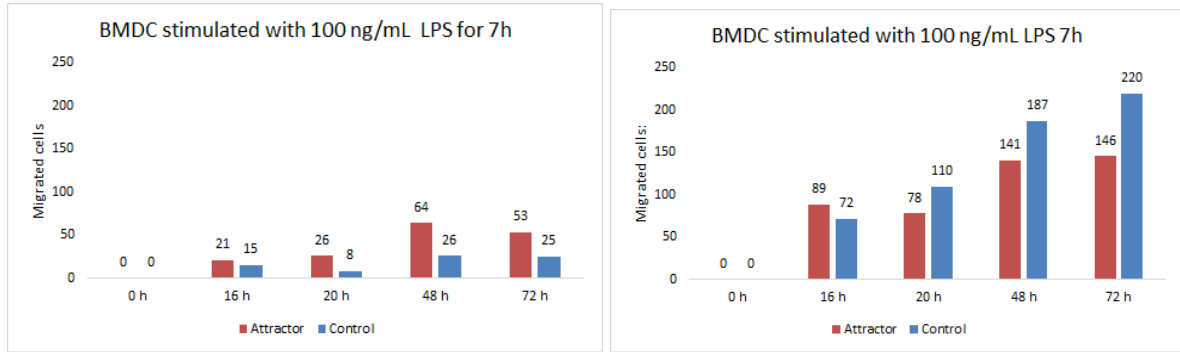
(b) Stimulation attractor: 100 ng/mL LPS 5h

Figure 4.11:

BMDCs localization in different areas of the device 24h and 48h after loading: a) BMDCs distribution was analyzed in different subareas of the network after 24 h after loading, according to strategy explained in 4.3.1 b) BMDCs distribution was analyzed in different subareas of the network after 48 h after loading, according to strategy explained in 4.3.1

In later experiments involving LPS stimulated dendritic cells it was difficult to observe a clear directed migration as in the first experiments. Many reasons were proposed in order to explain such results and they will be further discussed. Bonding problems seems to be the most probable cause for undirected migration. They were evaluated in a second time for every device by observing letters and numbers filling with medium, as explained in section 4.1.1.

In two experiments DCs were stimulated in petri dish with with 100 ng/mL LPS for 7h. In one experiment it was decided to investigate whether adherent unstimulated BMDCs could be used as migratory cell. It was found that migration was very reduced, as shown in Figure 4.12a, even though there was still a trend towards the attractor side. Another device, reported in Figure 4.12b, seemed to have a bad bonding, especially in the migratory side, when it was refilled with fresh medium during device preparation. It was therefore decided to use it upside down, in this case non-adherent BMDCs were used as migratory cells. In both cases migration wasn't clearly directed towards the attractant compartment, and way more cells migrated in the device loaded with non-adherent iBMDC. In these experiments the control side was loaded with a larger amount of BMDCs compared to the first experiments involving BMDCs.

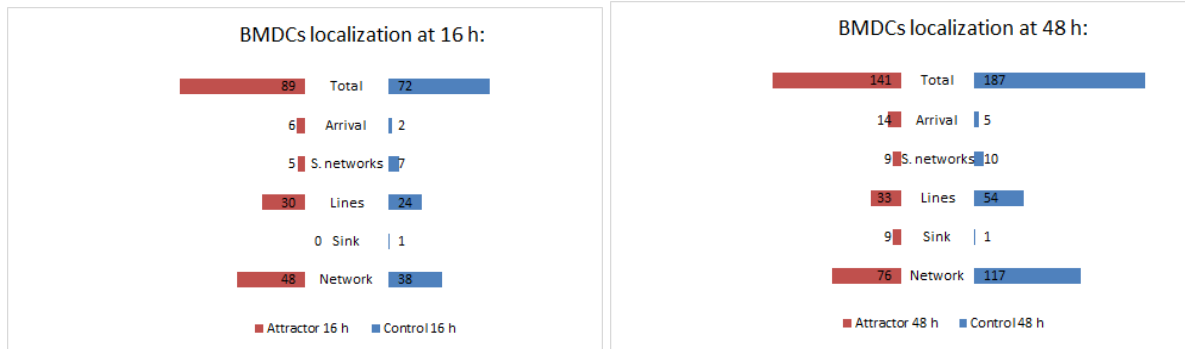


(a) Stimulation attractor: LPS 100 ng/mL 7h, Migratory cells: adherent iBMDC (b) Stimulation attractor: LPS 100 ng/mL 7h, Migratory cells: non-adherent iBMDC

Figure 4.12:

Chemotactic response of iBMDCs towards LPS stimulated BMDCs: (a) BMDC (iBMDC) migrated towards attractor (red) vs. control (blue) compartment. (b) BMDC migrated towards attractor (red) vs. control (blue) compartment.

In these experiments, it can be observed that BMDC continued to enter the networks also after 20 hours, as in both experiments migrating cells relatively augmented in the following 24 hours. In the second experiment also after 72 hours more cells had entered the network. Comparing the localization of cells in the experiment of Figure 4.12b at 16 hours and 48 hours, it was noticed an increased migration towards the control subareas already at 20 hours (data not shown) the same relative differences between subareas were maintained at 48 hours, see Figure 4.13, and after 72 hours (data not shown).



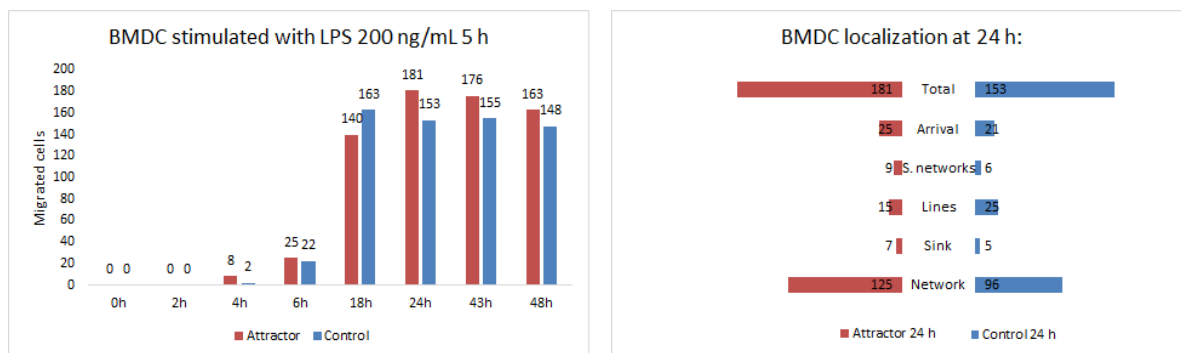
(a) Stimulation attractor: 100 ng/mL LPS 7h (b) Stimulation attractor: 100 ng/mL LPS 7h

Figure 4.13:

BMDCs localization in different areas of the device 16h and 48h after loading: a) BMDCs localization was analyzed in different subareas of the network 16 h after loading, according to strategy explained in 4.3.1, experiment of 4.12b. b) BMDCs localization was analyzed in different subareas of the network after 48 h after loading, according to strategy explained in 4.3.1, experiment of 4.12b.

In a final experiment cells were stimulated with an higher dose of LPS (200 ng/mL) for 5 h, it was decided not to scrape cells from the petri dish and to instead loose them with EDTA. In this more alive BMDCs were loaded on the attractor compartment and many cells survived

in the compartment up to 4 days. Migration was monitored as reported in Figure 4.14, and also in this case there was not a clear directionality towards the attractor compartment. No significant changes were either observed 4 days after. One possible reason is the incomplete Corona bonding of the device network noticed in a second time. Anyway it can be observed that, respect to previous experiments, more cells entered the network already after 18 hours, maybe reflecting a general higher concentration of chemotactic stimuli. In order to give a complete picture of the experiment, it must be said that more cells had been loaded in both attractor and control compartments compared to the previous experiments. Cell distribution in different subareas did not show any particular trend, as depicted in Figure 4.14b, and it can be assumed that a chemotactic gradient did not form inside the device.



(a) Migrated BMDC at different time points

(b) Stimulation attractor: 200 ng/mL LPS 5 h

Figure 4.14:

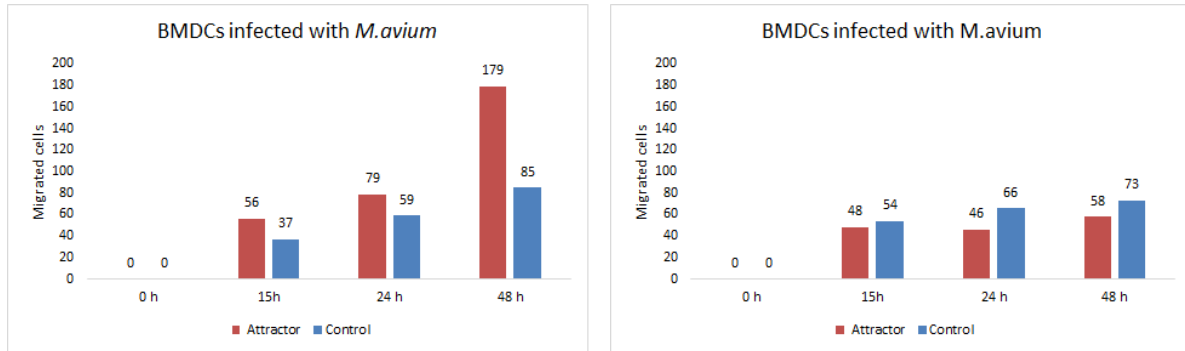
Chemotactic response of BMDCs towards LPS stimulated BMDCs and distribution 24 h after loading: (a) BMDC migrated towards attractor (red) vs. control (blue) compartment. (b) BMDCs localization was analyzed in different subareas of the network after 24 h after loading, according to strategy explained in 4.3.1.

BMDC infections with *Mycobacterium avium*:

The devices were then in experiments were it was evaluated chemotaxis towards bacterial infections. Immature BMDCs were first loaded on the attractor compartment and after 3-4 h were infected with *M. avium* administrated from the lateral channel, as explained in section 3.2.7.

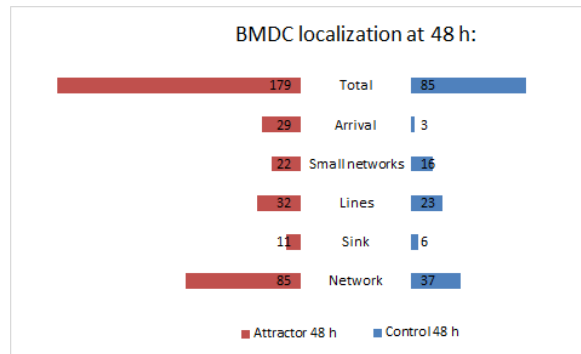
In the first two experiments the control compartment of one device was filled with some immature BMDC while in the other device control was filled with medium, as depicted in Table 4.2. Cells were counted 15 h after administration and no clear response was observed. At EVOS system bacteria seemed to be too few and not colocalized with cells. No response was observed 24 hours after infection and therefore a second bacterial administration was performed. After other 24 hours a response direct to the migration compartment was observed by evaluating cell distribution in different subareas: more BMDCs had entered the left attractor network and cells localized in the attractor small network and arrival compared to the control side, as depicted in Figure 4.15a. In this case cells were found in both lower and upper attractor lines, while in the control lines they were just in the lowest ones. After the second bacterial administration migration was instead more or less homogeneous inside device of Figure 4.15b. Cell load in the attractor compartment differed for the two devices, more cells were actually

loaded in device of Figure 4.15a.



(a) BMDC migrated towards *M. avium* infection

(b) BMDC towards migrated *M. avium* infection



(c) BMDC Localization at 48 h experiment of Fig. 4.15a

Figure 4.15: **Chemotactic response of BMDCs at 15 h, 24 h and 48 hours towards *M. avium* infections:** Migration towards attractor (red) vs. control (blue) compartment at 15 h, 24 h, and 48 h after a second bacterial administration. Control: medium b) Migration towards attractor (red) vs. control (blue) compartment at 15 h, 24 h, and 48 h after a second bacterial administration. Control: unstimulated c) BMDC localization 24 hours after the second administration of *M. avium*, analyzed according to strategy explained in 4.3.1 experiment reported in Figure 4.15a.

When the experiment was attempted a second time, many bacteria were detected in migratory and control sides. Cell migration was very contained in this experiment, as shown in Figure 4.16, and the differences between attractor and control subareas were minimal:

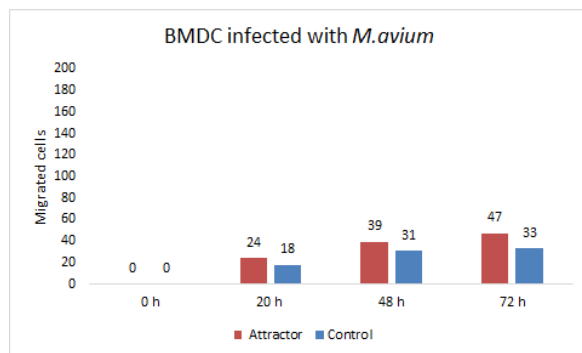


Figure 4.16:

Chemotactic response of BMDCs at 20 h, 48 h and 72 hours towards *M.avium* infections: Migration towards attractor (red) vs. control (blue) compartment at 20 h, 48 h, and 72 h after a second administration of *M.avium*. In this experiment bacteria were administered for a longer time and many bacteria were found in the migratory compartment after 20 hours.

In this experiment there was a lower cell load of BMDCs within the attractor compartment compared to the experiment reported in Figure 4.15a and this fact was also pointed out in experiment of figure 4.15b. From these results it can be speculated that the amount of BMDC loaded and the MOI resulting after bacteria administration in the attractor side are important for the creation of a functional chemotactic gradient within the device.

BMDCs behavior and motility inside the device were observed across several experiments and further considerations are reported in section 4.4.1.

4.3.4 MF2.2D9 and RF33.70 recruitment towards antigen presentation reactions

Fourth generation devices (type 1) were then employed in a series of experiments in order to assess the chemotactic response of MF2.2D9 and RF33.70 towards antigen presentation reactions. Compared to BMDCs these cell types showed a completely different dynamic within the device. Cells moves fast in every part of the device and may respond quickly to strong chemotactic gradients.

As reported in Table 4.3, different cell mixtures and stimulation conditions were tested to investigate whether in fourth generation device it was possible to chemotactically influence the migration of these cell types, since third generation device did not fit this purpose. Experiments were performed on device type 1 that were all well bonded, according to section sssec:bondingres.

Migratory side	Attractor side	Stimulation of attractor side	Control side	Medium
RF33.70 and MF2.2D9 1:1	BMDC*	100 ng/mL LPS 5h and 10 uM peptide 1h	Unstimulated BMDC	2% FCS
RF33.70 and MF2.2D9 1:1	BMDC and MF2.2D9** 1:2	100 ng/mL LPS 5h and 10 μ M peptide 1h	Unstimulated BMDC	2% FCS
MF2.2D9	BMDC and MF2.2D9** 1:2	100 ng/mL LPS overnight and 10 μ M peptide 1h	Medium	2% FCS
RF33.70 and MF2.2D9 1:1	BMDC and MF2.2D9** 1:3	in-channel stimulation***	Unstimulated BMDC	2% FCS

Table 4.3: **Experimental setups of antigen presentation reactions and RF33.70 and MF2.2D9 chemotaxis experiments:** Recruitment of OVA cells was evaluated towards differently stimulated DCs in order to investigate cross-talk between the two cell types. *: + 20 ng/mL GM-CSF; **+ 20 ng/mL GM-CSF + 10 μ M Ovalbumin 323-339 peptide; *** in-channel stimulation: in channel stimulation was performed with 200 ng/mL of LPS and 10 μ M Ovalbumin 323-339 peptide administrated for 4 hours. For further specification see section 3.2.7

MF2.2D9 migration in a test device without attractor reaction:

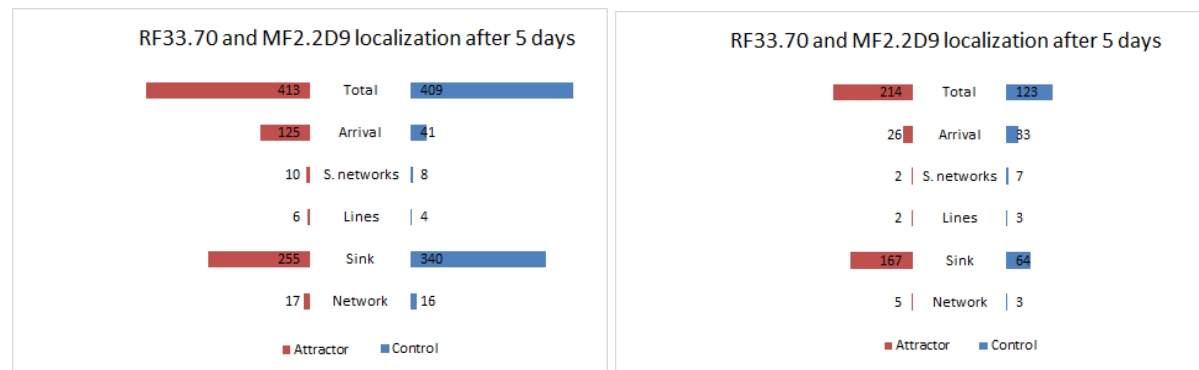
During loading strategies studies one test device Type 1 was loaded with VIOLEt BQ labelled MF2.2D9 cells in the migratory compartment, and unlabelled and unstimulated MF2.2D9 on the control and attractor sides. No stimulus was present within the device and it was possible to fill homogeneously both attractor and control side. Cells entered after 1 hour and 24 hours later most of the cells migrated towards the sink subareas, 76 cells were in the left side and 16 in the right. There were in the other subareas were 15 cells still showing mobility. This result may indicate that this cell line do not accumulate in network spaces, as BDMDC, but that they migrate towards open spaces like the sink when there is more access to fresh medium.

Cell retention by interactions with BMDCs:

In the first experiments, depicted in the first and the second line of Table 4.3, Deep Red labelled MF2.2D9 and CMFDA labeled RF33.70 and stimulated BMDC/antigen presentation reactions were loaded on a device type 1. The control side was not completely filled with unstimulated BMDC. Both devices were well bonded. Most of the loaded MF2.2D9 and RF33.70 cells seemed to be dead since the beginning, and no cell entered the network during the first 2 days. On the fifth day the devices were examined again and a surprising result was observed in the device were MF2.2D9 and RF33.70 migration towards stimulated BMDCs.

Observing cell distribution inside the different subareas, it appear that relatively many cells were retained in the arrival compartment, as depicted in Figure 4.17a, see Sv¹. Moreover BMDCs seemed to interact with them by stretching dendrites through the 2x2 nm filter, see Sv². Violet BMQC-labeling of RF33.70 was no longer detected by the EVOS system microscope, but Deep Red dye was still detected in some MF2.2D9 cells. Anyway it was not longer possible to determine to which cell line belonged retained cells. Some MF2.2D9 cells, and probably also some RF33.70, seemed also to have entered the attractor and the control compartments, as some fluorescent Deep Red dye was observed inside there (data not shown). Moreover, by observing cell morphology it seemed that among the retained cells in the arrival compartment there were some BMDCs, escaped from the attractor compartment. From this experiment it was hypothesized that some degree of interaction and cross-talking between BMDCs and T cell hybridomas was possible to happen inside the devices. Retention was not

observed in the experiment testing antigen presentation reactions, as depicted in Figure 4.17b, most of the cells were found in the left side of the sink, but no clear retention in other attractor compartments was observed.

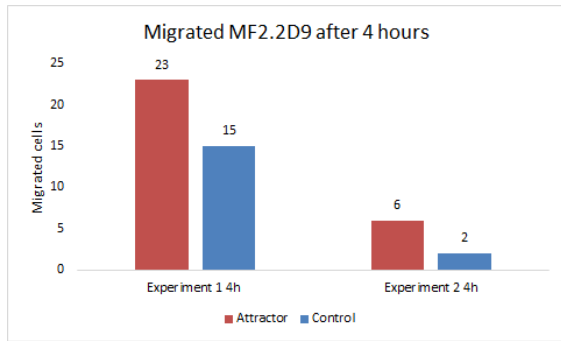


(a) Attractor: BMDCs stimulated with LPS for 5 h (b) Attractor: BMDC antigen presentation reaction

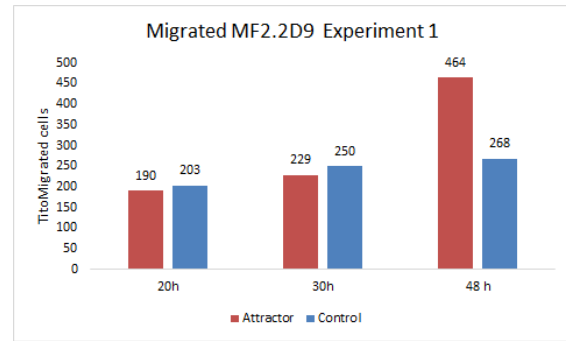
Figure 4.17:

Localization of a mixture of RF33.70 and MF2.2D9 towards BMDCs or antigen presentation reactions: (a) RF33.70 and MF2.D9 (mixture) localization was analyzed in different subareas of the network 5 days after loading, according to strategy explained in 4.3.1. (b) RF33.70 and MF2.D9 localization was analyzed in different subareas of the network 5 days after loading, according to strategy explained in 4.3.1.

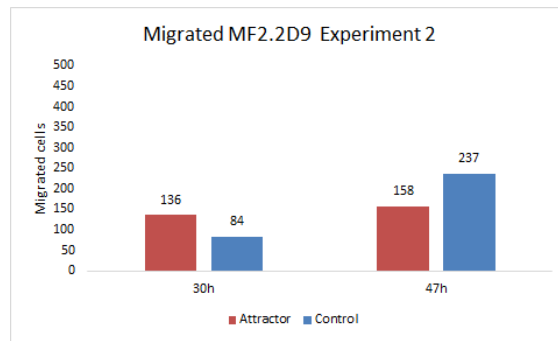
Another experiment was performed trying to evaluate the timing of chemotaxis when using these cell lines. Chemotaxis of Deep Red labeled MF2.2D9 was evaluated towards a differently timed antigen presentation reaction. Two devices were both filled on the attractor side with BMDC matured one night with 100 ng/mL LPS and loaded with 10 $\mu\text{g}/\text{mL}$ of peptide for one hour on ice and inside the device. Deep Red labeled MF2.2D9 were loaded with BMDCs in the attractor chamber at 1:2 ratio. Devices were monitored during the first 3-4 hours and at 20, 30 and 48h cells were counted in one device while in the other cells were counted at 30 and 48 h. In the first device, cells entered one hour after loading and a fair migration was observed during the first 4 hours, in another device, migration during the first 3-4 hours was more contained, as can be seen in picture 4.18b. Migration differences in the two devices were maintained in later time points, as depicted in Figure 4.18b and 4.18c. This high variability can partly be explained in terms of amount of cells loaded into the device, but this fact regarded just the migratory compartment that was loaded with more MF2.2D9 in the first experiment. Between 30 and 48 hours cells in sink subareas greatly augmented and this fact is responsible for a switch in the complexive amount of cells present in left(attractor) and right(control) areas. This fact happened in the left sink subarea of the experiment depicted in Figure 4.18b and in the right sink subarea of experiment depicted in Figure 4.18c.



(a) Attractor: antigen presentation reaction, after 4 hours



(b) Attractor: antigen presentation reaction, late hours



(c) Attractor: antigen presentation reaction, late hours

Figure 4.18:

Chemotactic response of MF2.2D9 towards antigen presentation reactions: a) Migration towards attractor (red) vs. control (blue) compartment at 4 h . b) Migration towards attractor (red) vs. control (blue) compartment at 20, 30 and 48 h c) Migration towards attractor (red) vs. control (blue) compartment at 30 and 48 h

When cells distribution in the different subareas was compared between the first and the late hours, see Figure4.19, in both devices MF2.2D9 and RF33.70 localized mostly inside the network during the first hours while in the later hours, most of the cells were found in open spaces such as the sink subareas and the arrival compartments. Moreover the difference of cells in attractor and control arrivals seemed to be irrelevant compared to experiment in Figure 4.17a.



(a) Attractor: antigen presentation reaction

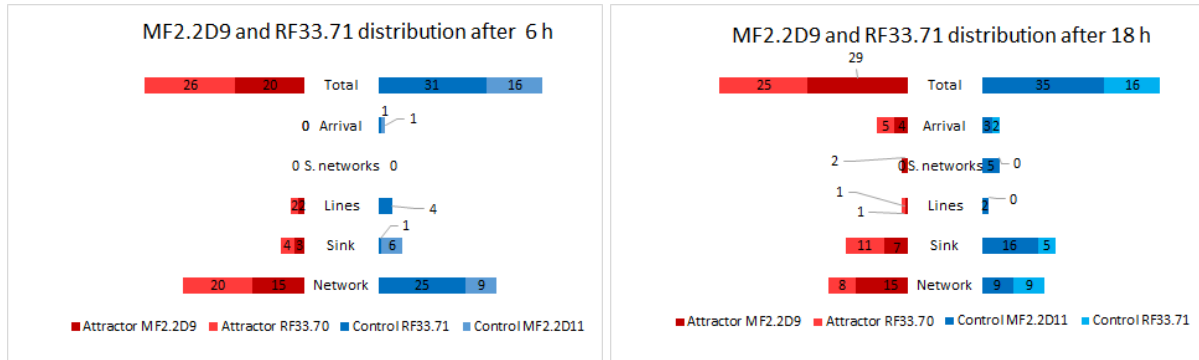
(b) Attractor: antigen presentation reaction

Figure 4.19:

Localization of MF2.2D9 towards antigen presentation reactions: (a) Deep Red-labeled MF2.2D9 localization was analyzed in different subareas of the network 4 h after loading, according to strategy explained in 4.3.1. (b) Deep Red-labeled MF2.2D9 localization was analyzed in different subareas of the network 20 h after loading, according to strategy explained in 4.3.1.

From this experiments it was thought that cell migration of MF2.2D9, and maybe also RF33.70, needed to be evaluated during the first 24 hours. It was also hypothesized that the antigen presentation reaction was inefficient and a new strategy was tested.

It was decided to try a last experiments were BMDCs, collected without scraping, were activated in channel using 200 ng/mL of LPS and 10 μ M administrated from a lateral flow for 4 hours. CMFDA-labeled MF2.2D9 were added to stimulated BMDCs after 4 hours and then CMFDA-labeled MF2.2D9 and Deep Red-labeled RF33.70 were loaded in the migratory at 1:1 ratio. Migration was supposed to be monitored with a Time-Lapse at EVOS system between the h 6 and 18, but due to technical problems, only the first four hours were monitored, i. e. until the tenth hour. Cells started to reach the arrival compartment in front of the attractor/control side during the seventh hour, but still few cells (5-7) from the network had reached the arrival subarea in front of the attractor/control sides at the tenth hour. Cell distribution at 18 h seems to confirm the hypothesis that MF2.2D9 and RF33.70 tend to accumulate in the sink compartment, as depicted in Figure 4.20 Most of the cells were still migrating inside the network/sink, with no particular overall direction, and it was thought that a chemoattractant stimulus towards other compartments of the device was not present.



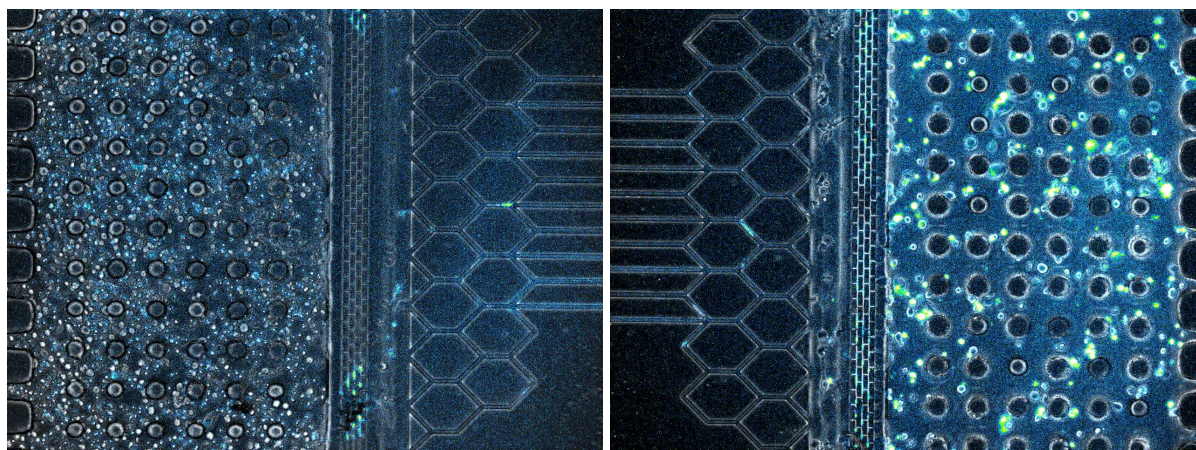
(a) Attractor: antigen presentation reaction

(b) Attractor: antigen presentation reaction

Figure 4.20:

Localization of MF2.2D9 and RF33.70 towards antigen presentation reactions: a) Deep Red-labeled RF33.70 and CMFDA labeled MF2.2D9 was analyzed in different subareas of the network 6 h after loading, according to strategy explained in 4.3.1 b) Deep Red-labeled RF33.70 and CMFDA labeled MF2.2D9 was analyzed in different subareas of the network 18 h after loading, according to strategy explained in 4.3.1

At 24 hours the situation seemed not to have changed and cells were counted at the light microscope. There were few cells inside the network (21), most of the cells were in the sink (53) and respectively 12 and 15 cells in front of the arrival compartments. At 48 h hours the situation seemed to have changed again: some BMDCs had exit the attractor and the control compartment and were maybe interacting with MF2.2D9 and RF33.70 in the arrival compartment. It was therefore decided to monitor again the device for 2 hours with the EVOS system. As depicted in Figure4.21, many Deep Red labeled RF33.70 cells had entered in the attractor compartment, compared to the control. Deep Red dye was found on both filter structures and, as it can be observed in Figure 4.21, the dye intensity is much was much less in the attractor compartment than in the control. This may suggest that a more sustained cell proliferation of RF33.70 cells took part in the attractor compartment, triggered by cytokines production during antigen presentation reactions. A more sustained proliferation would imply CellTracker dilution in RF33.70 progeny. CMFDA-labeling could not be detected and it cannot be said whether MF2.2D9 had passed or not the filter barriers. Cells were more alive and motile in the attractor compartment, as can be observed in Sv³ and compared to Sv³.



(a) RF33.70 channel Deep Red attractor compartment (b) RF33.70 channel Deep Red attractor compartment

Figure 4.21:

Different Deep Red CellTracker dye intensities in cells within attractor and control compartments: Deep Red-labeled RF33.70 were able to enter the attractor(a) and the control(b) compartments of the device, as traces of the dye are found in the structure of both filter. Images were taken at EVOS system and belong to a scan of the whole device using the same settings, a consistent difference in dye intensities can be observed in the two compartments. Images were equally stretched in Fiji.

4.4 Cell migration and interactions, in real-time observations in the Fourth Generation Device

Some interesting phenomena and facts regarding cell migration and interactions inside the device have been noticed throughout several experiments. Cell migration and decision-making can be evaluated in Real-Time at different time-points during ongoing immune reactions inside the device. BMDCs showed diverse amoeboid migratory modes: some cells were elongated and stretched, while some others had a more rounded and blebbing motility. Observing migrating MF2.2D9 and RF33.70 migration in Real-Time enable the viewer to speculate upon paths and interactions between two cell types in early and late time point of experiments.

4.4.1 BMDC behavior and migration in fourth generation device

Upon loading on attractor, control and migratory compartments BMDC had a rounded morphology due to the fact that they were kept in ice before loading. Once inside the device they start to stretch within 2-3 hours. In the attractor, migratory and control chambers, which are 28 μm high, they were often attached to the pillars of the chamber and exhibited a 2D migration with a broad lamellopodium, when they moved from a pillar to another, as can be observed in video Sv⁵. The first cells usually enter the network 4-5 hours after loading but most of the cells entered within 16-18 hours. As reported in section 4.3.3, in some experiments entrance and migration were mostly concluded after 24 hours, while in other experiments cells continued to enter in the later hours, as in the experiment of Figure 4.12b.

Cell migration during a probable chemotactic gradient was observed in Real-Time in one occasion, i.e. the experiment reported in Figure 4.9a. The left (attractor) side of the network,

where most of the cells localized, was imaged across a period of 2 h with pictures taken every 5 min. Inside the network cells exhibited multiple migratory morphologies, as can be observed in video Sv⁶. They often showed an elongate shape and protruded extensions, especially at the leading edge, while some of them seemed to possess a blebbing motility, like the cell on the left part of the video Sv⁶. Some cells had a morphology in-between this two migratory modes with a rounded rear and a protruding front during motion. Few completely round cells seemed to be stuck inside the channels, as the cell close to the symbol E in video Sv⁷. BMDCs often passed and squeezed along each other, remaining in touch for several minutes before separating and continuing on their way, as it can be observed videos Sv⁶, Sv⁷ and Sv⁸. In all the videos, it is easy to observe that cells did not completely occlude the channel, but they rather slid along the walls of the channels or pushed themselves against opposing walls. This means that confinement is not complete in 8 μm wide microchannels. In video Sv⁸, it can be observed how cells polarize before entering the network. In this video it is also possible to notice that in 2 cells, the cell already inside the left channel and the cell moving horizontally under the G symbol, have a lagging rear that sticks on the side of the channels stopping their movement, this is pointed out also in video Sv⁹. From a qualitative point of view, the complex translocation of moving cells was quite reduced across the two hours of observation, since most of the cells do not move more than 100-200 μm . Anyway few cells displayed a faster locomotion like the first cell entering the first channel from the left in video Sv⁸, that traveled 422 μm inside the network in 50 min of observation, with a mean instantaneous speed of 8.4 $\mu\text{m}/\text{min}$. Most of the BMDCs seemed to change direction very often moving forward and backward. This phenomenon was noticed especially in the line compartment, as can be visualized in video Sv⁷.

By observing videos and pictures of attractor and control compartments loaded with dendritic cells, a particular behaviour of dendritic cells was noticed. Some cells tended to adhere to the 2 nm large filter and stretched dendrites through the filter, as noticed in video Sv². When a longer time lapse, BMDC cells were indeed found able to squeeze through the filter slots. Across an observation time of 4 hours some many squeezing and infiltrating behavior were observed, as reported in video Sv¹⁰. Anyway only a cell with a small size completely passed across the filter, the phenomenon will therefore need further investigations.

4.4.2 MF2.2D9 and RF33.70 cells migration and behaviour

In the network it was possible to observe migration of MF2.2D9 and RF33.70 in Real-Time. The network provides a space where cell paths and migration can be observed and tracked, as for example in video Sv¹¹. This video comes from the later Time-Lapse of the last experiment involving MF2.2D9 and RF33.70, the tracking has been done manually with the plug in Manual tracker of Fiji. Only few MF2.2D9 were detected moving in this part of the network, their paths seem to be more determined than those that were observed in the previous time point of the experiment (6-10 h), when some MF2.2D9 had a more undecided behavior, often stopping and interacting with other MF2.2D9 and RF33.70 encountered in network intersections. A BMDC escaped from the attractor (or control) compartment is tracked in green and can clearly be recognized by its different amoeboid motion.

The speeds of the tracked MF2.2D9 were comparable with the previous work of Ryan Hannam, speeds were almost all between 7 and 15 $\mu\text{m}/\text{min}$ plus one cell with a top speed of 22 $\mu\text{m}/\text{min}$. Automated tracking using Track Mate v.25.1 plug in was attempted in order to test whether this procedure can be applied to Celltracker labeled migrating cells. It was difficult for the

software to identify cells labeled with a cytoplasmic CellTracker dye as a single object and to distinguish between two cells interacting, and further elaboration will be needed to correctly visualize the paths. As it can be observed in Sv¹², tracking inside the maze-structured network resulted to be way more geometrically organized, and it would be easier to utilize for further studies of cell behavior and migration paths than unconstrained movements inside the migratory compartment.

It was also possible to evaluate from a qualitative point of view interactions between cells migrating inside the network. Upon meeting in network intersections, both MF2.2D9 and RF33.70 were sometimes passing each other through a squeezing behavior, as can be observed in video Sv¹³, where a Deep Red labeled RF33.70 squeezes over a MF2.2D9, or interacting for several minutes before changing direction, as depicted in video Sv¹⁴. Some cells, that displayed high speeds and a kind of predetermined direction, were also seen to push away interacting cells, like the cell tracked in yellow in video Sv¹¹.

Across several experiments it was noticed that CellTracker dyes tend to be concentrated at the rear of the cell, in the so-called uropod. Many cells seemed to interact upon meeting in network intersections by remaining attached to the rear of other cells, that had accumulated more dye respect the front. Upon those meetings, one cell seems to drag the other one from the back of the cell, as depicted in Figure 4.22. Images can be visualized in time-lapse in the first part of video Sv¹⁵. In the second part of the video another Deep Red labeled RF33.77, initially squeezing over a MF2.2D9, is later redirected by another MF2.2D9, always from the uropod. The cell is first dragged backwards to another channel and then, after releasing, it repolarizes and exits the network. These observations may implicate a functional role for the uropod in coordinating and directing migration and will be further discussed.

Finally, since some dendritic cells were able to invade the network, autonomously or thanks to filter damages occurred during devices microfabrication, some interactions between them and MF2.2D9 and RF33.70 were observed, see video Sv¹⁶. Here a dendritic cell in front of the minor network is protruding some dendrites while it interacts with several cells, some of them are Deep Red labeled RF33.70, some are CMFDA-labeled MF2.2D9 and some others might be other BMDCs escaped from the network. BMDC squeezing through the filter were previously supposed to interact with cells on the other side, as it was noticed in the experiment reported in Figure ?? and in video Sv². The video Sv¹⁶ is a complete picture of the phenomenon.

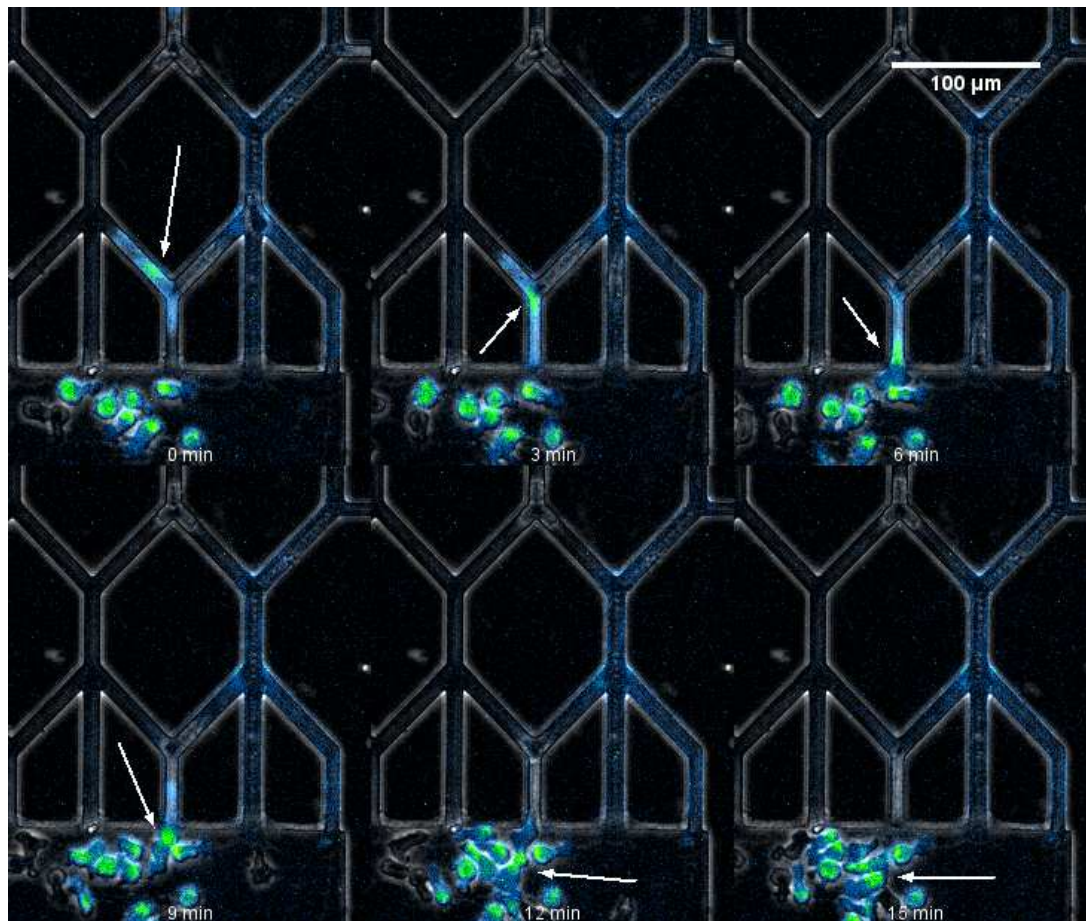


Figure 4.22:

Interaction from the uropod region between two RF33.70 cells: RF33.70 cells were labeled with Deep Red Celltracker, that mainly localizes in the cell rear. During image processing a different LUT was generated using the Green-Blue fire combination in Fiji. In this manner the areas with maximum signals appear green and the other points are brilliant blue. The white arrows are always pointing at the back of the two cells, where also most of the dye is localized. At 0 min two RF33.70 cells are interacting with each other, their rear is in contact, as pointed by the arrow. At min 3, 6 and 9 the cell on the right seems to drag the other one from the rear. Finally the two cells exit from the network and, at min 15 they are still in contact with their back.

Chapter 5

Discussion

The novel design of the fourth generation device provides new experimental conditions that urged to be understood through several tests and experiments. Numerous difficulties and problems, such as sterility and bonding, needed to be solved during this work in order to fully benefit from its potentials. Results and problems encountered in this work will now be analyzed and discerned. A definitive solution for some problems has not been applied yet, but based on this experience it is now possible to have a concrete approach to them.

5.1 Device fabrication and operations

PDMS-glass bonding: Corona treatment, and sometimes Oxygen plasma, resulted to be troublesome during the bonding of fourth generation devices and needed therefore to be optimized during the present study. There are many possible reasons for unsuccessful bonding when using these procedures. First, fourth generation design presents a more complex architecture with higher number and dimensions of loading chambers surrounding an elaborated network. This fact may reduce the zones of PDMS actively taking part in bonding formation, and therefore bonding formation along every feature needs to be facilitated since it could require more time. During Corona bonding the discharge is applied manually to the surface and surface coverage results are therefore variable. Moreover, the two surfaces can be rearranged within the first five minutes while after plasma treatment the bonding is initiated immediately³⁸. Filling up the devices with water during bonding formation and stabilization time can therefore create a too high pressure and compromise bonding formation. Another reason identified for unsuccessful bonding while using the first Corona bonding procedure is the non-evaporation of the organic alcohols and water from the PDMS, and in consequence, in Corona bonding procedures, it was decided to bond the devices one day after the washing steps. The time of PDMS treatment was maybe too long and powerful causing an excessive concentration of surface silanols and a rearrangement of the surface chemical bonds as it has been shown for oxygen plasma bonding procedures⁴⁶. Thermal and mechanical stress cause further surface cracking after surface activation⁴⁰. For this reason, an even pressure was applied by using a round lid covered with a clean glove to the activated surfaces. In both Corona and oxygen plasma bonding it has been observed that keeping the device at high temperatures after bonding procedure increase the strength of the bond and the devices was therefore kept at 70 – 80° C for 10 min³⁹.

Corona bonding is both low-cost and time-saving since it does not require the use of a vacuum chamber. However the use of Corona bonding needs to be optimize for every application

in order to obtain satisfactory reproducible results³⁸. The amended bonding procedure for Corona bonding granted an apparently successful bonding of the PDMS onto the cover glass. Later, as reported in section 4.1.1, bonding was lost in some experiments. Also filtering damage needs to be addressed and it was maybe due to a too long exposure to the corona discharges during channels reactivation. Considering all the problems mentioned above it is questionable whether Corona bonding completely fits fourth generation devices and their application.

Still, as mentioned in section 2.3.1, PDMS hydrophilicity after oxygen plasma treatment decreases rapidly and can be improved by extending the curing time of the polymer, or by organic solvents extracting procedures^{41,47}. Both procedures consistently reduces the number of low molecular weight PDMS chains in the bulk material, but they would also increase the cost and the time necessary in device production. Since the plasma procedure determined during this work resulted to be the most sterilizing step it may be recommended for fourth generation devices. Rapid filling with sterile water of the mounted device after plasma bonding should be performed at Nanolab on a clean bench and it is likely to maintain PDMS hydrophilicity⁴⁸.

Bonding problems, especially those noticed during device employment in cell experiments, need to be taken into account while interpreting results, since incomplete bonding clearly affected gradient formation and cell recruitment inside the device.

Sterility in fourth generation devices: Sterility is very important since cells loaded into the device need to be alive during 24-48 hours for an optimal application of the device. Bonding by Corona does not seem to provide the same degree of sterility of oxygen plasma bonding, since manual application of Corona discharges does not completely cover the whole surface exposed to it. Very good sterilization was achieved during ethanol washing, but still some concern can be express regarding the amount of ethanol retained inside PDMS. Ethanol is a low swelling solvent in PDMS that does not deform the polymer, and ethanol sterilization does not change the rate of oxygen diffusion inside PDMS^{47,49}. Anyway an increased surface hydrophobicity was noticed after ethanol evaporation and this fact, together with ethanol retention, can possibly reduce device feasibility for cell cultures. Exposure to 302 nm UV light resulted to be inefficient, but adjusting the exposure time may be a good solution and further tests should be done in this direction.

Also the steps before bonding procedures were carefully examined. For example, the water used after organic alcohols washing of the glas coverlid might be have been a source of infections and it was therefore decided to eliminate this step from the washing procedure. Also administration practices can play a role in infection establishment and it was therefore important to optimize them.

Loading strategies in fourth generation devices and master types: One of the limiting step in third generation device use was the low and uneven cell loading in different compartments of the device. Low cell load have been solved by increasing the height of loading chambers from 9 to 28 μm and by punching inlet and outlet holes closer to the cell storage compartments. Nevertheless uneven distribution of cells in front of the attractor and the control networks was still an issue and the low number of cells loaded in the attractor side was addressed as a cause of poor response to cell-produced chemokine gradients. Also in the fourth generation design, loading compartments of 9 μm resulted to be inefficient for proper cell loading with dendritic cells and T cell hybridomas. Devices type 2 could not be

used in experiments with these cell types. It is therefore recommended to avoid such a design for the future, at least when big and sticky cells such as dendritic cells are employed.

The strategies found during this work increased the amount of cells loaded in the devices and loading was evenly distributed in front of the major network. Anyway, the initial channel designed for cell loading in the attractor/control compartments resulted to be unsuitable. The ramifications in the higher part of the attractor compartment, designed in order to provide an even distribution of cells in the attractor/control compartments, constituted a block for flowing cells that stopped and stuck to each other hindering compartment filling. Loading in attractor/control compartment was therefore performed from the lateral feeding channel, that was initially designed for in-channel administration of bacteria and bioactive molecules. Loading time was adjusted to 30-40 min max when all the wells were filled at once. It should be stressed out that 10 min is the ideal time to reduce loading procedures' bias and make devices more user-friendly. Indeed it is still difficult to load a satisfactory number of cells when a light microscope is not used to constantly monitor loading procedures. Loading problems could be solved by augmenting the height of loading channels and cell compartments, while all the features should be well developed in order to avoid cell blocks.

Cell preparation and survival: Cytotoxicity is to a certain level tolerated in macro experiments, but in this case it is deleterious, because of the relatively low number of cells that are loaded inside the device and that are required to be more functional as possible in order to produce strong and sustained chemokine gradients. Therefore implementation of overall cell survival within the device is important. This could be achieved first by reducing infection within the device, second by improving cell preparation routines. CellTracker staining procedures were tested for general cell toxicity and cell activation and did not result deleterious for MF2.D9 cells and RF33.70, see section 4.2.2. Even though activation of primary bone marrow-derived (BMDC) dendritic cells was not impaired during staining procedures many cells were actually dying during long handling procedures. For this reason, it was decided not to stain these cells. BMDC detaching and preparation resulted to be important in order to load viable cells on the devices. Many cells died during scraping, while the employment of non adherent BMDC or EDTA detached cells increased the number of living cells during assay. This procedure can indeed be found in a protocol for chemotaxis assay in microchannel³³. Mutu dendritic cells (1940) were then proposed as an alternative model in order to avoid staining procedures and reduce animal use. This cell line is a novel murine dendritic cell line created from a transgenic mouse expressing the oncogene SV40LgT under the control of CD11c promoter and with GFP as a reporter gene⁵⁰. Mice present dendritic cells tumorigenesis, predominantly in the spleen and in the liver, affecting especially the subtype CD8 α positive of conventional dendritic cells from which the cell lines are derived⁵⁰. Cells are already mature and do not require LPS maturation. They could therefore be employed for studying mature dendritic cells chemotaxis.

Administration of bioactive molecules/bacteria in-channel Even though the use of pipette plugs seemed to be useful during food dye simulations of diffusion dynamics inside the device, it was later found that their use is potentially damaging in fourth generation devices, because small displacements of the plugs create internal currents compromising experiments. Therefore it is suggested to adopt permanent plugs that would not be moved over time.

During administration of bacteria to cells already loaded in the attractor channel, some prob-

lems regarding spread of bacteria and loading have been observed. In order to avoid bacteria diffusion to migratory and control wells in the device, it is suggested to permanently plug the attractor compartment after bacterial administration. Finding the right combination between administrated bacteria and BMDC loaded into the attractor chamber is still troublesome, since a positive chemotactic response was observed just in one occasion, after a second administration of bacteria. Indeed bacteria and dendritic cells were loaded from the same channel, if the later feeding channel is too full with cells delivery of the bacteria to the attractor chamber can be hindered. The time of 2-3 h in between cell loading and bacteria administration was evaluated. Moreover it is important to have enough viable cells inside the device in order to

Gradient diffusion inside the device: Our preliminary experiments suggest a longer time for gradient formation in fourth generation device, compared to third generation, where dye accumulation in front of the migratory compartment started within 2 h. They also suggested that established gradient might be maintained longer, thanks to the draining function of the sink compartment. It has been argued that slow diffusion microdevices do not fit rapid leukocytes chemotaxis Kim and Wu²⁴. Therefore, when rapid moving cells such as T-cells are employed, it would be optimal to reduce the time for gradient formation within the device.

Moreover the longer the time is, the more the device is prone to any kind of disturbance, i.e. infections, metabolic wastes derived from cells, lost of bonding and chemokines draining from attractor/control chamber wells. The difficulty to induce the dye to consistently diffuse throughout the network, as it was evidenced in some experiences, may be due to excessive draining from the other wells of the attractors. This phenomenon was noticed while administration routes were tested with food dyes and it is another reason for proposing to permanently plug two of the attractor side wells after cell loading procedures. Diffusion was faster when the device was not covered by medium, and the sink is indeed able to drain dye surplus maintaining a correct gradient across the major network. This phenomenon could be exploited by combining a recirculating pumping mechanisms to the device and creating an hybrid system between active convective flows and passive diffusion where cells are not directly exposed to shear stress, as inside the device reported in⁵¹. For example the feeding channel could be part of a circulating mechanism. This flow would not interest migrating cells, and may push chemokine produced by attractor cells toward the major network more efficiently.

Moreover it should be considered that chemokine production by biological activity in most cases is not likely to be a continuous flow. For example, in dendritic cells, it is rather a burst of inflammatory chemokines released upon activation stimulus followed by linear upregulation of constitutive chemokines in maturing cells¹⁴. Anyway our predictions comes from empirical observations of the system that was in a state of non-equilibrium. A more detailed characterization of the time and the modalities of gradient diffusion should be performed in the future.

5.2 Chemotaxis assays and antigen presentation reactions

The potential use of the fourth generation device in chemotactic assays relies on the correct establishment of a chemotactic gradient, depending on many factors such as bonding efficiency of the PDMS, cell load and viability, and diffusion of chemoattractant molecules that were previously discussed. A further important factor is that attracting cells are producing significant amounts of chemokines and that migrating cells are prone to respond to them. Flow cytom-

etry analysis did not show any considerable change in some activators markers of of BMDC, MF2.2D9 and RF33.70 after staining procedures. Anyway only one dye was tested, CMFDA, and probably more tests should be done to be confirm these preliminary results.

Bone marrow-derived dendritic cells chemotaxis: In BMDC chemotaxis experiments, stimulation of BMDCs with LPS was usually performed on petri dish inside the incubator. Stimulation for 30 minutes or 5h-7h would be a maturation stimulus, that induce upregulation of inflammatory chemokines, which are abundantly produced by dendritic cells during the first hours following a strong maturation stimulus such as LPS¹⁴.

During the first experiments a clear directed response towards the attractor compartment was observed thanks to the strategy identified in section 4.3.1, see Figures 4.10afig:butterfly31gen24. Since the same dynamic was observed in the experiment reported in Figure 4.15c during dendritic cells chemotaxis towards *M. avium* infection, it may be suggested that whether a gradient of chemotactic molecules is present inside the device BMDC will have similar distributions with a neat difference between attractor and control subareas. Such a response is comparable to the chemotactic responses obtained when BMDCs were used in third generation devices⁴³. Since such a neat response was not observed in other experiments, it is possible that a chemotactic gradient was not present inside the devices. Regarding LPS stimulated cells, the most significant causes for inconclusive results are inefficient bonding and unwanted activation of control BMDCs, whose amount loaded on the devices increased during experiments. Indeed, flow cytometry results showed that even non-adherent and carefully handled BMDC had a considerable population positive for CD86. Therefore, unstimulated BMDC may not be a perfect internal control in such experiments. Regarding in-channel infections of BMDC, non optimal ratio between alive BMDC and bacteria loaded on the attractor compartment, and bacterial contamination during administration routes seem be determinant causes for undirected and reduced migration.

In most of the experiments, complexive migration of dendritic cells inside the network seemed to be time-restricted during the first 24 h. Moreover, most of the cells did not advanced towards sink, attractor or control compartments, and were retained in the network. This fact needs to be further analyzed and taking into account the acquired knowledge regarding gradient formation and cell response times. In case of positive results, it could be explained as a ligand-induced downregulation of dendritic cells receptors for inflammatory chemokine in maturing dendritic cells¹⁴. In later time points BMDCs may start to attract each other. Indeed a few dendritic cells reach open spaces, whereas of the cells is retained within the network. In one occasion, a second consistent migration was observed between 20 and 48 h after loading, see Figure 4.12. This result is difficult to interpret, but it might mean that part of the cells sensed a chemotactic stimulus in a second time.

Chemotaxis of T-cells: T lymphocytes isolated from mouse spleen did not show autonomous migration inside the device, and may not be suitable for chemotaxis assays in such a microchannel device.

On the contrary, both MF2.2D9 and RF33.70 T cell hybridomas showed consistent motility and migration across all device subareas. During the first experiments most of the migrating MF2.2D9 and RF33.70 probablt died because they had been kept on ice too long time, since in further experiments, where cells were not kept in ice more than 1 h, the first cells enter

the device one hour after loading. Anyway the experiments highlighted possible long term interactions between BMDC and T cell hybridomas, whereas a significant evaluation of antigen presentation reactions was not possible because of the late-timing of observation. The reaction was established again, but it was chosen to fully mature dendritic cells during the night in order to speed up antigen presentation reaction. Even though a slight localization of MF2.2D9 in front of the attractor chamber was observed in one device, see Figure 4.18c, when considering that the control compartment was loaded with medium (in order to avoid pure interactions with BMDCs), it does not seem that MF2.2D9 cells are sensible to antigen presentation reactions, in accordance to the previous results obtained by Ryan Hannam in third generation devices.

Since cytotoxic T cells have been shown *in vivo* to quickly respond to chemokines released by dendritic cells involved in antigen presentation reactions with T helper cells⁵², it was chosen to attempt again the antigen presentation reaction between MF2.2D9 and BMDC in an experimental setup where migration of MF2.2D9 and RF33.70 could be evaluated in Real-Time. Due to technical problems, this experiment was not optimally monitored. Moreover filters inside the device were damaged and allowed relocalization of attractant cells and invasion of attractor/control chambers by migrating cells. For these reasons it is not possible to properly evaluate the chemotactic response. The only observation that seems to suggest the occurrence of a sort of immunological reaction is the diverse dilution of Deep Red dye in RF33.70 cells found in the attractor compartment compared to the cells in the control compartment. Cell-tracker dilution may indicate that antigen presentation reactions have induced MF2.2D9 to produce IL-2 and stimulated RF33.70 proliferation⁵³.

Anyway these experiments were performed only a few times and with too many variants that do not allow to formulate further hypotheses. Right now, it is difficult to say whether or when chemoattractant molecules will start, and further investigations are needed. It is important to correctly tailor the activation of BMDC and investigate whether efficient antigen presentation reactions can be sped up inside the channel by providing the correct combination of stimuli to BMDCs⁴⁴. For example, CD40 stimulation is important to fully activate dendritic cells and maybe expression of CD40L on activated MF2.2D9 could result in more effective antigen presentation reactions⁵⁴. The high reproduction rate of these cell lines is a further reason to speed up the time of gradient formation inside the device, since experiments results might be compromised by the presence of too many cells. Finally, due to the high speed of migrating T cell hybridomas and according to the later localization of these cells in the open spaces of the device, such as the sink and the arrival subareas, it is likely that evaluation of chemotactic responses should especially take into account localization in front of the attractor chamber.

i

5.3 Cell Recruitment and Migration in Real-Time

The fourth generation network design provides diverse confined environments where direction of migration is either imposed, as in the linear channels between the major and the minor networks, or left up to cells, as in the maze of the major network. Even though a complete picture of all migration modes and behaviors of cells within the device cannot be delineated right now, some migratory modes and behavior compatible with models reported in literature were observed.

BMDC migration: Dendritic cells are able to protrude in open spaces thanks to their adaptability to the adhesive properties of the environment. They can indeed switch the rate of actine polymerization and protrude their anterior network even in the absence of anterior pulling forces²³. Myosin contraction is a second important mechanism in order to retract cell rear and generate hydrostatic forces that are probably contributing to cell migration in confined environments²². Moreover, dendritic cells there have non contractil phases where the rear of the cell is motionless and is passively dragged by the protruding front. Dendritic cells are able to move in absence of integrin-adhesion, but just in 3D environment¹⁶. Inside the network BMDCs have shown to be able to move, but the space they encounter cannot be defined three-dimensional because cells are often not filling the 8 μm width microchannels. The ability to couple protrusion and contraction in order to generate effective movement along the channels seem to be cell specific, and it might be a reason for the multiple morphologies observed inside the system. Often, the rear was observed lagging behind and sticking to the wells of the channels, apparently hindering forward displacement. Indeed a mechanism for functional dissociation of the front and the back of dendritic cells have been suggested¹⁶. In order to increase the confinement of migrating cells channels, 6 μm width may be an efficient improvement.

Some BMDCs were found able to protrude under intact filter and some of them were detected to have invaded integer devices. Gaps of 3 μm between lymphatics endothelial cells are sufficient for DCs and lymphocytes entry into lymphatic vessels⁶. Nuclear deformation of dendritic cells is necessary in 2 μm broad spaces³³. Some results could therefore be biased by this fact and the event will need further investigations, even though the number of DCs migrated in intact device is maybe negligible.

During migration in microchannels dendritic cells alternate moments of high speed with moments of low speed. This is predominant in immature dendritic cells and it has been hypothesized that the underlying mechanism is calcium regulation, which is responsible also for the directional persistence,⁵⁵.

T cell hybridomas: Labelling procedures for multiplexing resulted to be sometimes inefficient for long term observations. CMFDA CellTracker and Violet BMQ labels were not well detected by the EVOS system and further improvements needs to be established. However, the good labelling achieved with Deep Red CellTracker allowed for cell recognition in multiplexed experiments. Tracking of T cell hybridomas could be used in order to analyze motility and paths of T cells, and check whether a chemoattractant stimulus is present or not inside the device. Some qualitative differences were visible from the first hours of migration and later hours. However, most of these behaviours need to be further and more precisely collocated into a physiological context, depending on the correct timing and tailoring of immune reactions inside the device. MF2.2D9 were previously reported by Ryan Hannam to have 2:1 straight migration over paths presenting 90° turns in device of third generation. Fourth generation devices present an X-shaped network where the same analysis could be performed over several experiments. This could be used to investigate mechanisms regulating T cell migration and directions in lymph nodes and other interstitial tissues, where diverse models such as random migration and environmental guided migration have been proposed^{56,57}.

The uropods of T cell hybridomas have been observed to capture other cells and redirect their migration via adhesive mechanisms. Indeed, the role of this organelles and myosin II filled

structure is emerging, and it seems to be involved in several communication and interacting mechanisms among leukocytes,⁵⁸. Further investigations involving fluorescent label targeting subcellular components of the uropod, or transfection of fluorescently localized proteins, could be used in order to define molecularly specific functions of the uropod and subcellular components involved the adhesive cell recruitment observed during time-lapses.

The observation of uropod dynamics and the effects upon cell migration of MF2.2D9 and RF33.70 is a proof that the device provides a geometrically controlled environment where interactions between cells can be resolved at an high resolution, maybe at an higher level than intra-vital microscopy¹².

Chapter 6

Future Developments

The device is prone to be used in several application for the study of immune reactions in Real-Time. In order to fully benefit from its potential important parameter and technical improvements are needed. The the most important are control of immunological reaction timing and efficiency, application of more sophisticated imaging techniques in order coupled with efficient labelling techniques, and elaboration of mathematical models for tracking cell paths and interactions within the device. Moreover, device design could be ameliorated in order to speed up gradient formation and the amounts of cell loaded inside. All the features within the master used for the production of the device by soft lithography needs to be well developed on both sides, and increasing the height of loading channels is an important step to be taken into account in order to ameliorate device performance. Employing fibrin/collagen coating would moreover ameliorate the cell culture condition and migration within the device, or alternatively, the use of other materials such as hydrogels could be investigated in order to provide cells a more physiological microenvironment²⁴. Once optimal experimental conditions have been established, numerous applications of such a design are possible.

Behaviour and migration of different subsets of primary dendritic cells towards a multiple chemoattractant stimuli, such as viral and bacterial infections, could be investigated in such a design where a small amount of these rare cells could be loaded and monitored⁵⁹. In the same way, the migratory routes and tissue targets of locally imprintend effector lymphocytes or memory cells could be recreated in coculture systems inside the attractor chamber of the device⁴.

From a chemotaxis point of view we would like to address the mechanisms regulating naïve T cells and mature dendritic cells recruitment and retention inside T-cell zones in lymph nodes (LN), which are still not completely elucidated. We would like to use a systemic multicellular approach and are currently working on the introduction of LN stromal cells inside the system,⁶⁰.

Moreover, an alternative use of the device subareas could be used for studying antigen presentation reactions. Labelled and antigen loaded mature DCs could be loaded on the sink compartment and differently labelled T cells on the migration entries. In this way, transient and prolonged interactions between the two cell population could be evaluated, similarly to the visualization of antigen-presentation reactions during *in vivo* microscopy⁶¹.

Finally, the device could be employed in high resolution in order to visualize subcellular mechanisms regulating migrating cells movements and chemotaxis at a single-cell level, for example the role of diverse uropods components could be evaluated during cell-cell contacts. The device

is prone to be used in single-cells analysis that can be further integrated in order to have a complexive and detailed vision of migration during cell chemotaxis⁶².

Chapter 7

Conclusion

This work aimed to point out possible applications of our newly designed fourth generation device for studying cell migration and chemotactic recruitment. Several new procedures were tested and implemented in order to employ such a device in chemotactic and in real-time monitored studies of cell migration. The new design offer a broader network to be observed and multiple environments can be compared, such as migration in space with an imposed direction, lines, and a multiple choice environment were decision making of migrating cells can be visualised in Real-Time. A chemotactic response was observed in some occasions, and resulted to be strongly dependent on a proper microfabrication of the device, a correct way of stimulation of cells and the amount of cell loaded in the attractor compartment. Indeed these two latter aspect of the design need to be improved in order to augment the suitability of the design for biological experiments. Once established routines for cell loading and stimulation, migration of slow moving cells could be evaluated and compared using the strategies identified during this work. Instead, for the employment of rapid migrating cells, it is important to increase the speed of gradient establishment across the major network.

Real-time observation of cell migration during time-lapse, enlarge the range of possible applications of the device for the study of cell migration and chemotaxis at a single-cell level. The design resolve the structural determinants of the space surrounding cells, it is therefore possible to visualize how cells enter, move and interact in confined spaces.

Bibliography

1. Ivan K H Poon, Christopher D Lucas, Adriano G Rossi, and Kodi S Ravichandran. Apoptotic cell clearance: basic biology and therapeutic potential. *Nature reviews. Immunology*, 14(3):166–80, 2014. ISSN 1474-1741. doi: 10.1038/nri3607. URL <http://www.ncbi.nlm.nih.gov/pubmed/24481336>.
2. Antonella Pellicoro, Prakash Ramachandran, John P Iredale, and Jonathan a Fallowfield. Liver fibrosis and repair: immune regulation of wound healing in a solid organ. *Nature reviews. Immunology*, 14(3):181–94, 2014. ISSN 1474-1741. doi: 10.1038/nri3623. URL <http://www.ncbi.nlm.nih.gov/pubmed/24566915>.
3. Jacqueline Parkin and Bryony Cohen. An overview of the immune system. *Lancet*, 357(9270):1777–1789, 2001. ISSN 01406736. doi: 10.1016/S0140-6736(00)04904-7.
4. Bas J G Baaten, Andrea M. Cooper, Susan L. Swain, and Linda M. Bradley. Location, location, location: The impact of migratory heterogeneity on T cell function. *Frontiers in Immunology*, 4(OCT):1–11, 2013. ISSN 16643224. doi: 10.3389/fimmu.2013.00311.
5. Reinhold Förster, Asolina Braun, and Tim Worbs. Lymph node homing of T cells and dendritic cells via afferent lymphatics. *Trends in Immunology*, 33(6):271–280, 2012. ISSN 14714906. doi: 10.1016/j.it.2012.02.007. URL <http://dx.doi.org/10.1016/j.it.2012.02.007>.
6. Tim Lämmermann and Michael Sixt. The microanatomy of T-cell responses. *Immunological Reviews*, 221(1):26–43, 2008. ISSN 01052896. doi: 10.1111/j.1600-065X.2008.00592.x.
7. Sussan Nourshargh and Ronen Alon. Review Leukocyte Migration into Inflamed Tissues. *Immunity*, 41(5):694–707, 2014. ISSN 1074-7613. doi: 10.1016/j.immuni.2014.10.008. URL <http://dx.doi.org/10.1016/j.immuni.2014.10.008>.
8. Sussan Nourshargh, Peter L Hordijk, and Michael Sixt. Breaching multiple barriers: leukocyte motility through venular walls and the interstitium. *Nature reviews. Molecular cell biology*, 11(5):366–378, 2010. ISSN 1471-0072. doi: 10.1038/nrm2889. URL <http://dx.doi.org/10.1038/nrm2889>.
9. Samantha J Allen, Susan E Crown, and Tracy M Handel. Chemokine: receptor structure, interactions, and antagonism. *Annual review of immunology*, 25:787–820, 2007. ISSN 0732-0582. doi: 10.1146/annurev.immunol.24.021605.090529.
10. Charlotte L Weller, Sarah J Collington, Jeremy K Brown, Hugh R P Miller, Adam Al-Kashi, Peter Clark, Peter J Jose, Adele Hartnell, and Timothy J Williams. Leukotriene B₄, an activation product of mast cells, is a chemoattractant for their progenitors.

- The Journal of experimental medicine*, 201(12):1961–1971, 2005. ISSN 0022-1007. doi: 10.1084/jem.20042407.
11. William Rostène, Patrick Kitabgi, and Stéphane Mélik Parsadaniantz. Chemokines: a new class of neuromodulator? *Nature reviews. Neuroscience*, 8(11):895–903, 2007. ISSN 1471-003X. doi: 10.1038/nrn2255.
 12. Tim Lämmermann and Ronald N. Germain. The multiple faces of leukocyte interstitial migration. *Seminars in Immunopathology*, 36(2):227–251, 2014. ISSN 18632300. doi: 10.1007/s00281-014-0418-8.
 13. Patrick Blanco, a. Karolina Palucka, Virginia Pascual, and Jacques Banchereau. Dendritic cells and cytokines in human inflammatory and autoimmune diseases. *Cytokine and Growth Factor Reviews*, 19(1):41–52, 2008. ISSN 13596101. doi: 10.1016/j.cytogfr.2007.10.004.
 14. Federica Sallusto, Belinda Palermo, Danielle Lenig, Minja Miettinen, Sampsa Matikainen, Ilkka Julkunen, Reinhold Forster, Ralf Burgstahler, Martin Lipp, and Antonio Lanzavecchia. Distinct patterns and kinetics of chemokine production regulate dendritic cell function. *European Journal of Immunology*, 29(5):1617–1625, 1999. ISSN 00142980. doi: 10.1002/(SICI)1521-4141(199905)29:05<1617::AID-IMMU1617>3.0.CO;2-3.
 15. Yuan Liu and Guixiu Shi. Role of G protein-coupled receptors in control of dendritic cell migration. *BioMed Research International*, 2014, 2014. ISSN 23146141. doi: 10.1155/2014/738253.
 16. Tim Lämmermann, Bernhard L Bader, Susan J Monkley, Tim Worbs, Roland Wedlich-Söldner, Karin Hirsch, Markus Keller, Reinhold Förster, David R Critchley, Reinhard Fässler, and Michael Sixt. Rapid leukocyte migration by integrin-independent flowing and squeezing. *Nature*, 453(7191):51–55, 2008. ISSN 0028-0836. doi: 10.1038/nature06887.
 17. Shaun R. McColl. Chemokines and dendritic cells: A crucial alliance. *Immunology and Cell Biology*, 80(5):489–496, 2002. ISSN 08189641. doi: 10.1046/j.1440-1711.2002.01113.x.
 18. Stephanie S. Watowich and Yong Jun Liu. Mechanisms regulating dendritic cell specification and development. *Immunological Reviews*, 238:76–92, 2010. ISSN 01052896. doi: 10.1111/j.1600-065X.2010.00949.x.
 19. Alexander Link, Tobias K Vogt, Stéphanie Favre, Mirjam R Britschgi, Hans Acha-Orbea, Boris Hinz, Jason G Cyster, and Sanjiv a Luther. Fibroblastic reticular cells in lymph nodes regulate the homeostasis of naive T cells. *Nature immunology*, 8(11):1255–1265, 2007. ISSN 1529-2908. doi: 10.1038/ni1513.
 20. Miguel Vicente-Manzanares and Francisco Sánchez-Madrid. Role of the cytoskeleton during leukocyte responses. *Nature reviews. Immunology*, 4(2):110–122, 2004. ISSN 1474-1733. doi: 10.1038/nri1268.
 21. Audrey Gérard, a. E E Mertens, Rob a. Van Der Kammen, and John G. Collard. The Par polarity complex regulates Rap1- and chemokine-induced T cell polarization. *Journal of Cell Biology*, 176(6):863–875, 2007. ISSN 00219525. doi: 10.1083/jcb.200608161.
 22. Tim Lämmermann and Michael Sixt. Mechanical modes of 'amoeboid' cell migra-

- tion. *Current Opinion in Cell Biology*, 21(5):636–644, 2009. ISSN 09550674. doi: 10.1016/j.ceb.2009.05.003.
23. Jörg Renkawitz, Kathrin Schumann, Michele Weber, Tim Lämmermann, Holger Pflücke, Matthieu Piel, Julien Polleux, Joachim P Spatz, and Michael Sixt. Adaptive force transmission in amoeboid cell migration. *Nature cell biology*, 11(12):1438–1443, 2009. ISSN 1465-7392. doi: 10.1038/ncb1992. URL <http://dx.doi.org/10.1038/ncb1992>.
 24. Beum Jun Kim and Mingming Wu. Microfluidics for mammalian cell chemotaxis. *Annals of Biomedical Engineering*, 40(6):1316–1327, 2012. ISSN 00906964. doi: 10.1007/s10439-011-0489-9.
 25. Bx Stephen Boyden and D Ph. THE CHEMOTACTIC EFFECT OF MIXTURES OF ANTIBODY AND ANTIGEN ON POLYMORPHONUCLEAR LEUCOCYTES (From the Department of Experimental Pathology , John Curtin School of Medical Research , Australian National University , Canberra) Materials and Methods. *Assessment*, pages 453–466, 1962.
 26. Nina Kramer, Angelika Walzl, Christine Unger, Margit Rosner, Georg Krupitza, Markus Hengstschläger, and Helmut Dolznig. In vitro cell migration and invasion assays. *Mutation Research/Reviews in Mutation Research*, 752:10–24, 2012. ISSN 13835742. doi: 10.1016/j.mrrev.2012.08.001.
 27. Peter Friedl, Erik Sahai, Stephen Weiss, and Kenneth M. Yamada. New dimensions in cell migration. *Nature Reviews Molecular Cell Biology*, 13(11):743–747, 2012. ISSN 1471-0072. doi: 10.1038/nrm3459. URL <http://dx.doi.org/10.1038/nrm3459>.
 28. Matthew L. Kutys, Andrew D. Doyle, and Kenneth M. Yamada. Regulation of cell adhesion and migration by cell-derived matrices. *Experimental Cell Research*, 319(16):2434–2439, 2013. ISSN 00144827. doi: 10.1016/j.yexcr.2013.05.030. URL <http://dx.doi.org/10.1016/j.yexcr.2013.05.030>.
 29. Katarina Wolf, Regina Müller, Stefan Borgmann, Eva B. Bröcker, and Peter Friedl. Amoeboid shape change and contact guidance: T-lymphocyte crawling through fibrillar collagen is independent of matrix remodeling by MMPs and other proteases. *Blood*, 102(9):3262–3269, 2003. ISSN 00064971. doi: 10.1182/blood-2002-12-3791.
 30. Alexandre P. Benechet, Manisha Menon, and Kamal M. Khanna. Visualizing T cell migration in situ. *Frontiers in Immunology*, 5(July):1–12, 2014. ISSN 16643224. doi: 10.3389/fimmu.2014.00363.
 31. Roberto Weigert, Natalie Porat-Shliom, and Panomwat Amornphimoltham. Imaging cell biology in live animals: ready for prime time. *The Journal of cell biology*, 201(7):969–79, 2013. ISSN 1540-8140. doi: 10.1083/jcb.201212130. URL <http://jcb.rupress.org/content/201/7/969.full>.
 32. Michael Y. Gerner, Wolfgang Kastenmuller, Ina Ifrim, Juraj Kabat, and Ronald N. Germain. Histo-cytometry: A method for highly multiplex quantitative tissue imaging analysis applied to dendritic cell subset microanatomy in lymph nodes. *Immunity*, 37(2):364–376, 2012. ISSN 10747613. doi: 10.1016/j.immuni.2012.07.011.

33. Mélina L Heuzé, Olivier Collin, Emmanuel Terriac, Ana-Maria Lennon-Duménil, and Matthieu Piel. Cell migration in confinement: a micro-channel-based assay. *Methods in molecular biology (Clifton, N.J.)*, 769:415–34, January 2011. ISSN 1940-6029. doi: 10.1007/978-1-61779-207-6_28. URL <http://www.ncbi.nlm.nih.gov/pubmed/21748692>.
34. Matthias Mehling, Tino Frank, Cem Albayrak, and Savas Tay. Real-time tracking, retrieval and gene expression analysis of migrating human T cells. *Lab on a chip*, 2014. ISSN 1473-0189 (Electronic). doi: 10.1039/c4lc01038h.
35. Vijaykrishnan Ambravaneswaran, Ian Y Wong, Alexander J Aranyosi, Mehmet Toner, and Daniel Irimia. Directional decisions during neutrophil chemotaxis inside bifurcating channels. *Integrative biology : quantitative biosciences from nano to macro*, 2(11-12): 639–647, 2010. ISSN 1757-9694. doi: 10.1039/c0ib00011f.
36. Sangeeta N Bhatia and Donald E Ingber. Microfluidic organs-on-chips. *Nature biotechnology*, 32(8):760–772, 2014. ISSN 1546-1696. doi: 10.1038/nbt.2989. URL <http://www.ncbi.nlm.nih.gov/pubmed/25093883>.
37. J Cooper Mcdonald, David C Duffy, Janelle R Anderson, and Daniel T Chiu. Review - Fabrication of microfluidic systems in poly (dimethylsiloxane). *Electrophoresis*, 21:27–40, 2000.
38. Kathryn Haubert, Tracy Drier, and David Beebe. PDMS bonding by means of a portable, low-cost corona system. *Lab on a chip*, 6(12):1548–1549, 2006. ISSN 1473-0197. doi: 10.1039/b610567j.
39. J. Cooper McDonald and George M. Whitesides. Poly(dimethylsiloxane) as a material for fabricating microfluidic devices. *Accounts of Chemical Research*, 35(7):491–499, 2002. ISSN 00014842. doi: 10.1021/ar010110q.
40. H. Hillborg and U.W. Gedde. Hydrophobicity recovery of polydimethylsiloxane after exposure to corona discharges. *Polymer*, 39(10):1991–1998, 1998. ISSN 00323861. doi: 10.1016/S0032-3861(97)00484-9.
41. David T. Eddington, John P. Puccinelli, and David J. Beebe. Thermal aging and reduced hydrophobic recovery of polydimethylsiloxane. *Sensors and Actuators, B: Chemical*, 114(1):170–172, 2006. ISSN 09254005. doi: 10.1016/j.snb.2005.04.037.
42. Jinwen Zhou, Amanda Vera Ellis, and Nicolas Hans Voelcker. Recent developments in PDMS surface modification for microfluidic devices. *Electrophoresis*, 31(1):2–16, 2010. ISSN 01730835. doi: 10.1002/elps.200900475.
43. N Gopalakrishnan, R Hannam, G P Casoni, D Barriet, J M Ribe, M Haug, and Ø Halaas. Lab on a Chip Infection and immunity on a chip : a compartmentalised microfluidic platform to monitor immune cell behaviour in real time †. *Lab on a Chip*, 2015. ISSN 1473-0197. doi: 10.1039/C4LC01438C. URL <http://dx.doi.org/10.1039/C4LC01438C>.
44. Kaveh Abdi, Nevil J Singh, and Polly Matzinger. Lipopolysaccharide-activated dendritic cells: "exhausted" or alert and waiting? *Journal of immunology (Baltimore, Md. : 1950)*, 188:5981–9, 2012. ISSN 1550-6606. doi: 10.4049/jimmunol.1102868. URL <http://0-www.jimmunol.org.unicat.bangor.ac.uk/content/188/12/5981.full>.

45. Oyvind Halaas, Magnus Steigedal, Markus Haug, Jane a Awuh, Liv Ryan, Andreas Brech, Shintaro Sato, Harald Husebye, Gerard a Cangelosi, Shizuo Akira, Roland K Strong, Terje Espevik, and Trude H Flo. Intracellular Mycobacterium avium intersect transferrin in the Rab11(+) recycling endocytic pathway and avoid lipocalin 2 trafficking to the lysosomal pathway. *The Journal of infectious diseases*, 201(5):783–792, 2010. ISSN 1537-6613. doi: 10.1086/650493.
46. Shantanu Bhattacharya, Arindom Datta, Jordan M. Berg, and Shubhra Gangopadhyay. Studies on surface wettability of poly(dimethyl) siloxane (PDMS) and glass under oxygen-plasma treatment and correlation with bond strength. *Journal of Microelectromechanical Systems*, 14(3):590–597, 2005. ISSN 10577157. doi: 10.1109/JMEMS.2005.844746.
47. Jessamine Ng Lee, Cheolmin Park, and George M. Whitesides. Solvent Compatibility of Poly(dimethylsiloxane)-Based Microfluidic Devices. *Analytical Chemistry*, 75(23):6544–6554, 2003. ISSN 00032700. doi: 10.1021/ac0346712.
48. Alvaro Mata and Aaron J Fleischman. Characterization of Polydimethylsiloxane (PDMS) Properties for Biomedical Micro / Nanosystems. *Biomedical Microdevices*, 2:281–293, 2005. ISSN 1387-2176. doi: 10.1007/s10544-005-6070-2.
49. S C Skaalure. Characterization of Sterilization Techniques on a Microfluidic Oxygen Delivery Device. *Journal of Undergraduate Research*, 2(1):1–4, 2008.
50. Silvia a. Fuertes Marraco, Frédéric Grosjean, Anaïs Duval, Muriel Rosa, Christine Lavanchy, Devika Ashok, Sergio Haller, Luc a. Otten, Quynh Giao Steiner, Patrick Descombes, Christian a. Luber, Felix Meissner, Matthias Mann, Lajos Szeles, Walter Reith, and Hans Acha-Orbea. Novel murine dendritic cell lines: A powerful auxiliary tool for dendritic cell research. *Frontiers in Immunology*, 3(November), 2012. ISSN 16643224. doi: 10.3389/fimmu.2012.00331.
51. Amir Shamloo, Ning Ma, Mu-Ming Poo, Lydia L Sohn, and Sarah C Heilshorn. Endothelial cell polarization and chemotaxis in a microfluidic device. *Lab on a chip*, 8(8):1292–1299, 2008. ISSN 1473-0197. doi: 10.1039/b719788h. URL `example`.
52. Flora Castellino, Alex Y Huang, Grégoire Altan-Bonnet, Sabine Stoll, Clemens Scheinacker, and Ronald N Germain. Chemokines enhance immunity by guiding naive CD8+ T cells to sites of CD4+ T cell-dendritic cell interaction. *Nature*, 440(7086):890–895, 2006. ISSN 0028-0836. doi: 10.1038/nature04651.
53. Özcan Met, Søren Buus, and Mogens H. Claesson. Peptide-loaded dendritic cells prime and activate MHC-class I-restricted T cells more efficiently than protein-loaded cross-presenting DC. *Cellular Immunology*, 222(2):126–133, 2003. ISSN 00088749. doi: 10.1016/S0008-8749(03)00128-X.
54. Daphne Y Ma and Edward a Clark. The role of CD40 and CD40L in Dendritic Cells. *Semin Immunol.* 2009, 21(5):265–272, 2010. ISSN 1044-5323. doi: 10.1016/j.smim.2009.05.010.The.
55. Paola Solanes, Mélina L Heuzé, Mathieu Maurin, Marine Bretou, Franziska Lautenschlaeger, Paolo Maiuri, Emmanuel Terriac, Maria-isabel Thoulouze, Pierre Launay,

- Matthieu Piel, and Pablo Vargas. Space exploration by dendritic cells requires maintenance of myosin II activity by IP 3 receptor 1. 34(6), 2015.
56. Paulus Mrass, Janka Petravac, Miles P. Davenport, and Wolfgang Weninger. Cell-autonomous and environmental contributions to the interstitial migration of T cells. *Seminars in Immunopathology*, 32(3):257–274, 2010. ISSN 18632297. doi: 10.1007/s00281-010-0212-1.
 57. Judy Cannon, Francois Asperti-Boursin, Matthew Fricke, Kenneth Letendre, and Melanie Moses. T cell motility within lymph nodes fits a Levy signature (CAM1P.225). *The Journal of Immunology*, 192(1 Supplement):47.1, May 2014. ISSN 1550-6606. URL http://www.jimmunol.org/content/192/1_Supplement/47.1.abstract.
 58. Francisco Sánchez-Madrid and Juan M Serrador. Bringing up the rear: defining the roles of the uropod. *Nature reviews. Molecular cell biology*, 10(5):353–359, 2009. ISSN 1471-0072. doi: 10.1038/nrm2680.
 59. Gwendalyn J Randolph, Jordi Ochando, and Santiago Partida-Sánchez. Migration of dendritic cell subsets and their precursors. *Annual review of immunology*, 26:293–316, 2008. ISSN 0732-0582. doi: 10.1146/annurev.immunol.26.021607.090254.
 60. Alice E Denton, Edward W Roberts, Michelle a Linterman, and Douglas T Fearon. Fibroblastic reticular cells of the lymph node are required for retention of resting but not activated CD8+ T cells. *Proceedings of the National Academy of Sciences of the United States of America*, 111(Cxcl):12139–44, 2014. ISSN 1091-6490. doi: 10.1073/pnas.1412910111. URL <http://www.ncbi.nlm.nih.gov/pubmed/25092322>.
 61. Thorsten R Mempel, Sarah E Henrickson, and Ulrich H Von Andrian. T-cell priming by dendritic cells in lymph nodes occurs in three distinct phases. *Nature*, 427(6970):154–159, 2004. ISSN 0028-0836. doi: 10.1038/nature02238.
 62. ZiQiu Tong, Eric M. Balzer, Matthew R. Dallas, Wei Chien Hung, Kathleen J. Stebe, and Konstantinos Konstantopoulos. Chemotaxis of cell populations through confined spaces at Single-Cell resolution. *PLoS ONE*, 7(1):1–10, 2012. ISSN 19326203. doi: 10.1371/journal.pone.0029211.